REPORT DOCUMENTATION PAGE

AFRL-SR-BL-TR-98-

0381

1. AGENCY USE ONLY (Leave Blank)	2. REPORT DATE	3. REPORT TYPE AND DATES COVERED
	May 1996	Final

4. TITLE AND SUBTITLE
Optical and Electrical Characterization of Vandium-Doped SiC

5. FUNDING NUMBERS

6. AUTHORS
Jason R. Jenny

7. PERFORMING ORGANIZATION NAME(S) AND ADDRESS(ES)
Carnegie Mellon University

8. PERFORMING ORGANIZATION REPORT NUMBER

9. SPONSORING/MONITORING AGENCY NAME(S) AND ADDRESS(ES)
AFOSR/NI
110 Duncan Avenue, Room B-115
Bolling Air Force Base, DC 20332-8080

10. SPONSORING/MONITORING AGENCY REPORT NUMBER

11. SUPPLEMENTARY NOTES

12a. DISTRIBUTION AVAILABILITY STATEMENT
Approved for Public Release

12b. DISTRIBUTION CODE

13. ABSTRACT *(Maximum 200 words)*
See attached.

14. SUBJECT TERMS

15. NUMBER OF PAGES

16. PRICE CODE

17. SECURITY CLASSIFICATION OF REPORT	18. SECURITY CLASSIFICATION OF THIS PAGE	19. SECURITY CLASSIFICATION OF ABSTRACT	20. LIMITATION OF ABSTRACT
Unclassified	Unclassified	Unclassified	UL

Carnegie Mellon University

CARNEGIE INSTITUTE OF TECHNOLOGY

THESIS

SUBMITTED IN PARTIAL FULFILLMENT OF THE REQUIREMENTS

FOR THE DEGREE OF *DOCTOR OF PHILOSOPHY*

TITLE Optical and Electrical Characterization of Vandium-Doped SiC

PRESENTED BY Jason R. Jenny

ACCEPTED BY THE DEPARTMENT OF Materials Science and Engineering

MAJOR PROFESSOR	DATE 5/1/96
DEPARTMENT HEAD C. D. Rollett	DATE 1 May '96

APPROVED BY THE COLLEGE COUNCIL

DEAN	DATE May 1, 1996

Carnegie Mellon University
Pittsburgh, Pennsylvania

FINAL PUBLIC ORAL ANNOUNCEMENT

For the Degree of

Doctor of Philosophy

CANDIDATE Jason R. Jenny

TITLE OF DISSERTATION Optical and Electrical Characterization of Vandium-Doped SiC

DEPARTMENT Materials Science and Engineering

TIME 10:00 a.m., April 23, 1996

PLACE 2327 Wean Hall

EXAMINERS Professor M. Skowronski, (Advisor, MSE)
Professor G.S. Rohrer, (MSE)
Dr. W. C. Mitchel, (Co-advisor, Wright Patterson AFB)
Dr. H.M. Hobgood, (Northrop Grumman)

PLEASE POST

Optical and Electrical Characterization of Vanadium-Doped SiC

Jason Jenny

Department of Materials Science and Engineering

Carnegie Mellon University

Pittsburgh, Pennsylvania

April 23, 1996

Submitted to Carnegie Institute of Technology
in partial fulfillment of the requirements for the degree of
Doctor of Philosophy in Materials Science and Engineering

Abstract

The purpose of this investigation was to characterize the material produced by Northrop Grumman during an effort to obtain semi-insulating SiC. The semi-insulating SiC is needed to further develop devices operating at microwave frequencies. High temperature Hall effect, deep level transient spectroscopy (DLTS), optical absorption, Fourier transform infrared (FTIR) spectroscopy, and thermally stimulated current (TSC) measurements were employed in concert to examine the resultant boules. The polytypes examined were 4H, 6H, and 15R. The product of these experiments was that three levels were detected which were related to the vanadium incorporation.

The deepest level (at E_c-1.35 eV) detected in 6H-SiC as a part of these experiments was identified as the isolated substitutional vanadium donor level (0/+). This confirmed previous predictions about the depth of the donor level. Wafers were found whose Fermi level was pinned at the vanadium donor resulting in insulating crystals (extrapolated to 10^{18} Ωcm at RT). The donor level was occupied due to the partial compensation by the boron acceptor which is ubiquitous in undoped SiC samples.

The other level related to the isolated, substitutional configuration of vanadium is the acceptor level. This investigation was the first to discover the position of this level within the SiC band gap. DLTS and Hall effect evinced an acceptor level position of E_c-0.8 eV for the 4H polytype. Hall effect was employed exclusively to ascertain the position in the 6H polytype (at E_c-0.66 eV). This level was observed in samples whose boron acceptor and vanadium donor levels were compensated by the common donor dopant, nitrogen. The DLTS results also indicated that the vanadium level can be incorporated in concentrations up to $3x10^{17}$ cm^{-3}. At these concentrations, it is a viable deep dopant for the compensation of residual donor and acceptor species at room temperature.

The final deep level that was attributed to vanadium was a complex with another undetermined impurity. This complex introduces a deep level at E_c-0.78 eV as determined by optical admittance spectroscopy. It also responsible for an

the NIR band indicate that the defect also aligns itself along the c-axis. Based upon these polarization studies, the transition that results in this NIR absorption was classified as a $^3A_2 \rightarrow {}^3E$ intracenter absorption of a linear defect with a C_{3v} symmetry. The second element in the complex was not ascertained, but nitrogen was suggested as a viable candidate.

Acknowledgments

The order of the listing of names in this section has nothing to do with their relative importance. I feel that I should start with the academic side of things, since this thesis stems from academic pursuits. The first name that comes to mind is the big guy - Professor Skowronski. I could not have asked for a better match for an advisor. His insight and direction were critical in my obtaining this degree, and for my development as a student of science. His dedication to his work is inspiring, and something that I hope to emulate.

Moving on to other influential persons, I have to include several professors at CMU, including: Professor Mahajan, Professor Rohrer, and Professor McHenry. Among this list are the people whose classes and/or encouragement have tremendously aided me in this achievement. The other people at Carnegie Mellon who have been fun to work with include: George Biddle, Jackie Cushion, Suzy Smith, Carol Carter, Andrea McDivett, Heiskell Rogan, and Marge Cain.

The other aspect of my research for which I am very grateful relates to my summer experiences. Had it not been for my ventures to Wright-Patt in beautiful Dayton, Ohio, I would not have nearly as much to say about vanadium as I currently do. Not only was it nice to get away for the summer, but working with everybody at WL/MLPO was enriching for my professional development as well - Dr. Mitchel as my mentor, Dr. Hemenger as a guide, Laura Rea as a buddy, and Matt Roth as a friend. I also have to thank Dave Fisher, Tom Kensky, Ron Perrin, Bob Bertke, and Jerry Landis for their support while I was there. I should also acknowledge the people at SCEEE Services Corporation who were very

helpful with all of my questions. I am also very appreciative of Air Force fellowship funding that I have received during the past three years.

The last academic-type group to whom I would like to express my appreciation are the guys at Northrop-Grumman, especially Don Hobgood. Had it not been for their effort in vanadium-doping of SiC, I would have worked on another research project, which could not have been more stimulating.

Finally, I have my family and friends. I think that I should start with my fiancée, Stephanie. She has really made the past four years as enjoyable as I could have imagined. I really do appreciate her support. My parents have been a wonderful throughout my life. They have allowed me to pursue my own path, allowing me to make my own mistakes and decisions. I have also been fortunate enough to know and appreciate my grandparents. I have enjoyed their varied and unique perspectives, which have, to some measure, shaped the way I perceive and react to certain situations. My friends and other family members have made my place here that much more enjoyable.

I would also like to thank silicon carbide for a variety of reasons. The foremost is the difficulty I had in breaking samples. I found that I could drop it from a height of 6 feet and it would not break. However, I did find out that I could not run over it with a chair.

Table of Contents

List of Figures

Chapter 1-Introduction

Chapter 2-Experimental Conditions

Chapter 3-The Vanadium Donor

Chapter 4-The Vanadium Acceptor

Chapter 5-Other Vanadium Related Features in Silicon Carbide

List of Tables

Introduction

Since the initial studies of single crystalline silicon carbide in the 1950's,[1] the prospects for the implementation of the material using all of its advantages have been elusive. Its wide band gap characteristics as well as other desirable electronic properties were the main driving force for this initial work. However, two major stumbling blocks persisted which hindered the development of SiC. The first of the these stumbling blocks was the n-type character of most undoped crystals. Studies later showed that this character resulted from nitrogen contamination which was very difficult to remove. The more challenging obstacle was that the crystals were very small, at most 1.5 cm^2 platelets. With the small size, the wide scale implementation would never lend itself to viable, economically feasible SiC devices. This problem of crystal size required the development of a new technique which was partly based upon that of the Lely. Only after this new technique was introduced was the purification of the grown boules possible. Before discussing the aforementioned new technique, a discourse on the applicability of SiC will be conducted.

1.1 Silicon Carbide Properties/Materials Characteristics

In many ways silicon carbide is an extremely useful material for electronic applications. One of the principal advantages is the width of its band gap, which places it within a sub-category of semiconductors termed wide-band-gap. Shown in table 1.1 is a comparison with several other semiconductors, both conventional and wide-band-gap. From this table, several advantages are apparent.

Table 1.1-Important semiconductor properties of various conventional and wide-band-gap materials[2]

Property	Si	GaAs	GaP	3C SiC 6H SiC	Diamond	GaN
Band gap (eV) at 300 K	1.1	1.4	2.3	2.2 2.9	5.5	3.39
Maximum operating temperature (K)	600	760	1250	1200 1580	1400	*
Melting point	1690	1510	1740	Sublimes >2100	Phase change	*
Physical stability	Good	Fair	Fair	Excellent	Very good	Good
Electron mobility RT, cm^2/Vs	1400	8500	350	1100 600	2200	900
Hole mobility	600	400	100	40	1600	150
Breakdown field E_b, 10^6/V/cm	0.37	0.4	-	4	10	5
Thermal conductivity c_T, W/m	1.5	0.5	0.8	5	20	1.3
Sat. C. elec. drift vel. v(sat), 10^7 cm/s	1	2	-	2	2.7	2.7
Dielectric const. K	11.8	12.8	11.1	9.7	5.5	9

*-unreported

The theoretical maximum operating temperature is reported to be much higher (for the 6H polytype) than the reported materials, save diamond. As a result of this property, it can be employed in many novel applications. Possibilities include mounting SiC devices directly onto jet engines to monitor operating conditions. The principal advantage of this placement comes from the fact that all of the necessary calculations and modifications can be performed very close to the sensors, eliminating the weight of wires needed to transmit these signals to the devices presently employed or proposed by airline manufacturers. Another idea which capitalizes on this property includes placing a SiC device inside of an automobile combustion chamber to analyze the performance of each

cylinder independently. The timing could then be adjusted to correct for any drop in the performance of a single cylinder. Such a contribution in this case would manifest itself in a savings from the reduction of gasoline usage in a poorly performing engine.

The physical stability of SiC results, in part, from the very strong bonding between the silicon and carbon atoms. This property is necessary in application in outer space where very high energy photons can readily damage more weakly bonded materials. In 1963, suggestions were made attesting to the fact that SiC could also operate as an indicator of irradiation temperature and neutron flux.[3] The first studies concerning the effects of neutron and gamma-ray bombardment of SiC took place in the early 1960's.[4] In a subsequent report, Canepa et. al.[5] indicated that SiC devices possessed a radiation hardness 100 times greater than that of other available Si devices. Although much of the current research into SiC has neglected this unique attribute, it is always mentioned as one prospect for the implementation of SiC devices.

Silicon carbide's breakdown voltage is yet another category where it exceeds other materials. This higher breakdown voltage will allow for the implementation of high-power devices using silicon carbide. An illustration of this is in placing SiC materials in a city's power distribution network. This would allow the system to operate at closer to 100% of its power rating (up from the current 66%) reducing the costs associated with building more carrying capacity. The current buffer is employed so that the equipment is not damaged in the case of a power surge. With a smart electrical system, the devices would automatically switch before the occurrence of equipment damage.[6]

The final important category where SiC greatly exceeds currently employed materials is that of thermal conductivity. A high thermal conductivity is crucial in the high-power application where large volumes of heat need to be dispersed in a short period of time so that the device does not break down from excess heat. An example of the need for high thermal conductivities can be seen with respect to the common Pentium processor. Large heat sinks coupled with cooling fans are required to sufficiently reduce temperatures and maintain device integrity. While SiC will probably not replace silicon in the future, its utility is clearly seen in this example.

While these bulk properties underscore the importance of SiC development, other device oriented properties further establish the potential dominance of silicon carbide in future markets. Two parameters used to gauge the viability of a given material include the Keyes figure of merit (KFM)[7], and the Johnson figure of merit (JFM)[8]. The KFM is used as a qualitative description of the thermal limitation of a material on its high frequency electrical performance. Conversely, the JFM measures the frequency and power product of a semiconductor transistor. Table 1.2 is a listing of the relative KFM and JFM for all of the materials that were previously compared to SiC. The numbers listed are normalized to silicon. The definitions used to establish these parameters are as follows:[9]

$$KFM = c_T \left(\frac{c v_s}{4\pi \varepsilon_R} \right)^{1/2} \qquad (1.1)$$

$$JFM = \frac{E_B^2 v_s^2}{4\pi^2} \qquad (1.2)$$

where c is the speed of light, v_s is the saturated velocity of carriers, and ε_R is the relative dielectric constant. From this table, silicon carbide would make a very effective material for high-speed and high-power devices. The current state of the technology will be discussed in the next sub-section along with some novel devices for which silicon carbide is especially useful. However, one other aspect of SiC needs to be mentioned before this issue is addressed.

One of the most curious features of the SiC system is its propensity to form structural modifications called polytypes.[10] By definition, polytypes are crystal structures whose chemistry is similar, but whose stacking sequence is different. The stacking sequence refers to the way in which close packed planes are stacked (i.e. {111} planes in cubic and {0001} planes in hexagonal crystals). Additionally, there are three classes of crystal structure found among the various polytypes, hexagonal, cubic and rhombohedral.

Table 1.2-Keyes' and Johnson's figures of merit for selected semiconductors[9]

Material	Normalized KFM	Normalized JFM
Si	1	1
Ge	0.27	0.1
GaAs	0.41	4.67
GaP	0.49	14.3
6H-SiC	5.1	262
Diamond	32	2601
GaN	0.46	16.7

Throughout this document, the most frequently used terminology will be that developed by Ramsdell.[11] This scheme uses two features of the crystal structure, the repeat distance of the stacking sequence and the base crystal structure (R for rhombohedral, C for cubic, and H for

hexagonal). As an example of this terminology, a sequence of layers whose crystal structure is hexagonal and after every 6 diatomic layers, the stacking sequence repeats itself is called 6H. The three polytypes that were examined as a part of this study are 4H, 6H, and 15R. As a manifestation of the polytypic

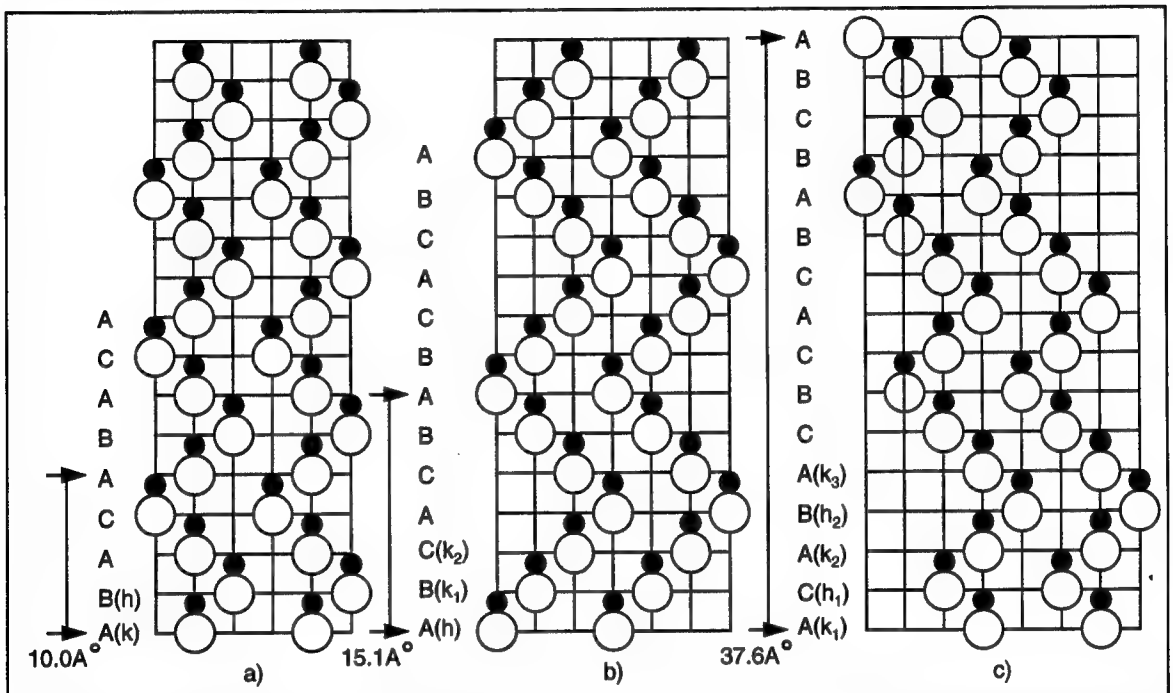

Figure 1.1-Stacking sequence of a)4H, b)6H, and c)15R polytypes. The type of inequivalent site is shown in parenthesis next to the type of plane

formation, inequivalent lattice sites are introduced into the crystal. Shown in figure 1.1 are schematics of the 4H, 6H, and 15R. Alongside the crystals are the positions of the inequivalent sites (1 hexagonal(h) and 1 cubic(k) for 4H, 1 hexagonal(h) and 2 cubic(k_1 and k_2) for 6H and 2 hexagonal(h_1 and h_2) and 3 cubic(k_1, k_2, and k_3) sites for 15R). The different sites in each crystal give rise to different crystal fields for the atoms occupying them. These different crystal fields result in the alteration of the absorption bands, photoluminescence features, and activation energies of defects which are subjected to them. These specific distinctions assist in the interpretation of features in the absorption spectrum which will be addressed in subsequent chapters.

Suggestions have been made proposing that the stoichiometry of the crystal aids in determining which polytype is grown.[12] In order to grow the various polytypes, the growth ambient is modified according to empirical relationships between temperature, pressure, and impurity content.[13, 14]

A principal result of the polytypic formation is the different band gap energies with the different polytypes. These range from 2.3 eV in the case of 3C to 3.4 eV in the case of 2H. The band gap varies as a function of the polytype's degree of hexagonality. The degree of hexagonality, η, is determined by dividing the number of hexagonal sites by the total number of inequivalent sites in the crystal (i.e. 0% for 3C, 33% for 6H, 40% for 15R, 50% for 4H, and 100% for 2H). As η increases, so too does the width of the band gap. Therefore, if a wider band gap is required for a given application, another polytype with a higher η may be substituted.

1.2 Device and Application Considerations

Silicon carbide has a great potential for a variety of electronic applications. These applications include light emitting diodes (LEDs)[15-17], bipolar transistors[18, 19], UV photodiodes[19, 20] and field-effect transistors (FETs). A partial list of the FETs that are believed to be suitable for development in the SiC system include: the metal oxide semiconductor FET (MOSFET)[21, 22], the junction FET (JFET)[23-25], and the metal semiconductor FET (MESFET)[19],. The first device to be successfully developed[20, 26, 27] and marketed[17, 19] in the SiC system was the blue LED.

Progress in the development of the SiC devices can be typified though an analysis of the improvement of operating parameters. As an example of these trends, the breakdown of p-n junctions improved from a reverse bias of 1000V[28,29] to 4500V[30] in a matter of 4 years from 1991 to 1995. Additionally, a silicon carbide p-n junction has been shown to withstand current densities as high as 60 kA/cm^2.[31] These considerable accomplishments give a glimpse of the viability of SiC as a high-power electronic material. Other studies have shown that the ratio of the specific on-resistance of comparable Si and 6H-SiC power MOSFETs is at least 100 for breakdown voltages above 200V.[32]

An application for which SiC is well suited is in ultraviolet (UV) detection. SiC's wide band gap allows for a sensitivity to UV radiation without interference from other longer wavelength sources. This is critical in applications where the UV signal to be detected is accompanied by other stray infrared (IR) or visible signals. Studies[33, 34] have shown SiC to be suited for this application, and p-n junctions fabricated resulted in very low leakage devices which can be employed in low light applications. These studies also showed successful operation of these devices to 500°C, exploiting yet another utility in the SiC system.

In addition to the previous application, two other roles exist for SiC. The first such application is as a candidate for a piezoresistor.[35] Semiconductors are currently used instead of conventional metal foils due to their higher strain sensitivity over the temperature regime. The other role for SiC is as a material for non-volatile random access memories (NVRAM). Due to the wide band gap and depth of impurity levels, trapped charges in SiC do not tend to possess sufficient thermal energy to recombine. In this role, the device would be placed into an on or off charge state, and could be left for significant periods of time,

without losing the charge. Extrapolation of data to room temperature for devices using a wet-oxide show that the storage time is on the order of 10^{14} s, or over 3000 millennia.[36]

One of the more useful semiconducting device classes in the SiC system is the field effect transistors (FET). Two very attractive properties of silicon carbide currently drive the development of this class of devices: SiC's wide band gap and its ability to operate at high temperatures. In 1987, a 3C-SiC/Si MOSFET was operated up to temperatures of 650°C.[38] SiC JFETs present a promising technology, given that a semi-insulating substrate is not required for their development. Table 1.3 is a listing of the currently studied SiC FETs, their best performance figures.[37] While SiC devices have improved within the last 10 years, a problem still persists. As the frequencies of the FETs approach the microwave regime, semi-insulating substrates are

Table 1.3-Listing of important transistor developments[37]

Type of device	g_m in mS/mm at room temperature	Highest temperature of operation (C)	Channel m at RT in cm2/Vs
Enhancement β SiC MOSFET	0.46 for Lg=5 μm	650	Low
Enhancement α SiC MOSFET	2.8 for Lg=7 μm	450	46
Depletion β SiC MOSFET	10 for Lg=2.4 μm	750	37
Depletion α SiC MOSFET	2.3 for Lg=5 μm	450	21
α SiC MESFET	4.3 for Lg=24 μm	450	300
β SiC MESFET	30 for Lg=24 μm	23	?
Depletion β SiC JFET	20 for Lg=4 μm	23	560
Depletion α SiC JFET	17-20 for Lg=4 μm	627	250

required for further development and refining of devices.[39] The semi-insulating wafers are necessary to isolate adjacent devices to reduce cross talk. More importantly, semi-insulating substrates are employed to reduce the parasitic capacitance inherent in devices grown on insulating material. Without carriers at the device boundaries, the capacitance in this region is negligible. Therefore, in addition to the need to develop larger diameter boules to reduce costs, a focus on the production of highly resistive boules is also necessary.

1.3 Growth of Large Diameter, High-Resistivity Boules

In order to make silicon carbide cost effective, it is essential to increase the size of the SiC wafers. The steps required to process a device are the same whether the devices are on a small or a large substrate. Therefore, the cost of processing a particular device is independent of the wafer size. If the processing was to be done on a 1.5 cm^2 Lely platelet and a 2" diameter (20.3 cm^2) wafer, the costs would be approximately the same, but the devices fabricated on the smaller wafer would cost thirteen times more than those on the larger wafer. Additionally, Lely crystals do not possess regular shapes, limiting the useful area even further.

From the 1950's until 1978 the predominant type of SiC growth was called the Lely technique.[1] In 1978, another technique, based upon the Lely technique, was introduced for the growth of boules of SiC.[40] This new growth was termed the modified-Lely, or physical vapor transport (PVT) method. Differentiation between these aforementioned techniques in future references will be made by referring to the older technique as simply, Lely, and the newer crystal growth

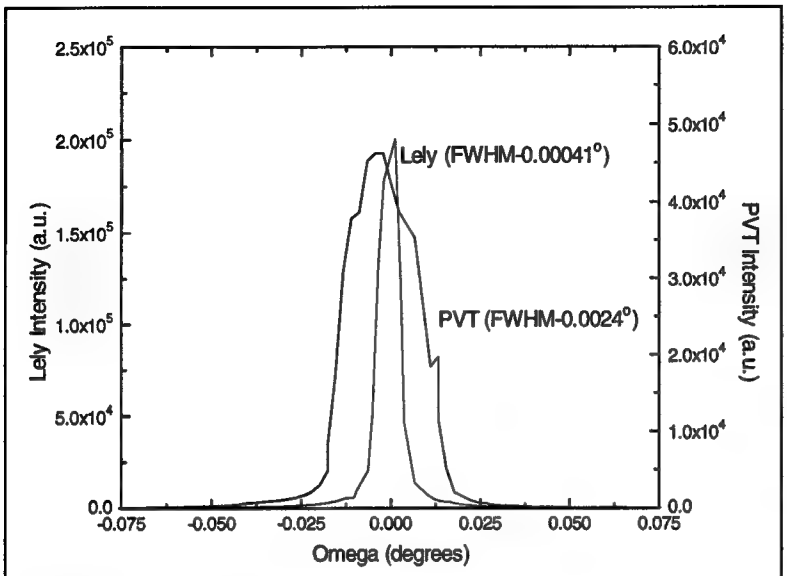

Figure 1.2-Typical rocking curves for: a) PVT and b) Lely grown crystals.[43]

technique, modified-Lely or PVT. The modified-Lely technique has gone through a scaling up from wafers of 14 mm diameters (18 mm lengths)[41] to the current published maximum of 60 mm (75 mm lengths).[42] Even with the advent of this new technique, the original Lely is not without utility.

Examining the structural properties of the resultant crystals, the Lely crystals possess a near-perfect structure not yet attainable in its modified relative. Plots of a Lely- and a PVT-grown SiC wafers' rocking curves are shown in figure 1.3. The full width at half maximum (FWHM) of the Lely crystal is significantly narrower than that of the PVT-grown crystal. An additional confirmation of the poorer crystal quality of the PVT grown wafers is evident when the wafers are placed in between polarized films which are oriented 90° with respect to each other. One useful tool for qualitatively establishing the crystallinity of a wafer is cross polarization. The experiment is performed by placing the wafer between two polarizing media oriented at 90° to one another. Figure 1.3 is a cross polarization image of a 2" diameter SiC wafer grown by the modified Lely technique. Clearly evident is a variation of shades which vary across the wafer. Due to the wafer's presence, the light's electric field is distorted sufficiently so that it is partly allowed to pass through the final screen. If the wafer were

homogeneous, the light would be constant across the wafer. Since it is not homogeneous, the light is altered differently at different points, indicating the presence of low-angle grain boundaries in the sample. In similar studies of Lely-grown material, no such variation is present, indicating a material of higher crystalline quality.

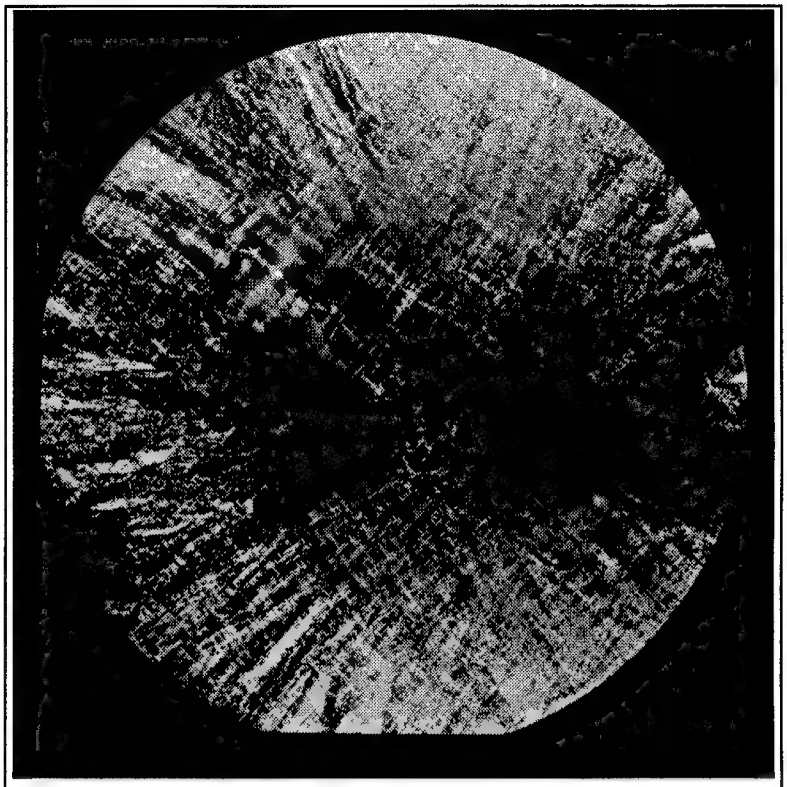

Figure 1.3-cross polarization image of a typical PVT-grown crystal. The variation in shade across the sample results from the occurrence of low-angle grain boundaries.

While the crystal quality of the PVT wafers are substantially poorer than the Lely, PVT is the only technique allowing for the production scale-up of SiC.

The other problem connected with the current state of the technology regarding the development of suitable SiC wafers concerns the presence of large quantities of impurities. Analytical studies performed on both Lely[44] and PVT[45] crystals show significant (>1ppm) concentrations of: N, B, **Fe**, **Na**, **Mg**, Al, **S**, **Cl**, **K**, **Ca**, **Ti**, V, **Cr**, **Ni**, and **Zn**. The elements listed in bold have not been proven to affect the electronic properties of the samples. In order to fabricate many of the SiC-based devices discussed in a previous sub-section, the substrates must be semi-insulating. There are two means of accomplishing this goal: growing purer material or doping with an impurity which produces a deep level. The next chapter will discuss the PVT growth conditions more specifically, but its operating

environment is extremely harsh. The PVT growth temperatures range up to 2300°C, at which point the majority of elements possess appreciable vapor pressures. As a result of this fact, there is very little likelihood of purifying the components of the growth environment sufficiently to reduce the resultant impurity transport within the reactor. This leaves the possibility of incorporating a deep level dopant into the SiC matrix which would pin the Fermi level deep enough to rid the mobile carrier bands of charges. The only element which has shown such a tendency is vanadium. A photo-electron spin resonance(ESR) study[46] has shown that it produces two deep levels, one of which (the vanadium donor) is near the middle of the silicon carbide band-gap.

1.4 Growth of Highly Resistive Boules/Research Objectives

As was alluded to in the previous section, the only means available to produce high-resistivity boules of silicon carbide is by employing a deep level dopant. This research is performed to characterize the development of such a boule. The techniques employed were: deep level transient spectroscopy (DLTS), high temperature Hall effect, optical absorption and Fourier transform infrared spectroscopy (FTIR). These tools were employed to determine how vanadium affects the optical and electronic properties of SiC.

The vanadium donor level was confirmed to reside at the mid-gap, and whole wafers were found whose Fermi level was pinned to this very deep donor level. Additionally, studies were made of the other levels which may impede the creation of these high resistivity boules. Two additional vanadium-related defects were discovered which produce levels within the SiC band gap: an

isolated vanadium acceptor and a vanadium complex. The vanadium acceptor level was found to reside 0.66 eV beneath the conduction band edge. Another level attributed to a vanadium complex was discovered 0.78 eV beneath the conduction band edge. Even if the Fermi level were pinned to either of these levels, the resultant crystals would still be semi-insulating at room temperature. However, semi-insulating material at higher temperatures (>600°C) is not attainable in the SiC system. These results indicated that vanadium possesses great potential as a deep level dopant in the SiC system.

2. Experimental Conditions

The purpose of this chapter is to convey the specific experimental procedures employed throughout the thesis as well as a cursory introduction to the techniques themselves. The experienced reader can skip the latter sections (2.2. - 2.1, 3.1, and 4.1 & 2.3. - 1.1 and 2.1). All of the other sections contain pertinent information regarding the experiments.

The research can be broken down into two types of techniques: electrical and optical. Before discussion can be conducted, an analysis of the samples' growth is necessary.

2.1 Physical Vapor Transport-Grown Silicon Carbide

All of the samples examined as a part of this study were grown in a physical vapor transport reactor. Such a reactor is shown in figure 2.1. The furnace is comprised of graphite elements which are replaced after each growth run. The reactor is heated by a water-cooled RF coil source to provide the >2100°C temperatures required to transport the SiC. The silicon carbide charge material is placed into the reactor. A seed crystal is then mounted onto a graphite susceptor in the center of the furnace. The reactor is closed and pumped down to vacuum and flushed with argon. Once this is completed, the reactor is heated to a high temperature for the growth. A temperature gradient of about 100°C is applied from the charge material to the seed crystal. This gradient is used to transport the material to create the SiC boules. Typical growth rates are from 0.5 to 1 mm per hour.[45]

There is a tendency for the boules to contain large amounts of impurities.[45] Such a problem stems from three facts: the high temperature used in growth, the graphite furnace elements, and impure charge material. The most critical factor is the high temperature. If not for the high temperatures, the other factors would not be as critical. At these temperatures, virtually all elements possess an appreciable vapor pressure. The impurities from the graphite elements and silicon carbide charge material cause the degradation of the material's purity.

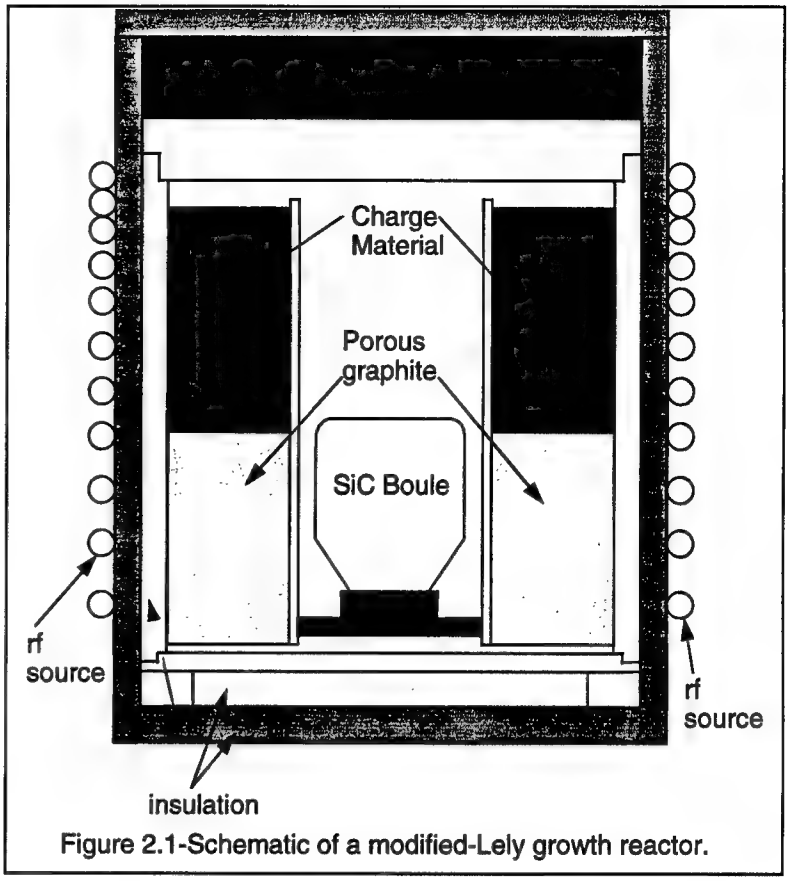

Figure 2.1-Schematic of a modified-Lely growth reactor.

2.2 Electrical Measurements

The purpose of this section is to discuss the electrical techniques used, as well as the means by which samples are prepared for the experiments. Following the discussion of the contact fabrication, the different techniques will be examined. During the course of this research, Hall effect (room temperature, low temperature-from 20 to 400K, and high temperature-from 295 to 1000K), deep

level transient spectroscopy (DLTS), and thermally stimulated current measurements were employed.

2.2.1 Contact Formation

For electrical measurements, two types of contacts are required: Schottky and ohmic. Hall effect and TSC measurements require ohmic contacts, while DLTS measurements use both ohmic contacts and Schottky barriers. In all cases, the sample surfaces were prepared with lapping and subsequent polishing with progressively finer diamond paste. Then, the samples are subjected to a 3 hour, 1150°C oxidizing anneal followed by an oxide etch in 50:50 H_2O:HF. These steps were employed to remove the native oxide as well as any residual surface damage from the cutting of the boules into wafers. All of the wafers used in the electrical measurements were sliced into 0.5 cm x 0.5 cm x 0.5 mm samples.

2.2.1.1 Schottky Barriers

The purpose of the Schottky barrier is to create a depletion layer in the crystal so that the occupancy of the traps within the layer can be modified by the application of electrical pulses. For these experiments, all of the DLTS measurements were carried out on n-type material. Therefore, the element selected for the Schottky barriers was the same as was used for ohmic contacts in the p-type samples, aluminum. For our samples, the aluminum provided a good barrier for the creation of a depletion region. The aluminum was applied by a magnetron sputtering system operating at a 360V bias while the samples were kept at room temperature. The plasma was created in a 5 milliTorr argon environment.

2.2.1.2 Ohmic Contacts

Four types of ohmic contacts were required for the range of samples examined as a part of this study. These types can be broken down by the sample/technique including contacts for: DLTS, n-type Hall, high-resistivity Hall/TSC, and p-type Hall.

For the DLTS samples, a circular Ti contact, 3 mm in diameter, was sputtered onto the carbon face of each sample. This procedure was used to form a broad area ohmic contact, and annealing was not employed because high quality ohmic contacts were not required for DLTS measurements. 2000 to 3000Å of titanium was applied in the same fashion as the aluminum.

On the n-type samples used in the Hall effect studies, either nickel or titanium was employed. Titanium was sputtered onto the samples, whereas nickel was applied using an electron-beam evaporation system. The thicknesses of the deposited films were between 3000 and 4000Å. Annealing was performed in a 90:10::N_2:H_2 forming gas environment at 900°C for 10 minutes. The metal was applied at the four corners of each sample required by the van der Pauw experiment. Prior to the contact deposition, the samples were wrapped in aluminum foil to mask off the corner regions. However, in some samples, the entire face was covered with the metal film, and black wax was applied to the corners. In this latter case, the unwanted metal was then removed via a generic metal etchant, either HCl:H_2O_2 or H_2SO_4:H_20.

The first two types of contacts were relatively easy to fabricate, while the latter two types of contacts proved to be more difficult. For p-type samples, aluminum

was applied via an electron beam evaporation system to a thickness of 4000Å. Aluminum was the natural selection because it is the shallowest p-type dopant in the SiC system. However, when annealing (700°C for 10 minutes) was performed, the contacts were invariably non-ohmic. The annealing process was altered with successive, shorter annealing steps. In between these steps, indium solder was applied to the sample and I-V measurements were performed to gauge the contact quality. Following this step and successive anneal, the contacts were often ohmic. The indium solder was found to be a crucial step in creating the desired contacts. Although the mechanism behind this was not examined, most likely, the indium diffused into the sample creating the necessary p-type character beneath the contact.

The most difficult contacts to fabricate reproducibly were those applied to the high-resistivity samples. Initially, the contacts were created using electron-beam-evaporated titanium (5000Å thick) followed by a 10 minute 900°C anneal. For samples prepared within the past year, 3000Å thick tantalum contacts were sputtered onto the samples. Rapid thermal annealing using an infrared heat source in an argon atmosphere was performed at 550°C for 60s. This latter schedule has created the majority of ohmic contacts to high-resistivity samples.

2.2.2 Hall Effect

Hall effect was a crucial element of this study. Other measurements can determine the ionization energy of both shallow and deep level defects. However, this is the only tool which would establish whether or not a certain growth environment resulted in the pinning of the Fermi level to a given deep

level. This determination is essential when attempting to study deep levels, and examine their effect in creating high-resistivity material.

2.2.2.1 Principles and Theory of the Hall Effect Measurement

Shown in figure 2.2 is a schematic of the basic Hall effect experiment. In this experiment, a current and a magnetic field are applied in mutually perpendicular directions. As a result of these applied fields, the Lorentz force (e(**vxB**), where v is the velocity of electrons and B is the magnetic field) is felt by the charge carriers in the third coordinate direction. A voltage (V_h) called the Hall voltage is developed to maintain the sample equilibrium. The direction of the voltage is determined by the type of majority carriers in the sample. If electrons are the majority carrier, they will initially be traveling in the opposite direction of the sign of the current (i.e. opposite the direction indicated by the arrow under the i in figure 2.2). Coupled with a magnetic field coming out of the figure, the force felt by the electrons will deflect them towards the top of the page. Similarly, if holes are the majority carriers, they will initially move in the direction of the current; and, with the same magnetic field, will deflect in the same direction as the electrons because the sign of the charge is opposite to that of the electron. Therefore, since the sign is opposite and the deflection the same, the voltage will

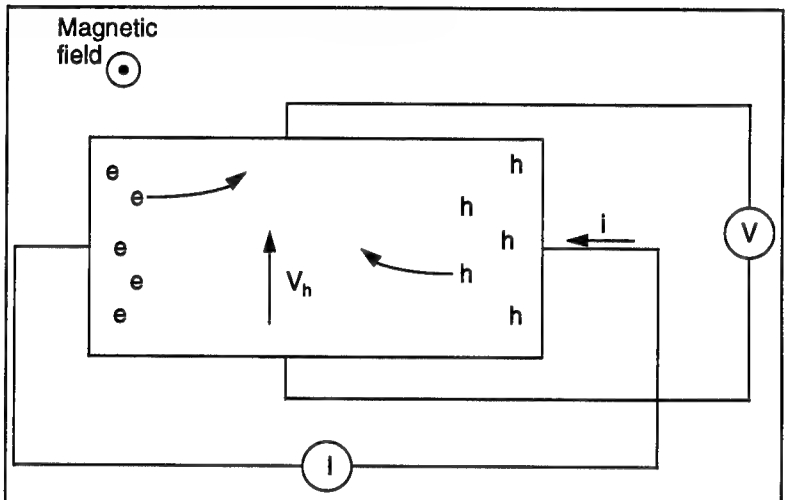

Figure 2.2-Schematic of a generic Hall effect experiment

be opposite. From this simple measurement, the type of carriers can be ascertained. Moreover, the concentration of carriers in the sample is determined based upon the magnitude of the Hall effect voltage according to the following relationship:[47]

$$\mathcal{E}_H=R_HJB=JB/N_e e \qquad (2.1)$$

where $\mathcal{E}_H$ is the electric field established by the Hall effect, R_H is the Hall coefficient, J is the initial current density, B is the magnetic flux density, e is the electron charge, and N_e is the concentration of carriers. With this information regarding the concentration of carriers, their mobility can then be calculated from the following relationship:[47]

$$\sigma=\mu_e(N_e e) \qquad (2.2)$$

where σ is the conductivity of the sample, and μ_e is the desired mobility. At a given temperature, mobility and carrier concentration are all that can be calculated. Such information yields a qualitative estimate about the quality and purity of the crystal. The full utility of the Hall effect is realized through the incorporation of one other component, temperature. By varying the temperature, the activation energy of the defect responsible for the charge carriers can often be determined. Many equations have been derived (from the charge balance equation, $n+N_a^- = p+N_d^+$) to extract these important parameters, however, a simple Ahhrenius relationship is most illustrative at this juncture:[48]

$$n=N_c\exp(E_c-E_f/kT) \qquad (2.3)$$

where n is the concentration of electrons, N_c is the conduction band density of states, E_c is the energy of the conduction band edge, E_f is the Fermi energy, and T is the temperature. This equation is also used for holes by replacing n, N_c and E_c-E_f with p, N_v, and E_f-E_v. The equation is valid provided that only a small fraction (<1%) of centers are ionized and that the semiconductor is nondegenerate (E_c-3kT<E_f<E_v+3kT). Other useful relationships will be introduced later in the text, where appropriate. An examination of this equation illustrates that if one plotted the natural logarithm of the carrier concentration divided by $T^{3/2}$ versus the inverse of temperature, a determination of the position of the Fermi level is made by calculating the slope of the line. Some nuances exist, but under most conditions, this procedure will indicate the depth of the principal impurity in a given sample. Not only can the depth of the level be determined, but also the total concentrations of the principal defect and compensating impurities. However, these two concentrations require that a significant fraction of the impurities be ionized (i.e. the previous equation will be invalid, and the other more complex equations need to be used). In most semiconducting systems, only low-temperature (to 400K) Hall effect is required to determine these parameters, because the ionization energies of most defects are close to the band edges. For example, the number of impurities shown to introduce electronic levels within 100 meV of the band edges in silicon, germanium, and gallium arsenide are: eight, twenty, and seventeen, respectively.[49] However, in silicon carbide, only one impurity (nitrogen at 85 meV in 6H)[50, 51] has been positively identified as introducing an electronic level within 100 meV of the band edge. Even for a relatively shallow (only nitrogen and aluminum are shallower) dopant such as boron, a minimum of 300°C is required to produce levels of ionization necessary to determine these parameters. High temperature Hall is also required, because the electronics of the Hall effect

experiment are not sensitive enough to determine the conductivity of the high-resistivity (~$10^{18}\,\Omega\cdot$cm @ RT) samples at room temperature.

The samples used in this study were square and sized from approximately 0.5 to 1.0 cm on a side. The contact configuration employed was devised by van der Pauw in 1958.[52, 53] In this method, four contacts (M, N, O, P) are applied to the periphery of a sample. Current is passed through two contacts(MN), the voltage is measured through the other two contacts(PO), and these two quantities are input into the following equation:

$$R_{MN,OP} = \frac{V_P - V_O}{i_{MN}} \tag{2.4}$$

where V_P-V_O is the voltage drop across the points P and O, i_{MN} is the input current (between M and N), and $R_{MN,OP}$ is the calculated resistance term. With the knowledge of the term $R_{MN,OP}$, its converse $R_{OP,MN}$, and the thickness of the sample, d, the resistance of the sample, ρ, is calculated through the following relationship:

$$\exp\left(-\frac{\pi d}{\rho}R_{MN,OP}\right) + \exp\left(-\frac{\pi d}{\rho}R_{OP,MN}\right) = 1 \tag{2.5}$$

where the only unknown is the resistivity, ρ. The calculation of the resistivity can

be reduced further:

$$\rho = \frac{\pi d}{\ln 2} \frac{R_{MN,OP} + R_{NO,PM}}{2} f \tag{2.6}$$

where $R_{MN,OP}$ and $R_{NO,PM}$ are the parameters which need to be measured, and f is calculated according to the following formula:

$$\cosh\left\{\frac{(R_{MN,OP}/R_{NO,PM})-1}{(R_{MN,OP}/R_{NO,PM})+1}\frac{\ln 2}{f}\right\} = \frac{1}{2}\exp\frac{\ln 2}{f} \tag{2.7}$$

While these measurements and calculations would be sufficient on their own, their converses, $R_{PM,NO}$ and $R_{OP,MN}$, were always measured to provide a check for any anomalies in the system. At this point, the Hall coefficient, R_H, can be calculated:

$$R_H = \frac{d}{B}\left(R_{MO,NP} - R_{NP,MO}\right) \tag{2.7}$$

which is then substituted into equation 2.1 to determine the concentration of carriers.

2.2.2.2 Equipment and Operation of the Hall Effect Systems

This section will focus on the two types of Hall effect systems employed throughout the study. The first type, low temperature, was used to study shallow defects in the silicon carbide system, including: nitrogen, aluminum, and boron.

The second type, high temperature, was used in the study of all other defects, including the vanadium acceptor and donor levels. High temperature Hall effect was also used to improve the understanding of the boron impurities. Schematics of both types of systems are shown in figure 2.3.

The following Keithly equipment was used in each system: a 705 scanner, a 619 multimeter, and a 220 current source. These programmable instruments were interfaced with 486 computer systems via IEEE 488 cards. The 220 supplies the current, the voltage was measured by the 619, and the 705 scanner was used to switch between the various configurations required by the van der Pauw technique. The current was directed from the electronics to the sample by a triaxial cable running into the sample chamber, then by a coaxial cable to the sample. In order to obtain the high impedance necessitated by the high resistivity samples, a unity gain amplifier was employed in the circuit. Using this amplifier, the inner shield of the triaxial cable and the outer shield of the coaxial cable were maintained at a voltage identical to that of the core conductor. Through this, the voltage losses were minimized which allowed for reliable current measurements as low as 100 pico-Amperes.

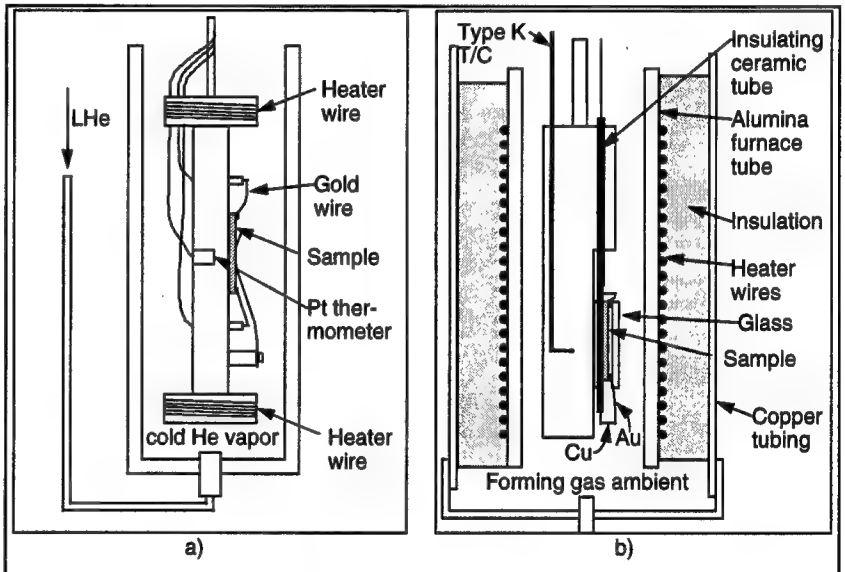

Figure 2.3-Schematics of a: a) low-temperature, and b) high temperature Hall effect systems

For the low temperature Hall effect, the computer controlled every aspect of the experiment. It allowed for setting the magnetic field, temperature, and automatically adjusted the input current to obtain the most appropriate voltage for the measurement. The temperatures used ranged from 20 to 400K. The temperature was measured using a Pt thermometer mounted inside the sample block. This range allowed for a significant ionization of nitrogen-doped samples, as well as a determination of the activation energy of samples doped with aluminum and boron.

For the high temperature Hall effect experiments, the magnetic field was set manually, and the computer took the readings necessary for the experiment. The temperature was measured with a type K thermocouple, and the samples were heated with Ni-Cr heater wire connected to a manually-operated DC power supply. The measurements were taken when the temperature stopped increasing. The current settings were performed manually to obtain voltage readings between 100 and 500 mV. The maximum temperatures in this study were 800°C. This allowed for a significant ionization of the boron levels, but was not sufficient to appreciably ionize the deepest defects.

2.2.3 Deep Level Transient Spectroscopy (DLTS)

While Hall effect is very useful in determining the depth of a given level, under normal conditions it can only be used to observe a single level in a given sample. For this reason, other tools, such as DLTS, are necessary to analyze other levels in semiconductors. These are mutually exclusive techniques, but can be used on different samples to further confirm the existence of a certain level. DLTS can also yield additional information about a defect not available through Hall effect measurements.

2.2.3.1 Principles and Theory of DLTS

In order to perform DLTS, a sample containing a depletion region is required. Such a sample can be created by reverse biasing one of two types of diodes: a p-n junction or a Schottky barrier. Due to the ease of creation and interpretation of resultant data, Schottky barriers were used in this study.

Before examining the DLTS experiment, a discussion of the capacitance measurement is in order. C-V profiling is usually performed before DLTS to determine the net carrier concentration as a function of the depth in the material. By applying a small, high frequency voltage to the sample, and measuring its respective phase shift after passing through the sample, the capacitance, C_s, of the sample can be determined. The sample capacitance can then be used to determine the width of the depletion region:[54]

$$C_S = \frac{\varepsilon_R \varepsilon_O A}{x_d} \tag{2.8}$$

where ε_R and ε_O are the relative permittivity of the material and the free space permittivity, A is the junction area, and x_d is the thickness of the depletion region. Simultaneous to the determination of the depth of the depletion region, the concentration of majority carrier centers is ascertained by analyzing the variation of the sample capacitance as a function of applied voltage(V_A):[54]

$$N_d(x_d) = \frac{-C_s^3}{q\varepsilon_R \varepsilon_O A^2}\left(\frac{dC_S}{dV_A}\right)^{-1} \tag{2.9}$$

where $N_d(x_d)$ is the concentration of donors at a distance x_d from the semiconductor-metal interface. With the information pertaining to the concentration of charge centers as a function of depth as well as reverse bias, the DLTS experiment is performed at a given reverse bias.

The process of DLTS involves creating the depletion region, injecting carriers into the region, filling electron or hole traps in the depleted region, and measuring the way those trapped carriers are ejected back into the sample.

Shown in figure 2.4 (Ref. 55) is a schematic of this process. The central part of the figure shows a typical capacitance variation as a function of time for a Schottky barrier diode. The insets a-c are used to show a schematic of the crystal at the different times along the capacitance transient. Shown in figure 2.4a is the equilibrium state of the crystal with all of the traps in the depletion region empty. Then the traps are filled with the forward bias pulse (figure 2.4b). At this point, the traps begin to empty as is shown in figure 2.4c. The rate at which the electrons leave the trap is determined by the sample temperature. The trap emission procedure is the central part of DLTS, and will be discussed further. This figure is only applicable to DLTS measurements performed on Schottky

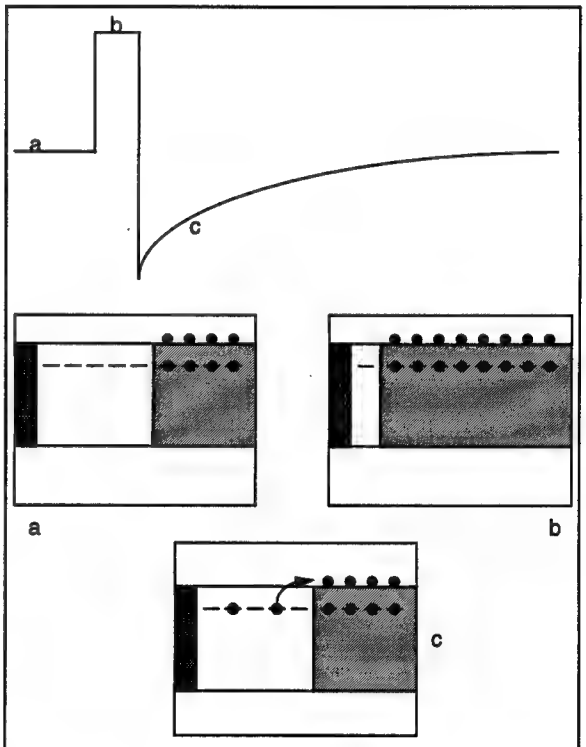

Figure 2.4-Capacitance pulse from a DLTS measurement with corresponding schematics for: a)quiescent capacitance, b) fully charged capacitance, and c) trap depopulation.[55]

barriers. If the diode were a p-n junction, both holes and electrons must be considered. On the left-hand sides of the insets in figures 2.4a-c holes should be introduced, which would contribute to the DLTS signal. The change in the capacitance would then be related to the ejection of holes from minority carrier traps in addition to the signal from electrons ejected from majority carrier traps. Although the signals can be separated, the interpretation is more facile in the case of the Schottky barrier.

As was alluded to earlier, the crux of the DLTS measurement relies on the study of the mechanism by which carriers are ejected into their respective bands to reestablish the equilibrium after the voltage pulse. The decay of the capacitance is represented by the following equation:

$$\Delta C(t) = \Delta C(t=0)\exp(-e_n t) \tag{2.10}$$

where e_n is the emission rate, and $\Delta C(t)$ is the change in capacitance (from the quiescent, i.e. $\Delta C(t=0)=C(t=0)-C(t=\infty)$) at a given time t. The emission rate is dependent upon the temperature at which the sample is held:

$$e_n = \sigma N_c v_{th} \exp\left(\frac{E_c - E_a}{kT}\right) \tag{2.11}$$

where σ is the capture cross section, N_c is the conduction band density of states, v_{th} is the thermal velocity of electrons, E_c-E_a is the depth of the level from the conduction band (in the case of electrons), k is the Boltzmann constant, and T is

the temperature. All that must be determined is the emission rate as a function of temperature.

Shown in figure 2.5 is a representation of how the capacitance transient changes as a function of temperature. If one were to model the shape of the exponential decay of the transient (figure 2.4), all of the information about the deep level could be ascertained in a single sweep of temperature. However, the more common method is to examine the transient at two times, t_1 and t_2 in the figure, and then sweeping temperature several times with a different t_1 and t_2. Shown in figure 2.5b is the difference in the capacitance plotted as a function of temperature. This difference in capacitance leads to the DLTS peak. The temperature input into equation 2.11 is the temperature at which the DLTS peak is a maximum, T_m. In order to determine the corresponding emission rate, the times t_1 and t_2 are analyzed. When the time constant of the transient decay $(e_n)^{-1}$ is equal to τ_{max},

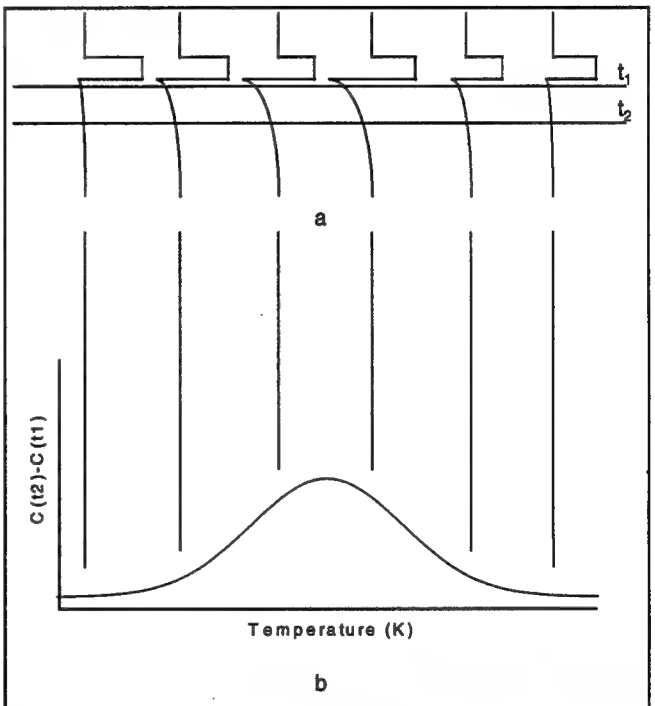

Figure 2.5-a) Capacitance transient versus temperature and)b manifestation in the DLTS signal

the DLTS maximum occurs. τ_{max} can be found in the analysis of t_1 and t_2 where:

$$\tau_{max} = \frac{(t_1 - t_2)}{\ln\left(\frac{t_1}{t_2}\right)} \qquad (2.12)$$

The emission rate and the temperature are then plotted in an Ahhrenius fashion, and the activation energy of the trap is then determined (eq. 2.11). The plot is extrapolated to infinite temperature, and the other trap descriptor, the capture cross section, is ascertained.

2.2.3.2 Equipment and Operation of DLTS

The DLTS apparatus employed in this study consisted of a Polaron 4600 unit coupled with a Boonton capacitance bridge operated in the boxcar configuration. This apparatus was connected to a Hewlett-Packard 9836 PC via a HPIB port. The Polaron S4900 cryo control unit temperature stage was capable of temperatures from 80 to 450K through the use of liquid nitrogen and resistive heating elements. In this temperature range, deep levels up to 0.8 eV (depending upon the capture cross section of the defect) were examined.

The typical reverse bias and filling pulse were -6 and +1 V, respectively. The setup called for the specification of the rate window as opposed to the individual times, t_1 and t_2. The common rate windows employed were between 1000 and 20 Hz.

2.2.4 Thermally Stimulated Current (TSC) Measurements

Although TSC was employed in only one aspect of the study, its role was essential for the confirmation of a hypothesis regarding the vanadium donor level. The samples that were examined for this measurement come from the high-temperature Hall effect study. The contacts used were ohmic, and the samples needed to be high-resistivity for reasons that will soon become apparent.

2.2.4.1 Principle of TSC Measurement

Where DLTS is used to analyze deep traps in conducting material, TSC is used to characterize the traps in high-resistivity material. The principle behind the measurement setup is to cool the high-resistivity sample, and then create a non-equilibrium configuration of carriers through the use of a external excitation source. At this point, the sample is heated at a constant rate, and a measurement is made of the current induced by the carriers on their return to the equilibrium configuration.

While this explanation may suffice for a general description of the process, a more detailed analysis is in order which can be found in various sources.[56-58]

The net carrier equation which is examined as a part of the TSC analysis is as follows:

$$\frac{dn_i}{dt} = -n_i\left(\frac{g_{i0}}{g_{i1}}\right)N_c\sigma_i v_{th}\exp\left(-\frac{E_i}{kT}\right) + n(N_i - n_i)\sigma_i v_{th} \qquad (2.13)$$

and

$$\frac{dn}{dt} = -\frac{n}{\tau_n} - \sum_i \frac{dn_i}{dt} \qquad (2.14)$$

where n_i is the concentration of electrons trapped by the ith trap, n is the concentration of free electrons, N_c ($\propto T^{1.5}$) is the conduction band density of states, τ_n ($\propto T^{\lambda}$) is the steady state lifetime of electrons in the conduction band, σ_i ($\propto T^{\alpha}$) is the electron capture cross section of the ith trap, v_{th} ($\propto T^{0.5}$) is the thermal velocity of conduction band electrons, N_i is the concentration of the ith trap, E_i is the activation energy of the ith trap relative to the conduction band minimum, μ_n ($\propto T^{\gamma}$) is the electron mobility, and g_{i0} and g_{i1} are the degeneracy factors of the ith traps when they are filled and empty, respectively. The Greek letters (α, λ, and γ) in the parenthetical expressions represent the temperature dependence of the expressions for capture cross-section, lifetime, and mobility, respectively. Additionally, the conductivity of the sample (σ_n) is related to the concentration of free electrons, n, by equation 2.2.

Typically, these differential equations, 2.13 and 2.14, are solved subject to an assumption about the retrapping rate versus the recombination rate of the free

carriers. With either case, the general form of the solution is similar to the following equation:

$$\ln\left(\frac{T_m^4}{\beta}\right) = \frac{E_i}{kT_m} + C \qquad (2.15)$$

where T_m is the temperature of the maxima of the Gaussian peak, β is the heating rate, E_i is the activation energy of the center, k is the Boltzmann constant, and C is a constant comprised of several factors which have at most a weak dependence on temperature. For the purposes of this study, only the activation energy of the defect was required. Therefore, the distillation of the constant was not required.

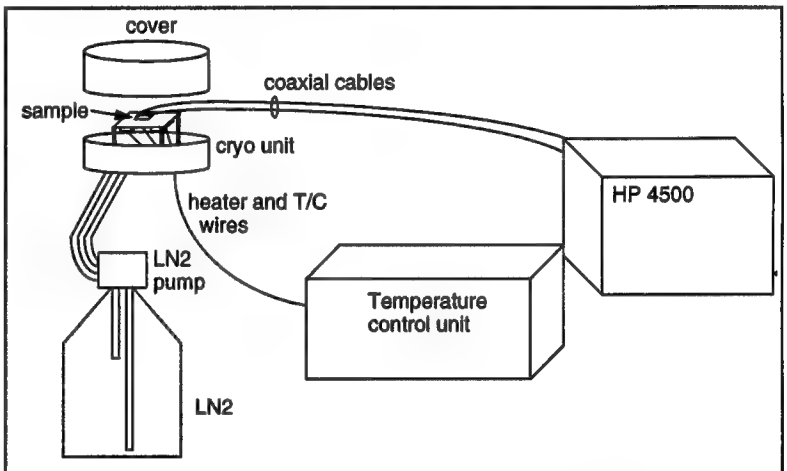

Figure 2.6-Experimental setup for TSC measurement

2.2.4.2 Operation of the TSC Measurement

Shown in figure 2.6 is the experimental apparatus employed in this study. The samples were mounted in the same Polaron S4900 cryo control unit that was the center of the DLTS investigation. The heating rate was controlled in the local mode setting of the DLTS interface. The sample leads were then connected from the cryo to the HP 4145A semiconductor parameter analyzer. The samples

were cooled to the starting temperature of 100K, and a flashlight was used to excite the carriers into non-equilibrium configurations. The 4145A was configured to bias two ohmic contacts with 2V. All external light sources were then removed from the sample, and the constant heating ramp was begun.

The heating rate was controlled by the temperature control interface. While it was not perfectly constant, the period of the variation was significantly less than the period of excitation of electrons to or from the electronic defects. For example, the FWHM of the narrowest TSC peaks was 83K, while the heating rate fluctuated within 1-2K.

The current was measured as a function of time. With knowledge of the heating rate, the time axis of the current-time plot was correlated to the sample temperature. The maximum variability in the heating rate was from 0.01 to 0.99K/s. The typical conditions ranged between 0.1 and 0.5K/s.

2.3 Absorption Measurements

The absorption measurements can be grouped into two types: diffraction grated optical and Fourier transform. The optical absorption measurements are intuitively simple. The Fourier transform studies yield much the same information as optical absorption, however, the explanation of its operation is more complicated.

2.3.1 Fourier Transform Infrared (FTIR) Spectroscopy

Fourier transform infrared spectroscopy is a powerful tool for characterizing vibrational modes as well as electronic transitions resulting from the incorporation of impurities. In this study, FTIR was used for both types of characterization. Since it can be used in the range from 10 to 55000 cm^{-1}, the utility of this experiment is apparent. Additionally, the resolution available is higher than that for optical absorption.

2.3.1.1 Principles of FTIR

The source for FTIR measurements is always white light. White light can alternatively be viewed as a series of point sources represented by a delta function at the frequencies which comprise the white light. The Fourier transforms of the delta functions are sine waves whose frequency is that of the delta function. The convolution of the sine waves is the raw spectrum observed in the FTIR experiment.

Shown in figure 2.7 is a sequence of graphics which illustrates this explanation. A series of ten equally spaced point sources are shown starting at a frequency of 1(arb. unit) and extending to 2.8 with an inter-source spacing of 0.2(figure 2.7a). A sample of three (highlighted by asterisks in figure 2.7a) Fourier transformed waveforms are shown in figure 2.7b. The final convoluted waveform is shown in figure 2.7c. If an inverse Fourier transform were performed on this function shown in figure 2.7c, the resultant graphic would be ten delta functions. If any of the initial points of light were absorbed, this would be evidenced in the resultant convoluted spectrum. Then, the final inverse Fourier transform would evince this difference as an absorption band in the absorption spectrum. The only question remaining is how the spectrum shown in figure 2.7c is generated experimentally.

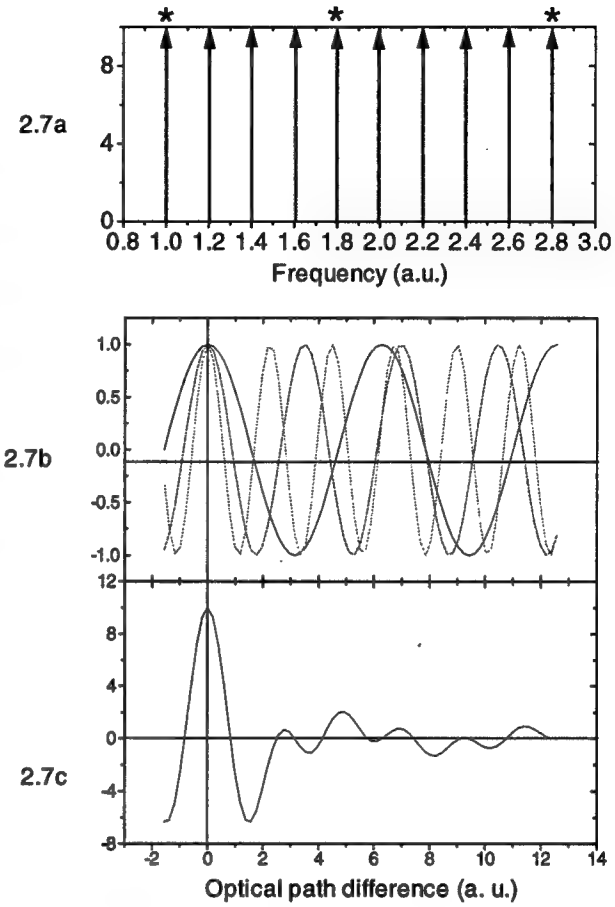

Figure2.7-a) White light broken into point sources, b) Fourier transforms of three of the individual sources, and c)convolution of the FT of all point sources.

Figure 2.8 is a typical schematic for a FTIR experimental setup, more commonly known as the Michelson interferometer.[59] This is the arrangement that is employed in the Bomem FTIR. The rays shown in the schematic represent the path of the traveling light. The equation of the electromagnetic wave at this point is: $E_0\cos(2\pi v_0 t-\phi)$, where E_0 is the amplitude of the light, v_0 is the wavelength, t is the time, and ϕ is the phase. The light then bounces off of a collimator mirror which acts to direct the rays so that they are now parallel. Then, the light hits the beamsplitter (B/S), and half (call this packet 1, $(E_0/2)\cos(2\pi v_0-\phi_2)$) of the light moves through, while the other half (call this packet 2, $(E_0/2)\cos(2\pi v_0-\phi_2-2\pi\delta/\lambda)$, where δ is the difference in the length of the paths) is reflected off of the beamsplitter. The normal to the B/S surface is oriented 45° with respect to the incident light. Packet 1 passes through the B/S, hits the fixed mirror and is reflected back to the B/S. Packet 2 is initially reflected is then directed to the moving mirror. Packet 2 is reflected off of this moving mirror and directed back to the B/S. If both the fixed and moving mirrors are at exactly the same distance from the B/S, packet 1 and 2 will recombine

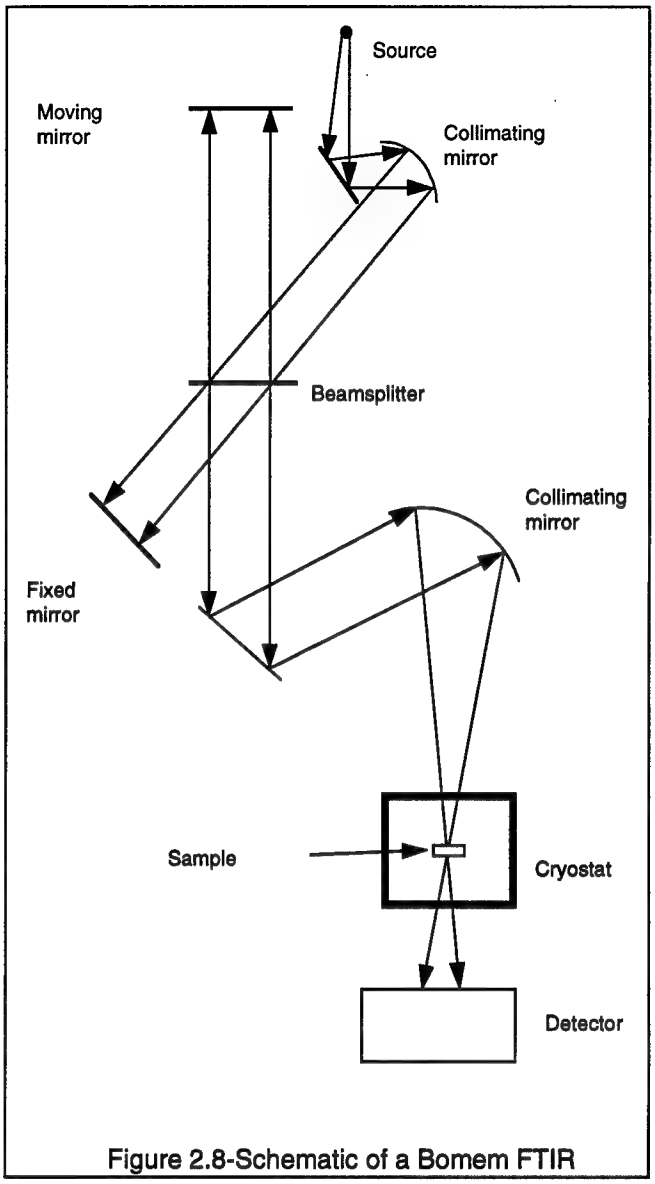

Figure 2.8-Schematic of a Bomem FTIR

constructively at the B/S and move on through the sample and to the detector. This condition is called the zero point displacement (ZPD). As the moving mirror moves away from the B/S, the packets recombine in a less constructive fashion.

Assuming that the light moves along the optical axis, or with very little deviation, destructive interference occurs when the path difference of the two packets, δ, is equal to $n\lambda/2$, where n is an odd integer. Constructive interference occurs when the path difference, d, is $m\lambda/2$, where m is an even integer. If the mirror moves with a fixed velocity, v, the difference in the path, δ, can be defined as: 2vt. The phase difference between the packets is then, $(4\pi vt)/\lambda$, or in terms of wavenumbers, σ, $4\pi\sigma vt \cos \alpha$. Assuming that the path of the rays is very nearly paraxial (i.e. α is small), the intensity of the resultant electrical signal is then:[60]

$$I(t) = \left(E_0^2 / 4\right)\cos(4\pi\sigma vt) \qquad (2.17)$$

From this, the interferogram (fig. 2.7c) is determined by integrating eq. 2.17:

$$I(I) = \int_0^\infty \left(E_0^2 / 4\right)\cos(4\pi\sigma vt)d\sigma \qquad (2.18)$$

This signal is then deconvoluted to ascertain the experimental spectrum.

When evaluating absorption experiments, two important parameters must be considered: the resolution and the signal-to-noise ratio, S/N. In a FTIR system, the resolution is increased by lengthening the path of the moving mirror. The raw spectrum of the FTIR signal is measured in finite elements along the path of the moving mirror. Therefore, if the number of elements is increased by

extending the travel of the mirror, the accuracy of the raw spectrum is increased. This then allows for a better resolution in the transformed spectrum, resulting in an increased experimental resolution.[61]

FTIR spectroscopy is carried out by coadding many scans. This coaddition is performed so that the determination of the interferogram can be more precise. Therefore, in order to increase the S/N ratio, the number of scans is increased. The increase in the S/N ratio follows from a parabolic increase in the number of sample scans, NSS (i.e. $S/N \propto NSS^{1/2}$).[61]

2.3.1.2 Operation of FTIR

The FTIR spectra shown in this document were taken on a Bomem DA3 spectrometer. The maximum resolution available in this unit is 0.003 cm^{-1}. This resolution is available because the moving mirror is capable of traveling up to 1.25m during the operation. This mirror travel is contrasted to the Bruker instrument employed during the early stages of the study; the Bruker mirror is capable of moving 10cm. The samples were mounted on a copper aperture with a dab of silver impregnated grease. This mounting was placed into a Janis continuous flow cryostat capable of liquid helium temperatures. The Janis cryostat used KRS-5 optical windows for the best transmission of the middle infrared spectrum (from approx. 400 to 6000 cm^{-1}). A Globar was used as the source for all of the experiments using this tool. For the measurements in the middle infrared, a Si:B photodiode was employed, while a InSb diode was used for the studies in the 5000 cm^{-1} region.

2.3.2 Diffraction Grated Optical Spectroscopy

While this form of optical spectroscopy is relatively simple, the information derived can be of great use in analyzing the samples. Much of the characterization of electrical defects in this study was assisted by diffraction grated optical absorption (hereinafter referred to as optical absorption or optical spectroscopy) experiments. The principal detractor to this method is the limited available resolution. This limitation is a result of the difficulty in constructing the device used to disperse light.

2.3.2.1 Theory of Optical Spectroscopy

During the advent of spectroscopy, the first tools employed much the same mechanism as that shown in figure 2.9. A white light source is shone upon a diffraction grating. This action separates the light into the spectrum which originally constituted the white light. An analysis of the diffraction grating follows the general description of the experiment. Now, the separated light is directed through an aperture which is used to select the desired wavelength of

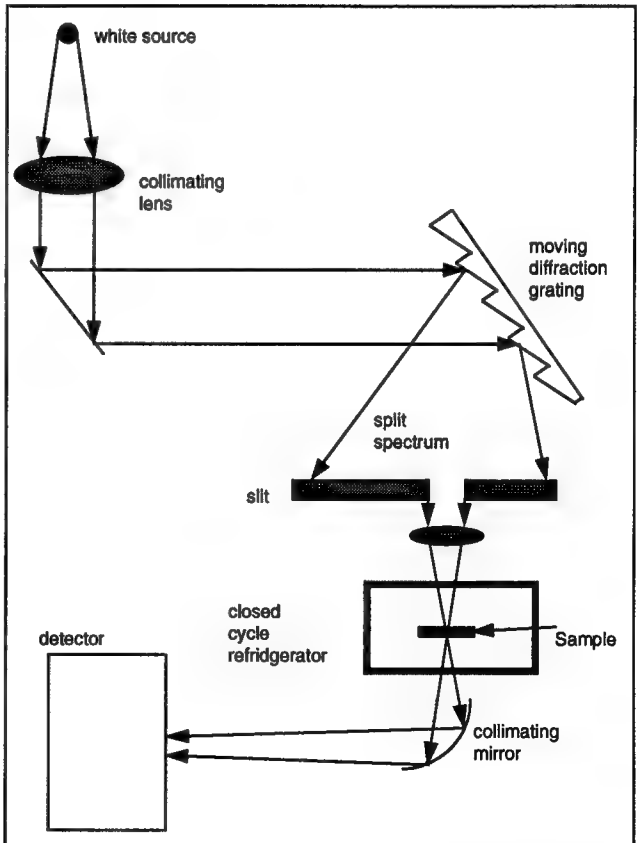

Figure 2.9-Schematic of a typical optical absorption experiment

light. This specific light is then passed through the sample, and onto a detector. As in FTIR, the incident photons produce an electrical signal which the computer reads as a function of the wavelength of light.

As was previously mentioned, the dispersor of light in this experiment is a diffraction grating. Shown in figure 2.10 is the edge of a typical grating.[59] It is created by cutting the groves into an aluminum coating that has been applied to a piece of optically flat glass. Typical spacing constants, d, are between 0.3 and 5 μm.

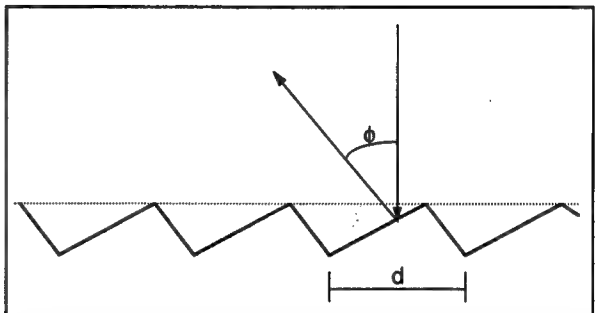

Figure 2.10-Diffraction grating employed for separating light into its respective components[59]

If the incident light is perpendicular to the plane of the diffraction grating, the angle of construction, ϕ, for light with a wavelength λ is found using the following equation:[62]

$$n\lambda = d \sin \phi \qquad (2.19)$$

where d is the distance between rulings, and n is the order of the diffraction. As the grating is rotated, the wavelength of light passing though the aperture is changed.

In this experiment, there are two classifications for resolution. The first of such classifications is the maximum experimental resolution, which is defined in part by the distance between the rulings on the grating. A functional relationship is as

follows:[59]

$$\mathcal{R} \propto nN \tag{2.19}$$

where $\mathcal{R}$ is the resolving power of the instrument, n is the number of the nth principal maximum, and N is the number of rulings in the grating. Therefore, as the number of rulings on a grating is increased, so to does the resolving power of the instrument increase.

Alternatively, the resolution of a given experiment is defined by the width of the slit through which the diffracted light is passed. In order to obtain higher resolution, the width of the slit is decreased. However, as the slit width is decreased, the amount of light passing through the slit is also limited. With the subsequent losses in the sample and cryostat, the smaller amount of light hitting the detector reduces the sensitivity of the experiment. From this, considerations need to be made with respect to a proper balance between experimental resolution and detection sensitivity.

From this experiment, the detector, source, and other noise in the system should be relatively constant. Therefore, in order to increase the S/N ratio, the time constant of the instrument needs to be increased. The time constant defines the length of time the instrument measures the absorption signal at any particular wavelength. This action increases the integration time of the detector, and thereby the detector signal, while not affecting the noise.

2.3.2.2 Operation of Optical Absorption Experiments

The optical spectrometer employed during these experiments was the Cary 05e. The photon energy range of this instrument varies from 0.5 to 4.2 eV. The widest band gap (4H SiC) examined was 3.4 eV, so that the Cary was sufficient to examine the entire spectrum of silicon carbide. Additionally, using the indium antimonide detector, and the globar source, the Bomem FTIR ranged up to 0.775 eV, so that these instruments complemented one another. The cooling of the sample was performed by a helium closed cycle refrigerator, capable of temperatures as low as 13K. The samples were mounted in much the same way as in the FTIR experiments, via silver impregnated grease on a copper aperture. In most of the experiments, a secondary illumination source was employed to modify the charge state of some of the impurities in the SiC matrix. This source was in the form of a 400 W halogen bulb, whose power was continuously variable from 1 to 100%. The maximum resolution of the instrument was 1.7 meV in the visible and 0.17 meV in the near infrared.

3. The Vanadium Donor

One attractive feature of silicon carbide is its ability to form high resistivity substrates. However, as was indicated earlier, much of the material is residually p- or n-type. Since the process of growing the boules cannot be made pure, other suitable means of achieving high-resistivity material must be developed. In other semiconductor systems, this is accomplished using intentional doping with elements whose electronic levels reside near the center of the band gap, as in the case of Cr-[63, 64] doped GaAs. In the first thirty years of silicon carbide development, no such element was known. Then, in 1992, a group in Germany[46] discovered that vanadium produced a deep donor level near the center of the band gap. This discovery of the vanadium donor level has led to the development of high-resistivity SiC boules grown by physical vapor transport utilizing vanadium doping.[39]

3.1 Prior Research

Prior to 1996, the research into the nature of the SiC:V can be broken down into two thrusts based upon the type of data extracted: structural and electronic. The first tool used in the discovery of vanadium in SiC was electron spin resonance (ESR), which coupled with absorption experiments, evaluated the structure of the vanadium impurity. However, the specific utility of vanadium as a deep level was not realized until another technique, photo-ESR, was employed. Photo-ESR allowed for the determination of the depth of the resultant donor level within the SiC band gap.

3.1.1 ESR/Absorption

The first report of the substitutional incorporation of vanadium into silicon carbide was published in 1990. Schneider et. al.[65] reported on the ESR and FTIR spectrum of vanadium. They determined that their ESR data possessed peaks related to the existence of vanadium on a silicon lattice site in the negative charge state (i.e. V_{Si}^{3+}). The data from FTIR experiments showed a spectrum of several sharp absorption lines in the region from 0.89 to 0.95 eV (figure 3.1). The absorption bands were interpreted as an intracenter transition of vanadium from the ^2E to the $^2T_2$ multiplet. These are doublet states, therefore this transition could only arise from vanadium in its neutral $3d^1$ configuration, or V_{Si}^{4+}. Since these bands disappear in heavily n-type samples, Schneider et. al. hypothesized that vanadium produces a deep acceptor level, $V_{Si}^{4+} + e^- \rightarrow V_{Si}^{3+}$, within the SiC band gap.

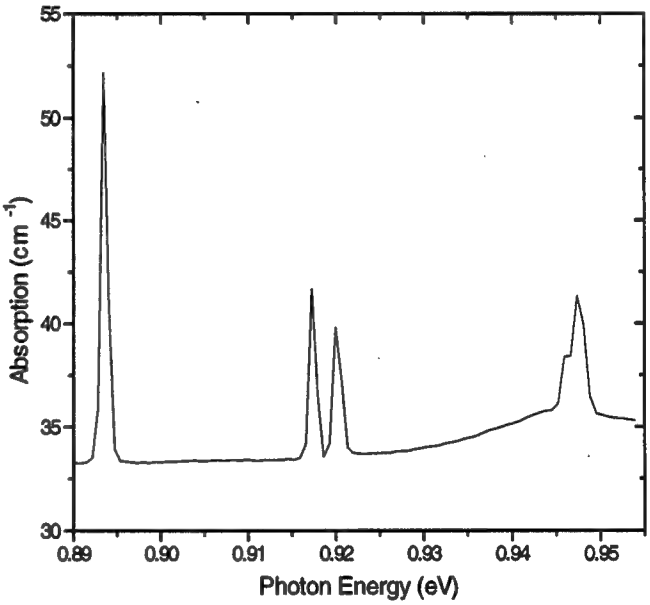

Figure 3.1-Near infrared absorption spectra from a vanadium doped sample.

Additionally, the ESR signal of vanadium in its $3d^1$ charge state was absent in p-type samples, which indicated that another deep level (a donor), $V_{Si}^{4+} \rightarrow V_{Si}^{5+} + e^-$, must also exist. From this initial work, the picture of the

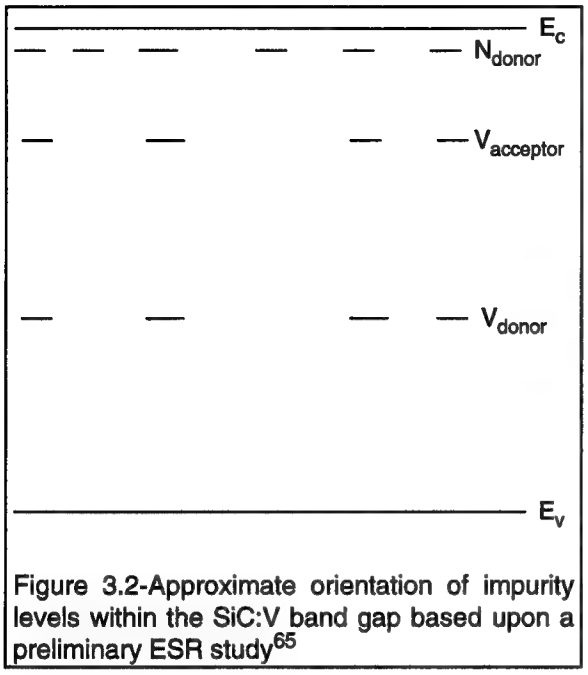

Figure 3.2-Approximate orientation of impurity levels within the SiC:V band gap based upon a preliminary ESR study[65]

electronic structure of vanadium in silicon carbide was thought to resemble that shown in figure 3.2. However, no experimental evidence existed relating to the depth of the respective levels.

The analysis of Schneider et. al. regarding the nature of the $3d^1$ absorption spectrum was based primarily upon conjecture due to the ubiquitous nature of vanadium. A confirmation of the relationship of the spectra to vanadium was made in 1993.[66] During that study, magnetic circular dichroism of the absorption (MCDA)-detected ESR was used to examine the nature of the absorption bands. The authors found that each possessed the requisite octet arising from the 7/2 nuclear spin of vanadium[67].

Other studies[68, 69] have been conducted which examine the selection rules associated with the intracenter transition in greater detail. These studies have rigorously specified the transitions and have modeled the intensities of the resultant bands. However, the majority of important work regarding the nature of vanadium in SiC is contained within the previous references of this section.

ESR is insufficient to determine the ionization energy of the resultant electronic levels. However, based upon other semiconducting systems, the vanadium donor level was thought to be deep, since it was attributed to a transition metal. Transition metal dopants commonly produce deep levels in semiconducting

systems.[70] In order to determine the ionization energy of the vanadium donor level, other techniques were employed.

3.1.2 Photo-ESR

The direct means by which researchers discovered vanadium to be responsible for a donor level was through the use of photo-ESR.[46, 71] Not only did they discover that vanadium possessed such a level, but also ascertained its position at 1.6 eV above the valence band edge. Figure 3.3 is a graph from their study. Shown in this figure is the ESR signal of the neutral vanadium, V_{Si}^{4+}, versus the photon energy of an external illumination source for a p-type sample. At 1.6 eV, the ESR signal starts to rise indicating that vanadium becomes populated with electrons from its initial $3d^0$ configuration, V_{Si}^{5+}, which is devoid of electrons. This rise is important for two reasons. First, it proves that there is a level in the band gap where vanadium transitions between the positive and neutral charge states (i.e. the donor level). Second, it establishes the position of the donor level near the center of the band gap. From these results, a study was undertaken to determine the viability of intentionally

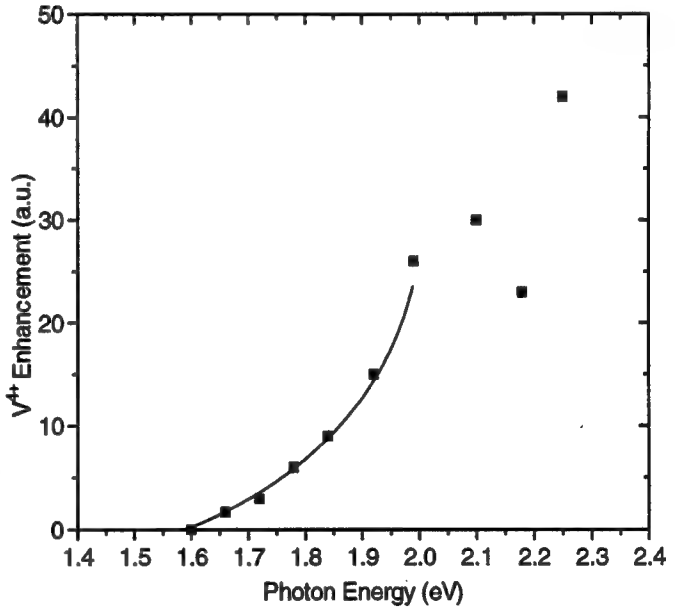

Figure 3.3-Photoenhancement of the ESR of V_{Si}^{4+} ($3d^1$) in weakly p-type 6H-SiC.[46]

incorporating vanadium to obtain high-resistivity material. We conducted an examination of the undoped material was conducted in order to determine whether it was suitable for eventual vanadium doping.

3.2 Examination of Undoped Material

This aspect of our research can be broken into two components, optical and electrical characterization. These undoped samples were grown using physical vapor transport at Northrop-Grumman (formerly Westinghouse). The optical characterization consisted of evaluating the characteristics of the near infrared and visible spectrum to determine whether any features were common to the undoped boules. The electrical characterization was employed to compare impurities in these boules to other known contaminants. Both types of characterization were employed toward the common goal of understanding the undoped boules by discerning the chemical and electrical nature of the principal impurity.

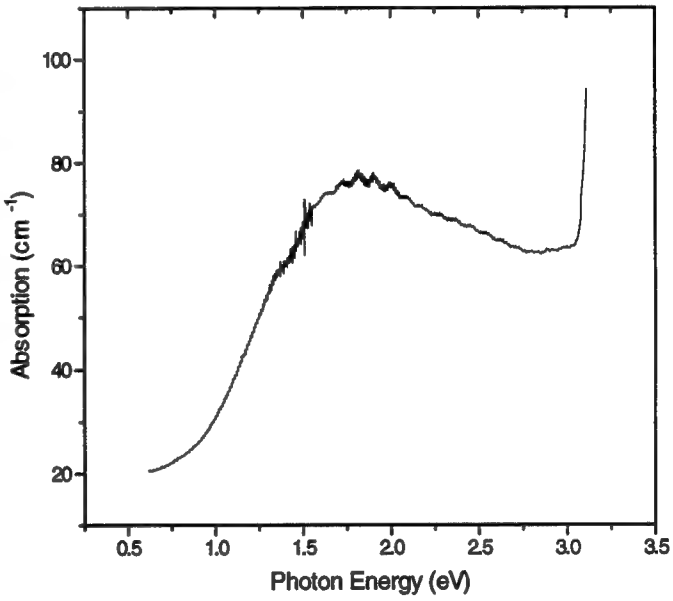

Figure 3.4-Low temperature (13K) absorption spectrum of a 6H-SiC sample contaminated with boron

3.2.1 Optical Characterization of Undoped Samples

The primary tool employed at this point was the Cary 5e spectrophotometer. In undoped samples, a wide featureless absorption band (fig 3.4) was noticed with a threshold at 0.70 eV, a maximum at 1.75 eV, which extended to the band edge. A band similar to this was observed in intentionally boron-doped 6H-SiC and interpreted as due to the photoionization of electrons from the valence band to empty boron acceptor levels.[72] However, due to the lack of specificity in figures, another element could cause the band observed in our undoped samples. Therefore, a study of the temperature dependence of the band was undertaken. The results of this study are shown in figure 3.5. As the temperature is increased, the threshold shifts toward lower energies.

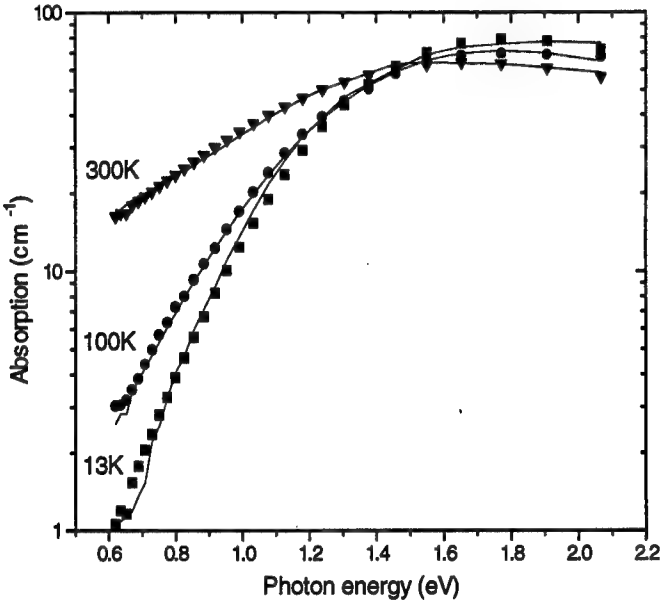

Figure 3.5-Photoionization band (lines) and their least squares fit (symbols) using formula 3.1 at three temperatures

The absorption spectra were collected at fourteen different temperatures so that the behavior of the band could be modeled and an activation energy of the

defect extracted. The equation used to model the behavior was adapted from:[73]

$$\sigma(E) = A\int_{L}^{\infty} \exp\left(-B^2\right)\frac{\left(E+\Gamma B-E_{opt}\right)^{\frac{1}{2}}}{E^3}\left(1+\Gamma\frac{B}{E}\right)dB \qquad (3.1)$$

where

$$B^2 = \frac{k_0(Q-Q_0)^2}{h\omega}\tanh\left(\frac{h\omega_0}{2kT}\right) \qquad (3.2)$$

E_{opt} is the energy associated with the optical ionization of the center (i.e. without a lattice relaxation), E is the energy of the incident light, $\sigma(E)$ is the absorption cross-section, A is a constant, and Γ is the broadening parameter which is defined below. During the fitting process, A, Γ, and E_{opt} were modified according to a least squares method to obtain the best correlation with the experimental data. Both A and Γ were changed for each temperature, while E_{opt} was assumed to be a constant (at 1.48 eV, based upon the fit) throughout the temperature regime. The lines in figure 3.5 represent experimental spectra, and the symbols represent the fit to that data using formula 3.1. In order to determine the quality of the fit, the parameters A and Γ were altered in such a way as to find the greatest deviation in Γ which resulted in a 10% increase in the sum of the squares. For the spectra taken at low temperature, Γ could be changed by up to 1% to bring about this 10% increase, while for higher temperatures Γ could only be modified by 0.3% before the sum was increased by 10%. Since such small alterations in these parameters resulted in much larger changes, the fits were deemed as representative of the processes occurring in the samples.

As was previously mentioned, the broadening parameter, Γ, was determined as a function of temperature. This dependence was further modeled by the following relationship:[73]

$$\Gamma = \frac{E_{ph,exc}}{E_{ph,0}} \sqrt{2(E_{opt} - E_{th}) E_{ph,0} \coth\left(\frac{E_{ph,0}}{2kT}\right)} \qquad (3.3)$$

where T is the temperature at which the absorption measurement was performed, E_{th} is the ionization (thermal) energy of the transition, $E_{ph,0}$ is the energy of the phonon associated with the ground state of the defect, and $E_{ph,exc}$ is the energy of the phonon associated with the ionized (excited) state of the center. E_{opt} was once again assumed constant and equal to the value used in fitting the spectral dependence of absorption (1.48 eV). The three free fitting parameters were: two phonon energies and ionization energy. Among these parameters, $h\omega_0$ is uniquely determined by the fitting procedure and is equal to 32 meV which is very close to the value for the lowest 6H-SiC LA lattice phonon mode.[74] As for the value $h\omega_{exc}$, boron is known to undergo a Jahn-Teller displacement[75] which frequently results in a softening of the phonon modes. Based on this fact, one expects that the energy of the phonon associated with the ionized state of boron should be less than that of neutral boron. In considering this, the best fit to eq. 3.3 occurs when the thermal ionization energy of the defect is in the 0.3 to 0.4 eV range. From the proximity of this value to that of boron as determined from Hall effect measurements[76], we can conclude that the absorption band is caused by the photo-ionization of electrons from the valence band to the neutral boron acceptor level.

3.2.2 Hall Effect Measurements on Undoped Samples

Room temperature Hall effect measurements on undoped 6H-SiC wafers frequently showed p-type conductivity with carrier concentrations in the $5x10^{14}$-$1x10^{16}$ cm^{-3} range and mobilities between 10 and 40 cm^2/Vs. Corresponding resistivities ranged from 60 to 3000 Ωcm. This work focused on crystals with higher than average acceptor concentrations, and the numbers above represent the upper limits of the contamination range.

Figure 3.6 is plot of the hole concentration versus inverse temperature for an undoped sample possessing resistivity in the lower part of the previously stated range. The curve in this plot is indicative of the ionization of a significant percentage of the dopant responsible for the carriers. In order to precisely determine the activation energy as well as concentrations of the principal dopant and compensating species, a fit to the data was made using the following relationship for a single level, partially

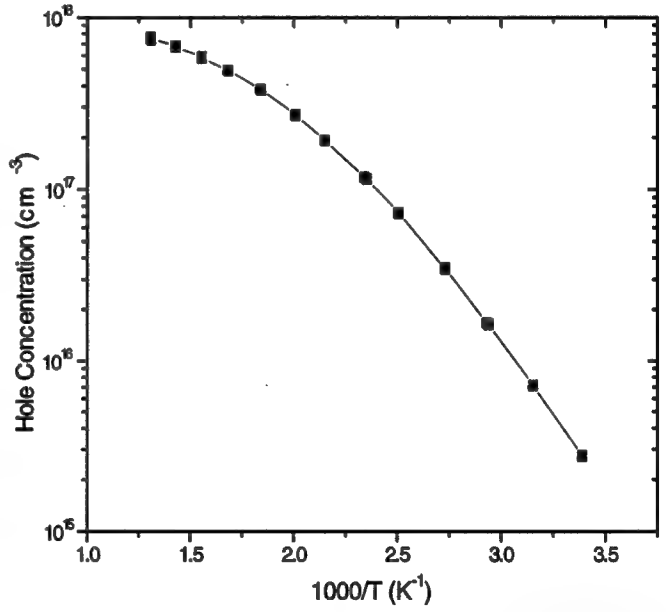

Figure 3.6-Hole concentration versus inverse temperature for an undoped 6H-SiC sample grown by PVT (line represents fit to eq. 3.4)

compensated defect:[77]

$$p_0 = \frac{2(N_A - N_D)}{\left[1+(N_D/\beta N_V)\exp(\varepsilon_A)\right]+\sqrt{\left\{\left[1+(N_D/\beta N_V)\exp(\varepsilon_A)\right]^2+(4/\beta N_V)(N_A-N_D)\exp(\varepsilon_A)\right\}}}$$

(3.4)

with $N_V = 2\left(2\pi m_h^* kT/h^2\right)^{3/2}$ and $\varepsilon_A = (E_A - E_V)/kT$

where the adjustable parameters were: the acceptor concentration, N_A, the donor concentration, N_D, and the ionization energy of the defect, E_A-E_V. For the impurity level spin degeneracy, β, a constant of 6 gave the best fit to the data, and the value 1^*m_0 was used for the effective mass of holes in the valence band.[78] For the sample whose Hall effect is shown in figure 3.6, the parameters extracted from the non-linear least squares fit were: activation energy - 0.321(±0.003) eV, acceptor concentration - 1.0(±0.01)x10^{18} cm^{-3}, and compensating donor concentration - 1.5(±0.15)x10^{17} cm^{-3}. The values in parentheses represent the deviations which result in a 10% increase in the sum of the squares to which the equation was fit. Altering either the acceptor concentration or ionization energy will greatly affect the quality of the fit. This indicates that these parameters are appropriate for this sample, and therefore the values discerned are reliable.

The activation energy extracted from the fitting procedure is in good agreement with the values obtained on 6H-SiC samples intentionally doped with boron.[76, 78] Spark source mass spectroscopy (SSMS) was also employed for determining

the concentrations of impurities in these samples. The concentration of boron (via SSMS) was found to be within a factor of two of the principal acceptor impurity observed using the Hall effect. Based on this SSMS, Hall effect, and optical absorption data, the dominant, acceptor-type impurity in the PVT-grown SiC boules was identified as boron.

As discussed above, fitting of high temperature Hall effect measurements allowed for the determination of the total concentration of uncompensated, substitutional boron acceptors (N_A-N_D). In the samples examined, this concentration ranged from $1x10^{17}$ to $5x10^{18}$ cm^{-3}, while that of the compensating species tended to lie in the range from $1x10^{15}$ to $2x10^{18}$ cm^{-3}. The likely sources for this contamination is the charge material and the graphite susceptor used in all growths of PVT SiC.

3.2.3 Correlation Between Hall Effect and Optical Measurements

By taking the concentration of boron from the Hall effect measurements, and correlating them to the intensities of the photoionization band absorption, an efficient means of determining the net concentration of boron acceptors is apparent. This correlation is shown in figure 3.7, where the abscissa is the

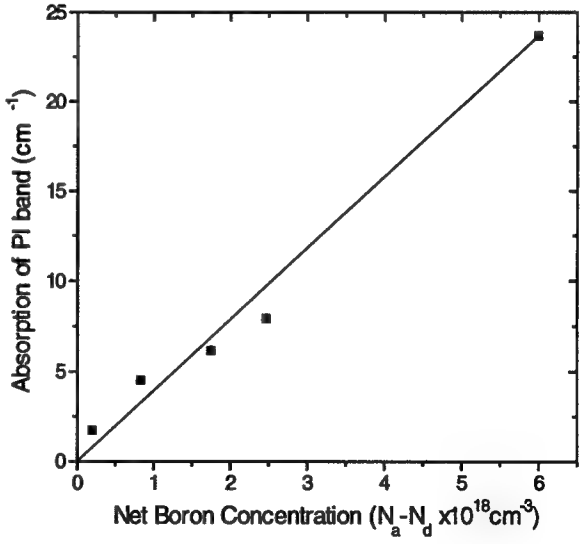

Figure 3.7-Correlation between the uncompensated boron concentration from Hall effect and the intensity of the photoionization band at 1.75 eV.

net concentration of boron impurities as determined by high temperature Hall effect measurements. The ordinate represents the intensity of the ionization band at 13K, which is determined by subtracting the background absorption at 0.55 eV from the maximum intensity at 1.75 eV. This correlation provides a secondary confirmation of the nature of the photoionization band. Additionally, this correlation can be used to obtain an approximation of the net boron concentration of a sample using optical spectroscopy. This method is easier than using Hall effect, because the difficulty in applying contacts is avoided.

3.3 Absorption Spectra of Vanadium Doped Samples

Once the study of undoped samples was completed, an examination of samples doped with vanadium was undertaken. Shown in figure 3.1 is the near infrared spectra of a vanadium doped sample. Clearly evident are the absorption bands attributed to the excitation of vanadium's $3d^1$ electron from the ^2E to the $^2T_2$ multiplet. Since the absorption experiments were made with a weak monochromatic probing light, the electron occupancy of traps is unaffected. From these two facts that: a) vanadium is present in its $3d^1$ charge state and b) the sample is in equilibrium, the Fermi level must be located between the vanadium donor (+/0) and acceptor (0/-) levels. For the highest resistivity SiC, the Fermi level should be pinned to the vanadium donor level, since this configuration produces a level nearer to the mid gap. Since the undoped samples are known to contain boron, the likely compensation process involved in creating material with the Fermi level at the donor level becomes apparent. If the vanadium concentration is higher than that of uncompensated boron, the electrons from the vanadium donor will completely fill the boron acceptors. The

excess electrons will remain on the vanadium atom pinning the Fermi level to its level near the middle of the band gap.

An examination of this compensation model was conducted using the following procedure coupled with the following two sections. The first step was to examine the effect of broad band illumination on the population of vanadium centers. This effect is shown in figure 3.8. Contained within the figure are two experimental absorption spectra taken at 13K. The dashed line represents the spectrum taken before illumination with a trans-band-gap halogen light source, while the solid spectrum was taken after 10 minutes of illumination. The number and relative intensities of the bands remained the same, but the intensities increased by 70% after illumination. This increase is due to the greater concentration of vanadium impurities in the $3d^1$ configuration. This shows that the vanadium donor is only partly occupied at thermal equilibrium. At this point, an exact determination of the compensation ratio is not possible, since the percentage of centers populated after illumination is unknown. Therefore, only an upper limit (0.65) for this ratio is available. However, these results demonstrate that there is a very

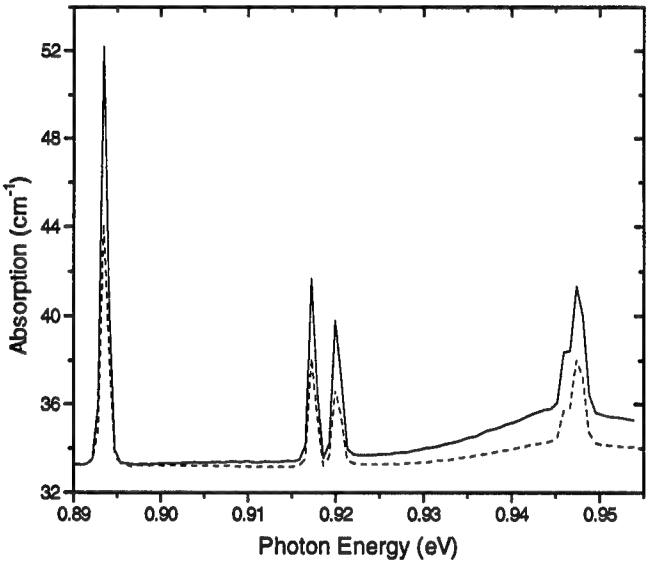

Figure 3.8-Effect of broad band illumination on the intensity of the vanadium crystal field absorption; dashed line-before illumination, solid line-after illumination

good possibility that the Fermi level is pinned to the vanadium donor level. The only other possibility is that it is pinned to the vanadium acceptor level.

Before continuing, a discussion of the rationale behind the exclusion of all other possible Fermi level positions is in order. For an understanding of the following argument, refer to figure 3.2. If the Fermi level were beneath the donor level, there would be no $3d^1$ absorption in the pre-illumination (dashed spectrum) sample, since all of the vanadium should be in the $3d^0$ configuration. If the Fermi level were in between the donor and acceptor levels, all of the vanadium in the sample should be in its $3d^1$ configuration, and there should be no increase in the post-illumination (solid spectrum) sample. Finally, If the Fermi level were above the acceptor level, all of the vanadium should be in its $3d^2$ configuration, and the pre-illumination sample spectrum would not contain the $3d^1$ absorption signal. From these arguments, the only means by which the sample illumination could increase is if the Fermi level were pinned to either of the vanadium deep levels.

To confirm that the Fermi level was pinned to the donor and not the acceptor level, high temperature Hall effect was carried out on the sample whose absorption spectra is shown in figure 3.8. The test to determine the position of the Fermi level in this sample is through the correlation of the Hall effect activation energy to that determined by the previous photo-ESR work.[46]

3.4 High Temperature Hall Effect

High temperature Hall effect measurements were performed on the sample whose absorption is shown in figure 3.8. The mobilities ranged from 140 (at 150°C) to 40 cm^2/Vs (at 470°C). The carrier concentration dependence on temperature is shown in figure 3.9. While the type of carriers could not be determined, the relatively high mobilities suggest that they are electrons. The squares represent the experimental data, while the solid line was fitted using a simple Arrhenius relationship (eq. 2.3) with the ionization energy as a fitting parameter. The least squares fitting method produced a value for the vanadium donor ionization energy of 1.35 eV (from the conduction band). Due to the difficulties associated with obtaining Ohmic contacts, only one sample was examined.

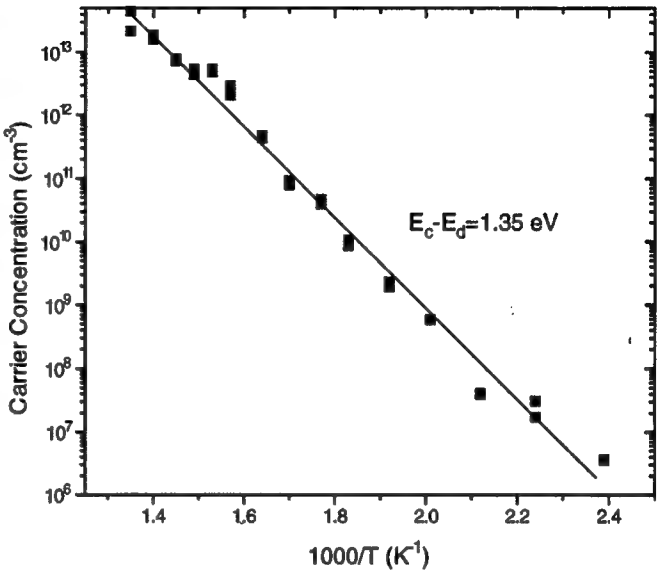

Figure 3.9-Carrier concentration in a SiC:V sample versus inverse temperature

As was previously mentioned, photo-ESR measurements have shown that the donor level is located 1.6 eV above the valence band (at 5K). While the techniques (photo-ESR & high temperature Hall effect) cannot be compared directly, due to the different temperatures and processes, E_v+1.6 eV and

E_c-1.35 eV would represent almost the same energy level, since $1.6+1.35 \sim E_{g\text{-}6H\text{-}SiC}=E_c-E_v$. The proximity of these values to one another is sufficient to indicate that they are one in the same.

3.5 Model of the Donor Compensation Process

With all of the information pertaining to the positions of levels, Hall effect, and absorption data in the previous sections, a simple schematic model can now be presented. Additionally, a confirmation of the chemical nature compensating species, which is the basis for these models, will be presented.

3.5.1 Schematic of Energy Levels

Shown in figure 3.10a-e are the processes involved in the previous experiments. The solid circles represent filled traps(electrons) and the blank circles represent unfilled traps(holes). The equilibrium configuration of electronic levels in an undoped sample is shown in figure 3.10a. One boron level is already filled due to the presence of a donor level in the upper half of the band gap. Once vanadium is added with its extra electron (figure 3.10b), the electron will drop into the empty boron orbitals. If the concentration of vanadium is higher than that of uncompensated boron (as is shown here), then all of the boron orbitals will be filled leaving extra electrons on the vanadium orbitals (figure 3.10c) pinning the Fermi level. Shown in figure 3.10d is the effect of the broad band illumination, where all of the levels are emptied into the conduction band. Once the illumination is turned off, the electrons fall into empty levels. Depending upon the relative capture cross sections, they will fall preferentially into either the

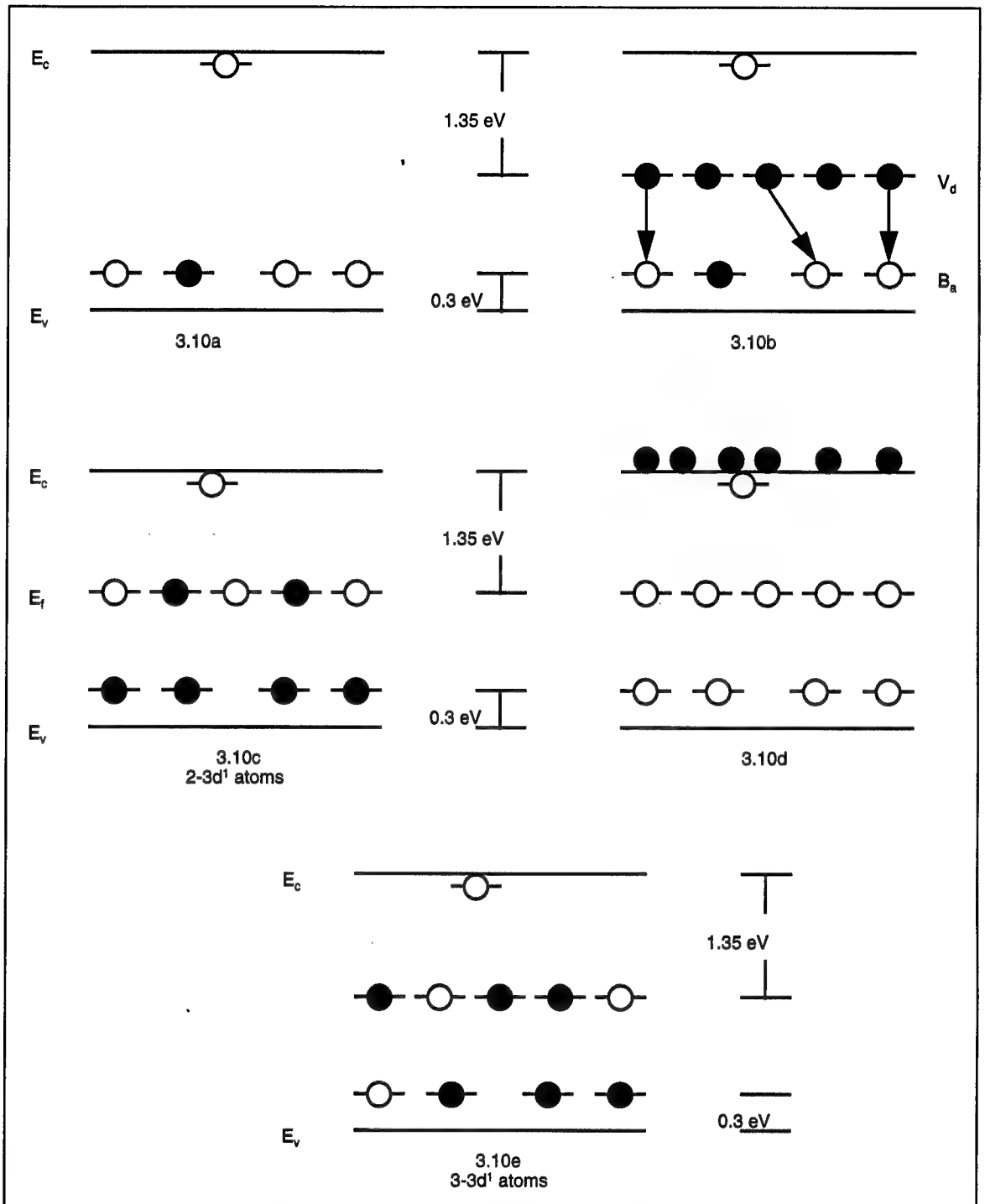

Figure 3.10-a)Equilibrium SiC band structure with only boron impurities, b)same sample with vanadium atoms added, but during quasi-equilibrium, c) equilibrium band structure with boron and vanadium, d) excitation of carriers to bands with white light irradiation, and e) resultant electronic structure with a preferential distribution of carriers towards the vanadium impurities, with an increased $3d^1$ concentration.

boron, vanadium, or other undetermined levels.

In figure 3.10e, the electrons preferentially fall into the vanadium level, which correlates with the observed measurements shown in figure 3.8. This sequence of figures represents the only explanation for the observations of the absorption/illumination and the Hall effect experiments. The only question which persists at this juncture concerns the nature of the compensating species. While boron was present in the undoped samples, the addition of vanadium may have introduced another acceptor beneath the vanadium donor level. In order to ascertain whether or not boron is in fact the acceptor level, thermally stimulated current (TSC) measurements were performed.

3.5.2 Confirmation of Boron via TSC Measurements

Shown in figure 3.11 is the experimental spectra derived from the TSC measurement of a SiC:V sample. Clearly evident are single Gaussian peaks centered about 300K. The different peaks result from altering the heating rate from 0.1 to 0.4 K/s in the order delineated by the

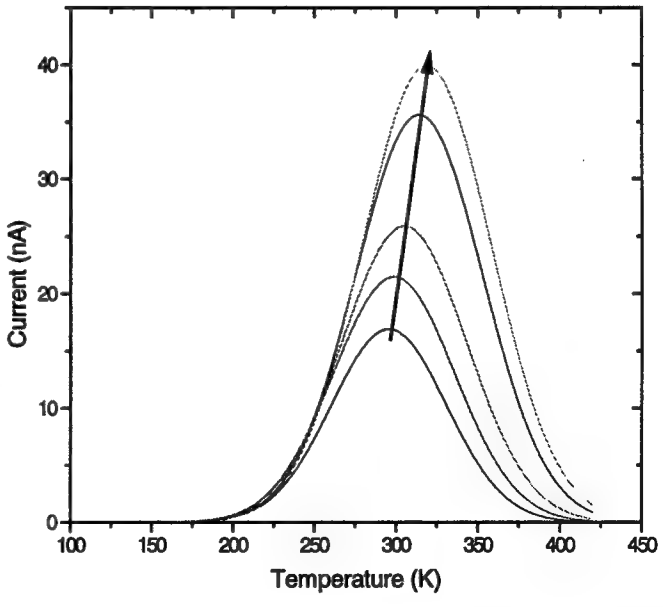

Figure 3.11-Thermally stimulated current spectra of an insulating SiC:V sample. The spectra were obtained at heating rates from 0.1 to 0.4 K/s in the order shown by the overlaid arrow

overlaid arrow. From this data, a fit was made to equation 2.17 which relates the heating rate to the activation energy in TSC. The power of T_m in the logarithm can assume values from 3 to 4.5 depending upon several factors which cannot be determined without more experimentation.

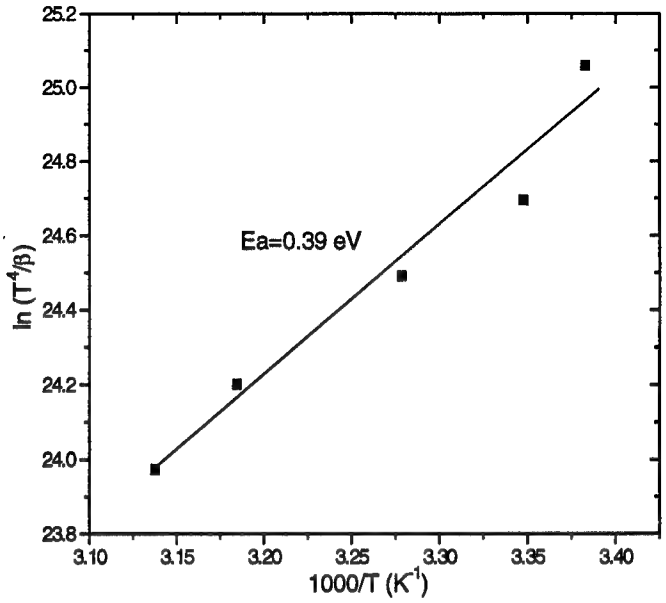

Figure 3.12-Plot of T^4/β versus reciprocal temperature which is used to determine the activation energy of the previous TSC spectra

However, when considering the total range (from 3 to 4.5), the activation energy does not change by more than 0.02 eV. The results of the fit are shown in figure 3.12. On the ordinate $\ln(T^4/\beta)$ is plotted versus 1000/T on the abscissa. From this plot, an activation energy for the center responsible for the TSC peak was determined. This value, of 0.39 eV, is very close to that of boron determined using Hall effect measurements. Thus, the principal compensating center in the vanadium doped samples is boron.

4. The Vanadium Acceptor

In order to fully exploit the advantages of the vanadium donor level, the other electronic levels imparted by vanadium into the crystal must be evaluated. These other levels may become a factor in the electronic character of SiC wafers, if sufficient care is not taken to avoid their introduction. The first level to be examined is the vanadium acceptor. Although complexes with other omnipresent impurities may be present (as is hypothesized in the next chapter), the isolated vanadium acceptor level is of prime importance. Its existence was verified in the very first examination of vanadium in SiC by ESR[65] even before the direct observation of a donor level. By definition, the number of acceptor states introduced into the band gap is identical to the number of donor states, since they result from the same impurity, substitutional vanadium. If these levels are close to one another, then this inquiry is moot, as the bulk electronic properties of the crystal will be similar in either instance.

4.1 Prior Research

As was previously mentioned, the very first examination of vanadium in SiC yielded the existence of the acceptor level at a position above the donor level.[65] During the years following the initial discovery, nothing more was mentioned regarding this level. Then, in 1995, Kunzer et. al.[79] proposed that the acceptor level was at most 0.62 eV from the conduction band. This hypothesis was based upon their statement that an absorption band in the near infrared (at 5000cm^{-1}) could be attributed to the vanadium acceptor $^3A_2 \rightarrow {}^3T_2$ intracenter transition. They concluded that since this band was observable in absorption and not in PL,

the final state ($^3T_2$) must be degenerate with the conduction band edge. Therefore, the distance from the conduction band edge of the acceptor level cannot be more than the energy of the transition, or 5000 cm^{-1} (0.62 eV). In the following chapter, the fact that no relationship exists between this absorption band and the vanadium acceptor level will be proven.

Yet in 1995, we published results which suggested that the acceptor level was 250 meV from the conduction band edge.[80] In this paper, we based this estimate upon the analysis of the vanadium bound exciton; which, in turn, was premised upon an analysis of the titanium bound exciton. This estimate was found to be too low.

4.2 Study of Nitrogen Doped Samples

In order to partly compensate the vanadium acceptor level, a shallow donor level must be added. Furthermore, this donor needs to be in sufficient concentrations so as to compensate the boron, and partially fill the remainder of vanadium acceptor levels. Therefore, an understanding of the vanadium acceptor level begins with an understanding of the principal donor species in the SiC system, nitrogen.

Nitrogen is the most studied element in the SiC system. It has been evaluated using PL[81-83], Hall effect[76, 78, 84-86], FTIR[50, 51, 87-92], optical absorption[93-98], and optical admittance spectroscopy[99, 100]. From these studies, much is known regarding the mechanism by which nitrogen influences both the electrical and

optical properties of the common SiC polytypes. These particular studies can be broken into two primary categories, electrical and optical analyses.

4.2.1 Electrical Properties of Nitrogen in SiC

Based upon the Hall effect studies referenced in the last section,[50,78,84] nitrogen in 6H SiC is known to form one donor level at 85 and two donor levels at about 140 meV below the conduction band edge. The presence of three distinct levels is a manifestation of the structure of 6H SiC. This polytype possesses one hexagonal (85 meV level) and two quasi cubic sites (140 meV levels). However, some Hall effect studies have shown that there is a variability to the activation energy based upon certain characteristics of the sample.[78]

The first study[78] to note such a variability correlated it to the number of compensating centers in the samples. This study gave no explanation for the unusual behavior, merely referencing articles[101-103] which did not support their claim. While they claimed that the compensating (minority) species controlled the activation energy of the defect, the references discussed the mechanism by which the majority species' concentration should influence this parameter. Van Daal's work was further supported by two other groups[76, 104] who claimed that altering the concentration of the compensation species altered the activation energy of the nitrogen levels. However, another author[105], claimed that the activation energy of the nitrogen donor (in 3C) is dependent upon the donor concentration and not upon the acceptor concentration. This latest work only covered a small concentration range with few samples, and may not be statistically significant. The first work[106] disputing the all previous authors' claims was put forth in 1993. In this article, Moore claimed that another center (a

doubly charged nitrogen donor) was responsible for these shallower activation energies. The only views that all of these authors support are the dependence of activation energy on other parameters, and the maximum energy of the nitrogen donor (85 meV for N on a 6H hexagonal site).

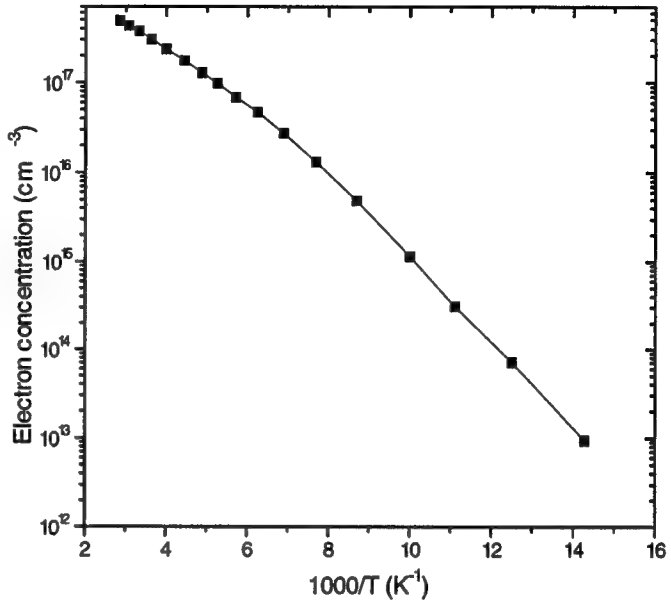

Figure 4.1-Low temperature Hall effect results from a nitrogen doped sample. The activation energy from the fit (line) was found to be 85 meV

A definite variation existed in the activation energies of the nitrogen-doped samples examined as part of this study. Shown in figure 4.1 is a plot of the temperature dependence of the carrier concentration of a nitrogen doped sample. The squares represent the experimental data, while the line is the fit to the data using a least squares fit of the following transcendental equation for a compensated, multi-level (j in all) sample:[77]

$$[N_a + n_0] = \sum_{j=1}^{M} \frac{N_{dj}}{1 + \beta_j^{-1} \exp(\eta + \varepsilon_{dj})} \qquad (4.1)$$

where M is the number of electronic levels contributing electrons to the conduction band, N_a is the concentration of acceptors, n_0 is the concentration of conduction electrons, N_{dj} is the concentration of jth donors, β_j is the impurity spin

level degeneracy, e_{dj} is the reduced activation energy for the jth level (see eq. 3.3), and η is equal to the natural logarithm of n_0/N_c. The best fit occurred when the number of levels was fixed at 1. From this fit, the three parameters extracted were: activation energy (84.6 meV), donor concentration (1.37×10^{18} cm^{-3}), and acceptor concentration (5×10^{16} cm^{-3}). In the Hall effect data, a variation in the activation energy from 35 to 85 meV was observed. However, not enough work was done to establish which of the currently accepted explanations was most representative of the trends in our samples. No samples existed with activation energies in the range from 50 to 75 meV, which suggests that there may be two types of shallow donors. This absence of such samples suggests that the latest interpretation of Moore may have some validity.

Reports from researchers using thermal admittance spectroscopy do not aid in sorting through the mystery of the nitrogen level in SiC. One group[100] claimed there to be only one level for the hexagonal, and potentially two (unresolvable) levels for each of the quasi-cubic sites of the 6H polytype. These levels are very near the values determined in the low-impurity limit of the Hall effect surveys (i.e. 83 meV for the hexagonal and 137 meV for the quasi-cubic sites). The other work stipulated that in the low-impurity limit ($<5 \times 10^{17}$ cm^{-3}), the admittance measurements exhibited levels at 80 and 110 meV for the two types of sites; however, above a net donor concentration of 1.5×10^{18} cm^{-3} levels at 30 and 40 meV existed. The existence of such levels support the more recent claim that there are other levels present in the samples possessing high levels of impurities.

4.2.2 Optical Properties of Nitrogen in SiC

Upon the introduction of nitrogen into silicon carbide, four features arise in the luminescence and absorption spectra depending upon the levels of doping. These features are: the nitrogen photoexcitation spectrum[107], free carrier absorption, the free carrier interband transition, and the nitrogen bound exciton.

The nitrogen photoexcitation spectrum has been studied in 3C[90], 4H[92], and 6H[50, 51, 91] SiC. This results from the excitation of electrons from the ground state of the nitrogen donor to other excited (hydrogenic) states. This spectrum appears as a set of bands in the middle infrared at about the ionization energy of the nitrogen level for the respective polytype.

At shorter wavelengths, the nitrogen affects the spectrum by introducing a broad free-carrier-like absorption band in the near infrared. Shown in figure 4.2 is a sample spectrum. This effect was studied by Beidermann[94] in 1965 who examined the bands in 4H, 6H, 8H, and 15R and in polarizations both perpendicular and parallel to the c-axis. It results from the excitation of electrons from the ground state of nitrogen to different states within the conduction band. In free carrier absorption, electrons are excited from states in the bottom of the conduction band minima to higher states. The reason why the bands resemble free carrier absorption is because the nitrogen donor level is sufficiently close to the conduction band edge, so that the electrons behave as though they were in the bottom-most states of the conduction band.

The third phenomenon of SiC:N, interband absorption, can also be seen in figure 4.2 at about 16000 cm^{-1}. Dubrovskii et. al.[98] stated that this band resulted from the transition of an electron from the filled nitrogen level to an upper conduction band minima. The transition occurred because the upper minima possessed a significant density of states, which augmented the likelihood of this transition. However, the authors did not indicate the specific upper conduction band.

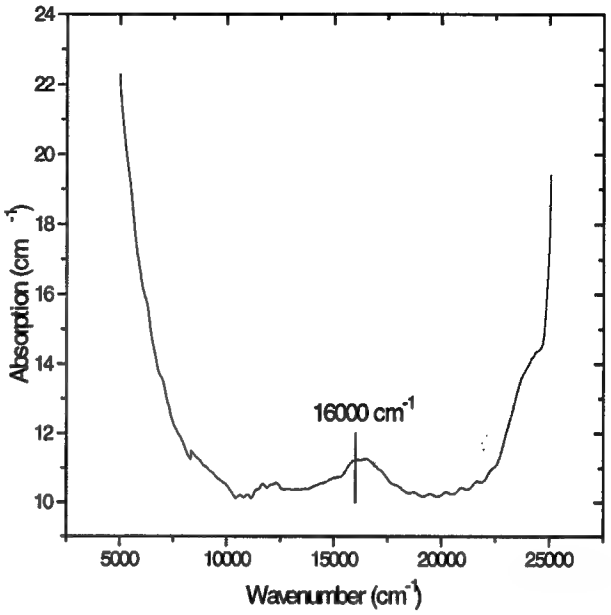

Figure 4.2-Optical absorption spectrum of a heavily N-doped SiC sample, evincing FCA and 16000 cm^{-1} bands

Finally, in the near band edge spectrum, nitrogen incorporation produces lines due to excitons bound to both ionized[96, 97] and neutral[83, 93, 95, 108] donors. Both are observable in absorption, while only the exciton bound to the neutral donor is seen in PL.

These features in the spectrum are useful tools in examining samples using optical techniques. The free carrier absorption band yields a rough estimate of the carrier concentration in a given sample. The bound exciton line can indicate whether the Fermi level for a sample is above or below the nitrogen levels, and

whether any nitrogen is present in p-type samples (i.e. excitons bound to ionized nitrogen).

4.3 Examination of a Boule with a Unique Doping Scheme

The two most proven means of characterizing electronic levels in semiconductors are Hall effect and DLTS. These are mutually exclusive techniques because the Hall effect requires that the Fermi level be pinned to the level in question, whereas DLTS necessitates that the Fermi level be shallower than the examined level. In order to use both techniques on a given boule to study the same defect, the Fermi level must change as a function of position along the boule. Initially, we believed that the vanadium acceptor level resided very close to the nitrogen levels. If this were true, the only possible way to examine these levels via Hall effect would be in the case of a vanadium doped boule whose nitrogen content was high on the seed end and decreased as the growth proceeded. A schematic of such a boule is shown in figure 4.3. DLTS could be performed on samples taken from the right part of the boule (nearer to the seed end), while the Hall effect samples could be taken from just left of where the nitrogen and vanadium concentration

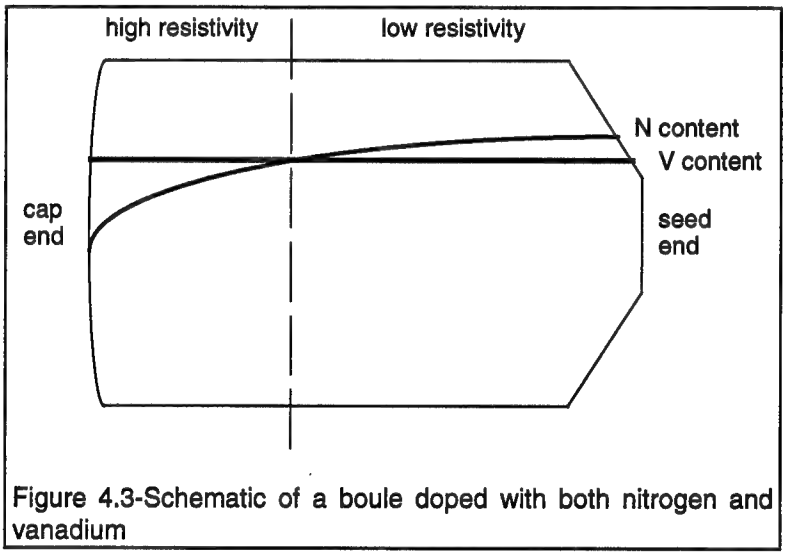

Figure 4.3-Schematic of a boule doped with both nitrogen and vanadium

lines intersect. This boule was grown in a PVT reactor, and wafered to produce both Hall effect and DLTS samples.

The experiments described in the following sections employed samples from this boule with the intent of understanding the electrical properties of the vanadium acceptor level.

4.4 DLTS of n-type Samples

Shown in figure 4.4 is the DLTS spectrum of a sample taken from a 4H SiC nitrogen and vanadium doped boule similar to that depicted in figure 4.3. C-V profiling revealed that the uncompensated nitrogen concentration in this sample was 1.5×10^{18} cm^{-3} at room temperature. As is evident in this figure, the DLTS signature of a deep level defect is present whose maximum ranges from 400 to 445K, depending upon the rate window. Additionally, the concentration of this defect is about 3×10^{17} cm^{-3}. In order to determine the activation energy of the defect responsible for the DLTS signal, a plot of e/T^2 versus reciprocal temperature was created, and is shown in figure 4.5. The activation energy was

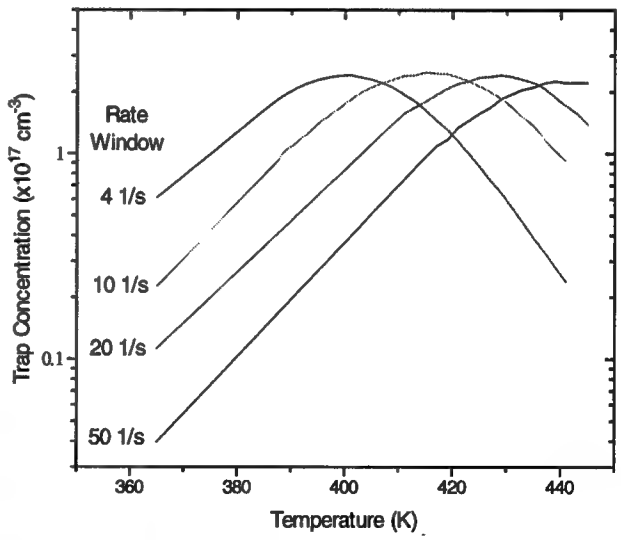

Figure 4.4-DLTS signal versus temperature revealing a deep level centered about 400K depending upon the rate window selection. The concentration of defects was 3×10^{17} cm^{-3}

extracted from this plot using equation 2.11. The activation energy of the defect was calculated to be 806(± 20) meV. The thermal velocity of electrons in this sample was calculated using a method devised by Green.[109] With this information, the temperature independent capture cross section was determined by examining a single point from figure 4.5 and was found to be 1.8×10^{-16} cm^2. No other levels were detected in these samples throughout the temperature range examined (90 to 450K). This fact coupled with the knowledge that these samples were intentionally doped with vanadium, suggests that this may be the sought after vanadium acceptor level.

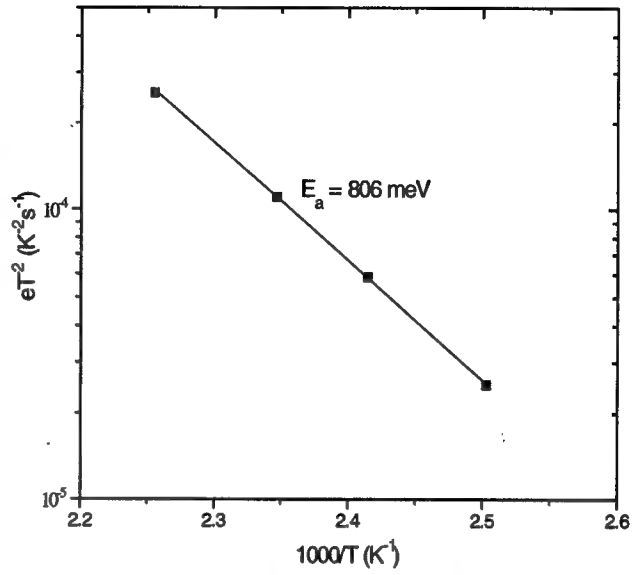

Figure 4.5-DLTS activation energy plot of a vanadium doped 4H sample shown in figure 4.4. The activation energy was found to be 806 meV, with a capture cross section of 1.79×10^{16} cm^{-2}

Additionally, since these samples were heavily doped with vanadium, the concentration levels as determined from the DLTS spectra are deemed to be the solubility limit of isolated, substitutional vanadium in silicon carbide. As a confirmation of this statement, secondary ion mass spectroscopy (SIMS) analysis was performed on samples from this boule, revealing a much higher concentration of vanadium than is observed in these measurements. This fact suggests that the additional concentrations of vanadium arise from crystal sites

other than the isolated, substitutional sites which contribute to these measurements.

The determination of the solubility limit is important in order to ascertain whether or not vanadium is a viable candidate for the creation of high-resistivity material. In the majority of grown crystals, the concentration of unintentional impurities in bulk grown SiC has been reduced to beneath the $3x10^{17}$ cm^{-3} level. These factors indicate that vanadium is a suitable deep level dopant for use in appropriate applications.

4.5 Model of the Acceptor Compensation Process

While DLTS measurements are useful in determining the ionization energy of vanadium acceptors, it is an indirect technique. The rationale behind attributing this 806 meV level to the vanadium acceptor stems from the fact that these samples were doped with vanadium and nitrogen. However, a complex or other intrinsic defect could be responsible for the observed signal. In order to provide the direct confirmation of the defect, optical absorption and Hall effect measurements are performed. A schematic of the compensation in samples whose vanadium acceptor is the principal active electrical defect will be presented. Additionally, an analysis of the differences between this and the donor level will be examined.

4.5.1 Optical Absorption/Illumination Experiments

Shown in figure 4.6 are two absorption spectra observed at 13K from a vanadium-doped 4H sample. Clearly visible are the characteristic $^2E \rightarrow ^2T_2$ intracenter transition absorption bands from the vanadium $3d^1$ center in the 4H polytype at 0.929 and 0.970 eV.[65] The solid line represents the spectrum taken under normal operating conditions, while the dashed spectrum was taken immediately following a 10 minute illumination with an above-band gap halogen source. Once again, the initial spectrum is assumed to be in equilibrium, and therefore the Fermi level in the sample is pinned to either the donor or the acceptor level. The other possible Fermi level configurations can be excluded due to the increase in the absorption spectrum as was discussed in section 3.3

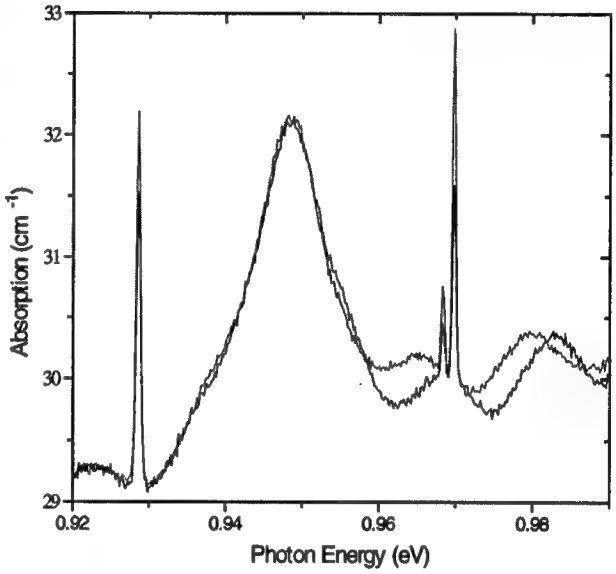

Figure 4.6-NIR absorption spectrum of a 4H V-doped SiC sample both before (solid line) and after (dotted line) illumination from a halogen source

If the Fermi level were pinned to the donor level, this increase would be the result of a rise in the population of vanadium $3d^1$ centers from electrons previously residing on boron centers (figure 3.10). Conversely, if the Fermi level were pinned to the acceptor level the increase in the signal would be the result of a different mechanism. Shown in figure 4.7 is a schematic illustrating the likely

mechanism in the case of 6H-SiC. In figure 4.7a, the nitrogen and boron levels are shown at E_c-85 meV and E_v+350 meV, respectively, with the nitrogen levels partly compensating those of boron. Then, two vanadium levels (at E_c-1.35 eV and E_c-0.66 eV) are added to the band gap (figure 4.7b). The position of the acceptor level (Ec-0.66 eV) was chosen based upon a determination of its location in the 6H polytype via Hall effect, as will be seen in the next section. The excess electrons on the nitrogen orbitals then fall into the empty vanadium acceptor levels in figure 4.7c. Another salient point is that under these conditions the Fermi level is pinned to the acceptor level. As light is shone on the sample, the electrons from all of the levels move into the conduction band (figure 4.7d). After the light is turned off (figure 4.7e), the electrons fall into the empty levels. With the low temperature experimental conditions, as the electrons fall into the traps, they do not have sufficient thermal energy to be excited out of even the shallowest of traps. Depending upon the respective capture cross sections, the electrons preferentially fall into the different levels present in the sample. In order to fill the vanadium acceptor levels, two electrons are required to fall into the same center. The statistical probability of capture of two electrons is significantly lower than that of one. Therefore, the concentration of vanadium centers in the acceptor level configuration would not be as high in the post-illuminated samples. Shown in figure 4.7e is the likely configuration after the light is turned off. The population of the $3d^1$ centers increases because some electrons do not fall back into the acceptor level. In order to confirm this model, Hall effect measurements were performed on the same sample that was the subject of the absorption experiments.

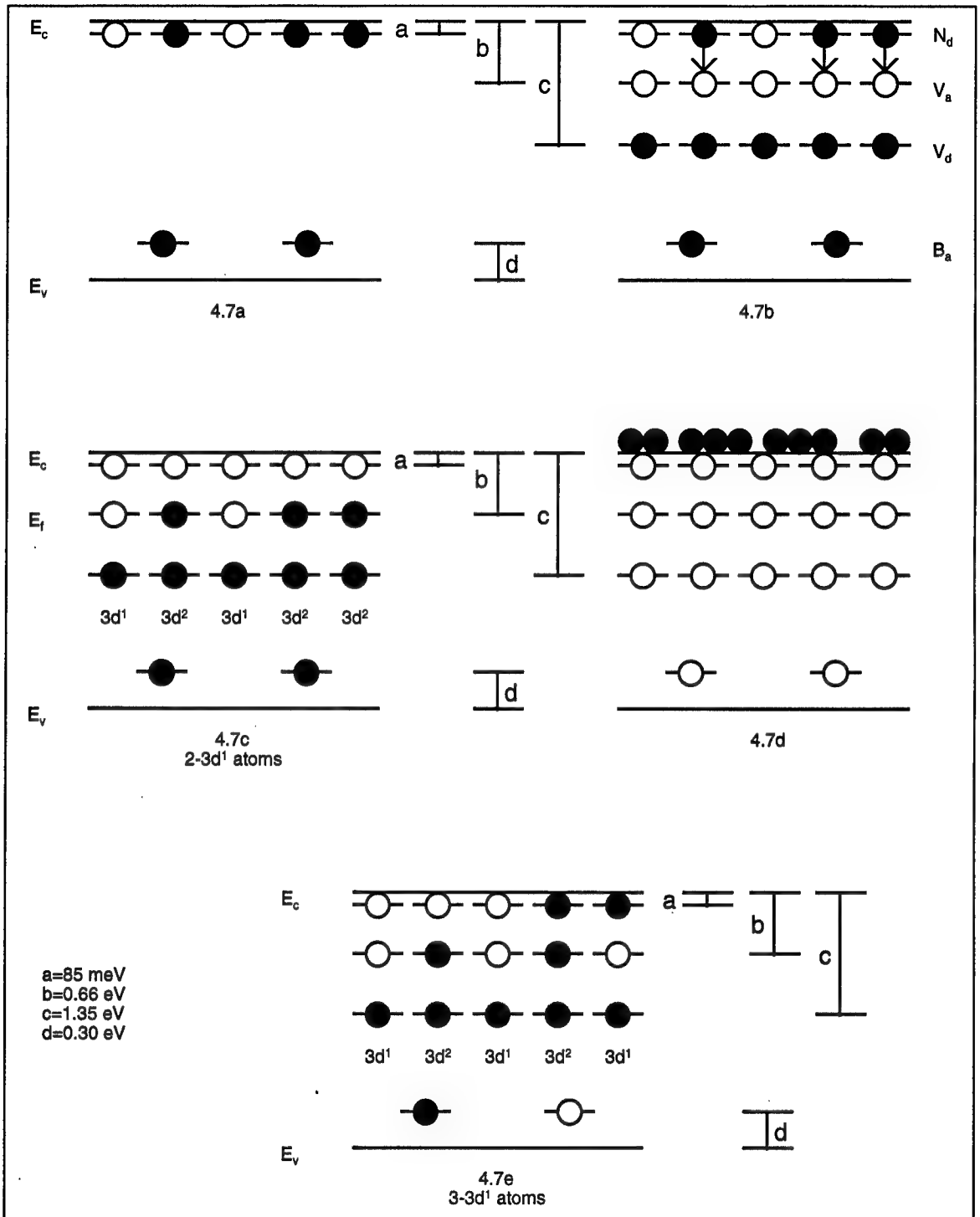

Figure 4.7-Model of the absorption/illumination results discussed in the previous sections- a)Equilibrium SiC band structure with nitrogen and boron impurities, b)same sample with vanadium atoms added, but during quasi-equilibrium, c) equilibrium band structure with boron, nitrogen, and vanadium, d) excitation of carriers to bands with white light irradiation, and e) resultant electronic structure with a preferential distribution of carriers towards the vanadium impurities, with an increased $3d^1$ concentration.

4.5.2 Hall Effect Examination of the Acceptor Level

Plotted in figure 4.8 is the resistivity of two vanadium-doped samples as a function of inverse temperature. The circular symbols represent the resistivity of a 6H sample , while the squares represent that of a 4H sample. The lines in the graph are a least squares fit of the Ahhrenius relationship between temperature and resistivity (modified for the conduction band density of states). The fitting parameter in each case is the activation energy of the defect. The ionization energy of the 4H sample was found to be 0.80 eV, or exactly the same as for the vanadium acceptor determined by DLTS. The position of the acceptor level in the 6H material was found to be 0.66 eV.

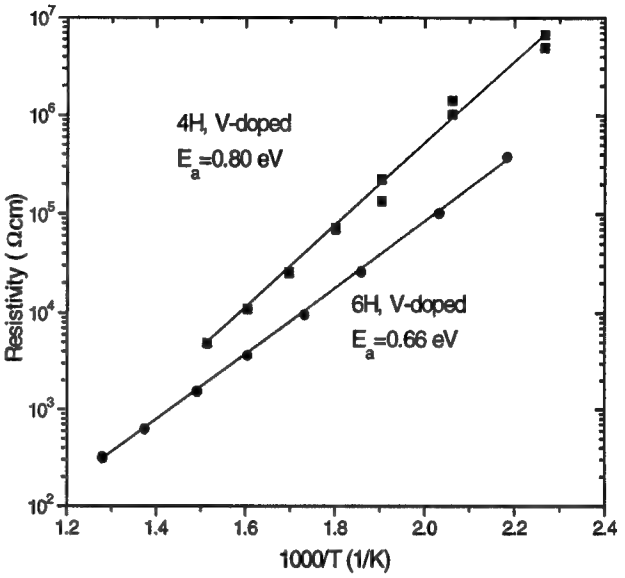

Figure 4.8-Temperature dependent resistivity measurements on both V-doped 4H (square symbols, Ea=0.80 eV) and 6H (round symbols, Ea=0.66 eV) SiC

The difference in the band gap of the 4H and 6H polytypes is 0.30 eV.[110] Evwaraye et. al.[111] has shown that the offset between the conduction bands in these two polytypes is 55% of this value, or 165 meV. This offset is nearly the same as the difference between the positions of the levels observed in the two polytypes. Additionally, localized defects (e.g. transition metals) have been

shown to produce levels dependent upon the vacuum energy level and not upon the energy of the conduction band minima.[112, 113] Coupling these two facts, the two levels observed in Hall effect are most likely the same defect. Moreover, the 4H sample is the same as the one used in the absorption experiments. These factors prove that this level is the vanadium acceptor level. The vanadium acceptor level is so deep that it may also be used as a dopant for the creation of high resistivity material. The depth of the level in the 4H polytype is nearly the same as the EL2 defect in GaAs, which is used in producing semi-insulating substrates for device development in that system.[114]

The tools used to prove the existence of both the donor and acceptor levels are similar. For example, Hall effect and absorption experiments focused on similar material (vanadium doped) and on similar features in the optical spectra (the $3d^1$ absorption bands). Additionally, the data extracted from these measurements are also similar (i.e. the increase in the $3d^1$ absorption when examining both the acceptor level and donor level). As a result of these similarities, some subtle distinctions must be underscored to prove that these levels are unique.

4.5.3 Differentiation Between the Acceptor and Donor Models

Two points comprise the proof necessary to deconvolute any ambiguity existing after these studies. The first point relates to the presence of two levels in the band gap. The second point is connected to the examination of another absorption band in the near infrared at 5000 cm^{-1}(0.625 eV). This 5000 cm^{-1} band can be used to differentiate between the acceptor and donor levels.

The first argument against the models proposed in the previous two chapters maintains that these two bands are not the donor and acceptor, but that both are donor levels of vanadium impurities on different substitutional lattice sites. The levels of hydrogenic impurities tend to exhibit this lattice site dependence; therefore, the activation energy of localized defects may also depend upon the local atomic structure (i.e. the tetrahedral symmetry around all atoms in the SiC lattice). This contention is eliminated with an examination of the illumination studies, each line in the vanadium absorption spectra changes in relatively the same fashion. If this argument were true, and the 1.35 eV level were due to the cubic site and the 0.66 eV level were due to the hexagonal site, one would expect that the line attributed to the hexagonal site would not change in the study of the 1.35 eV level, and the converse would also be true in the study of the 0.66 eV level.

In the figures depicting the absorption data of the $3d^1$ bands in the two samples, the remainder of the absorption spectrum is not displayed. The purpose of the investigation is to examine the vanadium centers, and therefore all other data was excluded in the analysis. However, another band at 5000 cm^{-1}(0.625 eV) exists supporting the differentiation between the acceptor and donor levels. This band is further studied in the next chapter, but one aspect is important to mention at this juncture. The activation energy of the defect responsible for this level is slightly deeper than that of the vanadium acceptor level (see section 5.2.3). In samples whose activation energy relates to the vanadium acceptor level, this additional band is always present. Whereas, for samples whose Fermi level is pinned to the vanadium donor level, this band was noticeably absent. This provides another non-electrical confirmation of the Fermi level position's

change in the various samples elucidating the different deep levels related to vanadium.

5 Other Vanadium Related Features in Silicon Carbide

Beyond isolated, substitutional vanadium, other electronic centers could result from the incorporation of vanadium; such as complexes with the other omnipresent impurities: boron, titanium, and nitrogen. These complexes may result in electronic levels, detracting from the semi-insulating behavior of the isolated vanadium impurity. In this chapter, a description of the vanadium bound exciton will be discussed. The exciton is an indicator of mechanism by which vanadium interacts with the SiC crystal. A discussion of a vanadium complex will conclude this chapter.

5.1 The Vanadium Bound Exciton

This research resulted from an analysis of the effect of vanadium on the optical absorption spectrum. Several small absorption bands were discovered near the fundamental absorption edge. Based upon the presence of these bands and an analysis of the nature of other transition element bound excitons (e.g. Ti), a determination of the position of the vanadium acceptor level was made. Based upon later experimental work (chapter 4), this estimate was found to be incorrect. The reason for this discrepancy has yet to be discovered.

5.1.1 Optical Absorption of Near-Band-Edge Absorption Bands

Shown in figure 5.1 is a typical near-band-edge, low temperature absorption spectrum of an intentionally vanadium-doped, high-resistivity 6H-SiC crystal. In addition to the well known crystal field absorption bands[65] elsewhere in the

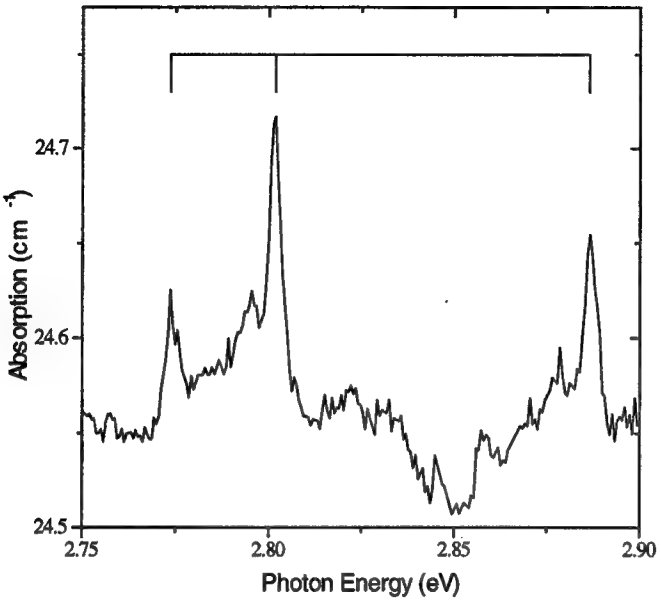

Figure 5.1-The near-band-edge absorption spectrum of a 6H-SiC crystal intentionally doped with vanadium

absorption spectrum, three weak absorption lines close to the fundamental absorption edge were discovered. These lines are located at 2.773, 2.801, and 2.886 eV.

The three line structure is quite common in the 6H-polytype of silicon carbide. Since this polytype has three inequivalent sites (a single hexagonal and two quasi-cubic), the absorption or luminescence bands which result from substitutional impurities typically exhibit three sets of no-phonon lines. This effect has been documented in the case of the $^2E \rightarrow {}^2T_2$ intracenter transition of vanadium[65] and in nitrogen-[81], titanium-[115], and boron-[116] bound excitons. This characteristic fine structure strongly

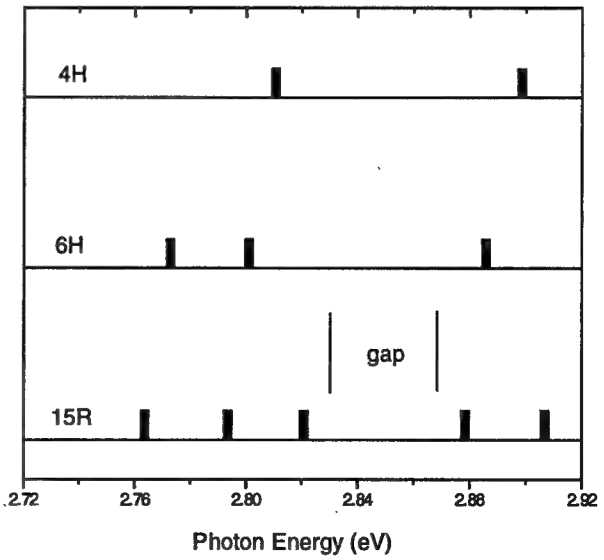

Figure 5.2-The peak positions for the near-band-edge absorption peaks in the 4H, 6H, and 15R polytypes

indicates that the near-band-edge absorption is due to a substitutional point defect.

Measurements on 4H and 15R polytypes further confirmed this conclusion. Depicted in figure 5.2 are the peak positions for three different polytypes. The structure of the lines depends upon the polytype examined. The difference lies in the number of inequivalent lattice sites each polytype possesses. The total number of sites in each polytype is equal to the total number of lines observed in the absorption spectrum. Additionally, a gap is present in each spectrum between two subsets of high-energy and low energy lines. This gap is indicated at the bottom of the figure. The number of lines on the high energy side of this gap is equal to the number of hexagonal sites in each polytype; and, the number of lines on the low energy side of this gap is equal to the number of quasi-cubic sites. The 15R polytype possesses five lines at 2.764, 2.794, 2.821, 2.879, and 2.907 eV; the 6H polytype possesses three lines at 2.773, 2.801, and 2.886 eV; and the 4H polytype has two lines at 2.811 and 2.899 eV. This correlation between the number of inequivalent lattice sites and absorption lines is strongly indicative of the substitutional nature of the responsible defect. Another important point is that the energy of the absorption bands do not shift with the band gap of the respective polytype (E_g=2.99 eV for 15R, 3.02 eV for 6H and 3.27 eV for 4H)[110].

5.1.2 Relationship of the NBE features to the Vanadium $3d^1$ Defect

The evidence for the chemical nature of the impurity responsible for the near-band-edge absorption lines is shown in figure 5.3. The intensity of the most pronounced line in the 6H near-band-edge spectrum (located at 2.801) is plotted

versus the intensity of the hexagonal line in the vanadium $3d^1$ $^2E \rightarrow {}^2T_2$ crystal field transition (located at 0.948 eV). This particular intracenter transition line is usually referred to as the α-line in the literature.[65, 68, 69]

The correlation between these two features is strong with small deviations due to the experimental error caused by the small intensities of the near-band-edge absorption. Besides the samples used to construct this figure, more than twenty other samples possessed neither the $3d^1$ absorption nor the near-band-edge spectrum and are represented by a single point at the origin. This point at the origin primarily includes samples which were either p-type or heavily n-type. Most likely, vanadium is present in these samples, but not in the $3d^1$ charge state. As was alluded to earlier, the 2.801 eV line is caused by the exciton bound to vanadium on one of the quasi-cubic sites. Of the three lines, this one exhibited the strongest absorption, and therefore was used in the correlation in figure 5.3, since the error in calculating the absorption intensity would be minimized. The α-line of the $^2E \rightarrow {}^2T_2$ transition was selected, because it exists as a singlet, and therefore provides the most direct correlation to the concentration of vanadium centers. At the high

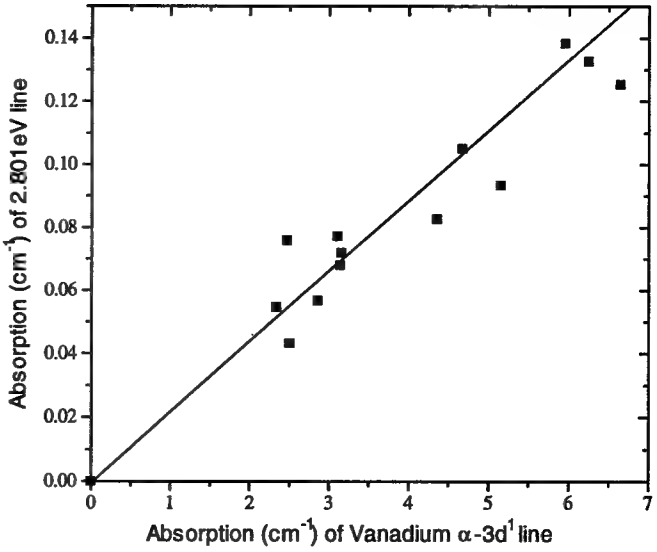

Figure 5.3-The absorption intensity of the 2.801 eV peak versus the intensity of the 0.948 eV peak due to the $^2E \rightarrow {}^2T_2$ intracenter transition of vanadium.

temperatures involved in growth, the distribution of the vanadium atoms among the three inequivalent sites is not expected to differ much, and should not affect the correlation.

5.1.3 Confirmation of the Chemical Nature of the Defect

An additional confirmation of the nature of the near-band-edge defect can be seen in figure 5.4. Shown in this figure is the change in absorption intensity caused by the illumination of each sample with above-band gap white light. As mentioned in the previous two chapters, this increase in the $3d^1$ absorption signal after illumination results from the increase in the density of vanadium centers in the $3d^1$ charge state. The results for three representative samples are plotted with two points for each sample connected by a line. As in figure 5.3, the vertical axis represents the intensity of the 2.801 eV band, while the horizontal represents the intensity of the α-line of the intracenter transition. The open symbols represent spectra obtained in the dark with a weak monochromatic probing light. The closed symbols represent

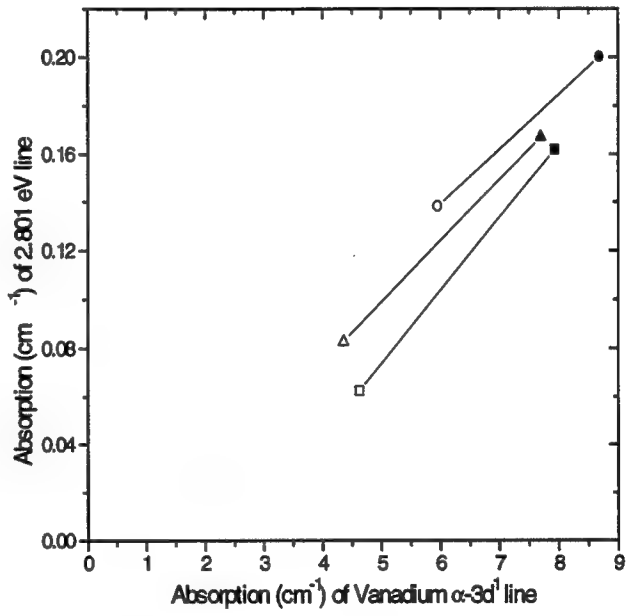

Figure 5.4-Effect of wide band illumination on the vanadium absorption features in partially compensated SiC doped with vanadium and boron. Open symbols-before illumination, closed symbols-after illumination

the respective absorption of the samples after five minutes of broad band illumination with a halogen lamp. All of the samples were taken from intentionally vanadium-doped 6H-SiC crystals partially compensated with boron or nitrogen (i.e. E_f pinned to vanadium donor or acceptor, respectively). Since the absorption of each sample changes at the same rate, both absorption features originate from the same state, namely the ^2E state of the $3d^1$ configuration of substitutional vanadium.

5.1.4 Discussion of the Nature of the Absorption Bands

The fact that the absorption bands are related to vanadium is the first step in their interpretation. The next step is to determine why they appear. There is no direct way to prove that these bands are related to excitons bound to vanadium, but a process of elimination leaves this as the only possible rationale behind their appearance.

Three types of electronic transitions from the ^2E state of vanadium can result in the appearance of narrow absorption lines in the visible part of the spectrum. These possibilities include: the intracenter transition between ^2E and higher excited crystal field states of vanadium (other than the $^2T_2$), vanadium donor-acceptor pair absorption, and excitons bound to neutral vanadium. The first possibility is quickly eliminated because the vanadium donor has only one electron on the 3d shell, and there are only two crystal field terms associated with this configuration: ^2E and $^2T_2$. As previously mentioned, the $^2E \rightarrow {}^2T_2$ transition is located in the 0.89-0.95 eV range.

The second possible interpretation of the near-band-edge absorption is a vanadium donor-acceptor pair(DAP) transition. In this case, boron is the only acceptor-type impurity possessing concentrations high enough to participate in this type of transition which implies a vanadium-boron DAP. That the DAP is responsible for the observed bands is unlikely because the energy of a DAP transition results from a transfer of an electron from the acceptor to the donor species.. In other words, the transition should be located at approximately the difference between the donor and acceptor activation energies. In the case of vanadium and boron, this difference is 1.2 eV, or well below the observed value of 2.8 eV. Even if the acceptor constituent of the DAP were another as yet unidentified species, the greatest possible value for the DAP would be the distance from the vanadium donor to the valence band edge (or 1.65 eV).

The only remaining interpretation of the near-band-edge absorption lines is the exciton bound to neutral vanadium. In the more prevalent SiC polytypes, impurity bound excitons have been identified for several different elements. Elements unambiguously identified as binding excitons include: N[81, 83, 93, 95-97, 108, 117], Al[118, 119], B[116], and Ti[115, 120, 121]. These excitons can be broken into two groups. The first type, seen with regard to the shallow impurities N, B, and Al, is caused by hydrogenic-like electrons and holes which bind to impurities. The energetic position of excitonic lines is related to the energy of the free exciton corrected by the binding energy of the exciton to the defect. As a result, the energy of excitons bound to a hydrogenic impurity shifts with the change of the value of the band gap in different polytypes.[119, 122]

The second type of bound exciton was reported in the SiC:Ti system, and corresponds to an electron occupying a tightly bound atomic-like state with the

hole in an extended hydrogenic orbit.[71, 123, 124] The tightly bound electron produces a $3d^1$ configuration and the exciton energy is expected to be independent of the polytype in much the same way as the energy of localized defects is independent of the conduction band edges.[112, 113] This structure of the titanium bound exciton results in a defect whose luminescence bands do not shift with the band gap energy, as observed in four SiC polytypes, 4H, 6H, 15R, and 33R.[121]

An exciton bound to neutral vanadium should resemble that of an exciton bound to titanium. The extra tightly bound electron from the exciton results in a $3d^2$ configuration, and the exciton energy is not expected to shift with band gap energies, as is seen in figure 5.2. The only apparent difference between the Ti- and V- bound exciton is the lack of corresponding photoluminescence in SiC:V. Upon inspection of the energy band diagram of 6H-SiC, one observes that the vanadium donor level resides 1.35 eV beneath the conduction band edge. The energy of the exciton is 2.76 to 2.91 eV, depending upon the lattice site and polytype where the exciton exists. Therefore, when the exciton recombines , the excess energy is transferred to the remaining electron in the following process:

$$3d^2(V) + h \rightarrow 3d^1(V) + h\nu \rightarrow 3d^0 + e_{cb} \qquad (5.1)$$

where the first term represents vanadium in its $3d^2$ configuration. The second term represents the hole which, along with the second electron on the vanadium, comprise the bound exciton. During the recombination process, the $3d^1$ state of vanadium is created and the energy associated with the recombination could, in principle, be emitted in the form of a photon. Instead, the hypothesis is that the energy (approx. 2.83 eV) is used to transfer the $3d^1$ electron (e_{cb}) to the

conduction band leaving vanadium in its $3d^0$ configuration. This Auger process would explain the lack of vanadium-bound exciton luminescence.

5.1.5 Explanation of the Relationship of the VBE to the Position of the Vanadium Acceptor Level

In a recently published journal article, we asserted that the position of the vanadium acceptor level resulted from an analysis of the structure of the vanadium bound exciton. The depth of the acceptor level was then determined to reside, at most, 250 meV from the conduction band edge. As seen in chapter 4, this estimate was found to be erroneous. The reason behind this error has not been ascertained, but the 250 meV estimate is based upon inference, and therefore thought to be much less reliable than the acceptor energy discussed in the previous chapter.

5.2 The V-X Complex

With the amounts of unintentional impurities present in the PVT-grown SiC, there is a real likelihood that the vanadium will form complexes with these elements. A priori, there is no way of determining the effect of such a complex on the electronic level structure of silicon carbide. During the course of an investigation into a set of absorption bands at 5000 cm^{-1}, a vanadium complex (V-N complex) was found. The fact that vanadium is present in this complex will be established, but due to the lack of proper experimental means (ESR) the second component cannot be ascertained unequivocally. A process of elimination will be used to

propose that nitrogen is the second element, forming a vanadium-nitrogen complex.

5.2.1 Review of Previous Research

The discovery of this defect stemmed from an examination of an absorption band (at 5000 cm^{-1}) found in the NIR. An review of a report about this band is critical toward an understanding of the complex's chemical nature. The report was the only means by which the primary chemical species of the complex could be ascertained. It also provides a tool for assisting in the determination of the second element in the complex.

5.2.1.1 Electronic Transition

The discovery of the V-X complex stemmed from an examination of an electronic transition observed in the near infrared spectrum of silicon carbide samples. Shown in figure 5.5 is this electronic transition observed in a typical 6H sample. The fine structure is defined by two no-phonon doublets at 5000 cm^{-1} and 4850 cm^{-1}. These

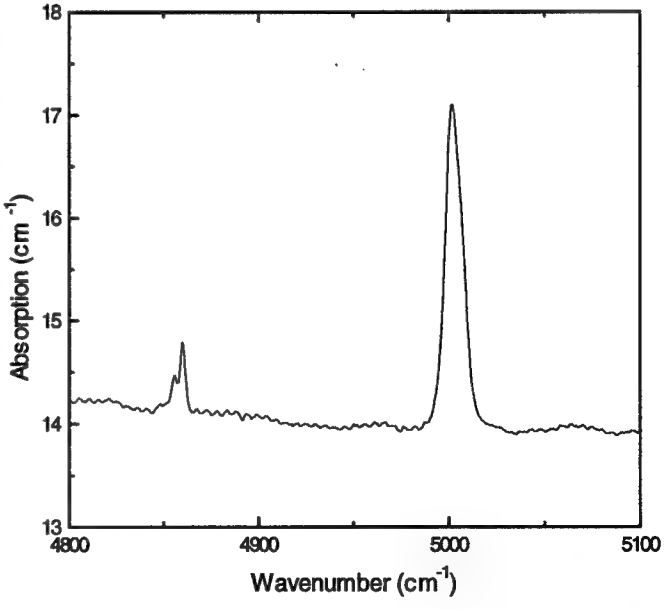

Figure 5.5-Absorption spectrum of the electronic transition of the V-X complex

bands are ubiquitous in n-type silicon carbide, and therefore most likely related to a common contaminant.

The next question to be asked pertains to the nature of the absorption band; whether it is electronic or vibronic. One means of differentiating between electronic and vibrational transitions is to examine the bands in both n- and p-type samples. Electronic transitions are dependent upon the charge state of the defect, and there from will only be observed in either p- or n-type material, not both. Conversely, vibrational transitions may shift with charge state, but will be present in both types of material. The 5000 cm^{-1} band were not observed in p-type samples, and therefore are likely related to an electronic defect. The energy position of the lines also supports this fact. The most energetic vibrational transition is related to that of hydrogen, and is at most 3300 cm^{-1}. Additionally, a set of phonon replicas is observed between 5500 and 6000 cm^{-1}. The replicas are shown in figure 5.6. Several of the replicas are related to SiC lattice modes, except for one at 683 cm^{-1} from the primary band, 5000 cm^{-1}. This specific phonon replica is important for the discussion in a future section regarding the vibronic transitions of this complex.

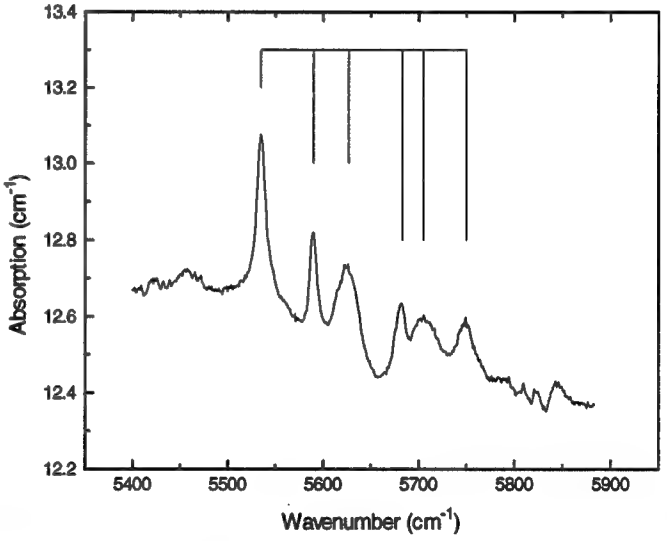

Figure 5.6-Phonon replicas of the 5000 cm^{-1} band

5.2.1.2 Review of a Previous MCDA-ESR Study of the Defect

In 1995, Kunzer et. al.[79] discussed the magnetic circular dichroism of the absorption (MCDA)-detected ESR. In this paper, they used MCDA to examine the effect of magnetic field on the absorption band at 5000 cm^{-1}. From this, they determined that the defect responsible for the absorption band possessed a nuclear spin of 7/2; and, the defect contained two electrons, based upon the observation of a second ESR band for the $\Delta m_s=2$ transition. From these factors, they concluded that the absorption bands resulted from the intracenter transition of the vanadium acceptor level, $^3A_2 \rightarrow {}^3T_2$. While we differ with their interpretation, their results that the nuclear spin of this defect is 7/2 and that it possesses two electrons support our current vanadium complex hypothesis. The only element lacking from the experiments of Kunzer et al.[79] was that they did not perform angular dependent measurements, which would prove whether or not this was an isolated-substitutional or a complex defect.[125]

A problem with their interpretation is that the transition they propose is orbitally forbidden. The absorption bands appear to be as sharp and intense as the vanadium $3d^1$ absorption bands, which are both spin and orbitally allowed. Not only are they orbitally forbidden, but one expects another orbitally allowed transition to the next excited state ($^3A_2 \rightarrow {}^3T_1$) at an energy only 80% greater than the 5000cm^{-1} band (i.e. 9000 cm^{-1}). This other absorption band has not been observed. In a similar arrangement of a $3d^2$ transition of V^{3+} in GaP, GaAs[126], and InP[127], the $^3A_2 \rightarrow {}^3T_2$ transition is a small peak on a much larger $^3A_2 \rightarrow {}^3T_1$ transition.

5.2.1.3 Possible Chemical Composition of the Defect, Based upon MCDA-ESR

In order to determine the elements of the complex an examination of the ESR data is necessary. This section is used to determine the chemical nature of the first element in the complex.

Shown in figure 5.7 is a chart of the elements which possess naturally-occurring, nuclear spins of 7/2. The bars represent the vapor pressure of the respective elements at 2100°C (i.e. within the PVT growth temperature range). The white bars are from elements whose 7/2 isotope is very near 100% of the natural

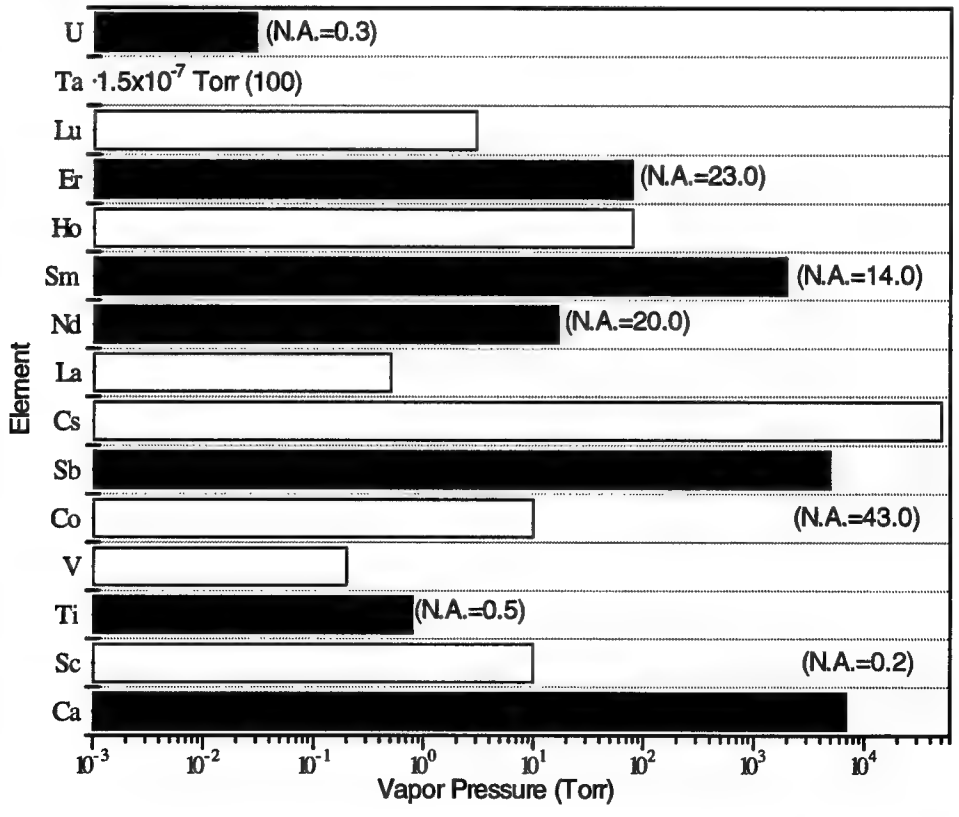

Figure 5.7-Vapor pressures of naturally occurring elemental isotopes with a nuclear spin of 7/2. White bars-N.A.≈100%, black bars-N.A.<100%.

isotopes of the element. Conversely, the dark bars show elements possessing isotopes with less than 100% natural abundance (N.A.). In the MCDA-ESR article, the ESR signal of the defect had only the octet representative of an element whose 7/2 nuclear spin isotope was almost 100% N.A. From this, all of the dark bars can be eliminated. This elimination leaves a total of seven elements. Eliminating rare-earth elements as well as Cs (whose covalent radii is more that twice that of Si), all that remain are lanthanum, scandium, vanadium, and cobalt. SSMS has been performed on many of these boules whether vanadium-doped or not, and there has been no record of lanthanum, cobalt, or scandium in any of the samples. However, atomic masses which are at or near integral multiples of either carbon and/or silicon must be excluded. This exclusion is necessary because the silicon and carbon atoms can form larger molecules when the subject is evaporated. For example, cobalt has a average mass of 59 amu which is very near that of the Si_2 (at 58 amu) and the C_5 (at 60 amu) molecules, and therefore, cobalt cannot be seen in SSMS. Conversely, the atomic masses of both scandium and lanthanum are sufficiently different from any Si_XC_Y molecules; therefore, they would have been observed if they had been present in these samples.

At this juncture, only vanadium and cobalt remain as possibilities for the first element of the complex. If cobalt were part of the complex, it would contribute five electrons to the atomic orbitals after four are consumed in bonding with the carbon near neighbors. In the Kunzer article, the defect was shown to possess two electronic particles (either holes or electrons). Therefore, the other element of a cobalt complex must be either a triple acceptor (to leave two electrons) or a triple donor (to leave two holes). No such defect exists in the SiC system, which means that cobalt cannot be part of this complex.

From this, the only possible element that may contribute to the observed ESR signal is vanadium. Thus, Kunzer et. al. were correct in their analysis that vanadium was responsible for the examined octet. Since vanadium is known to be part of this complex, a study of the nature of the defect was performed with to further comprehend its structure and chemical composition.

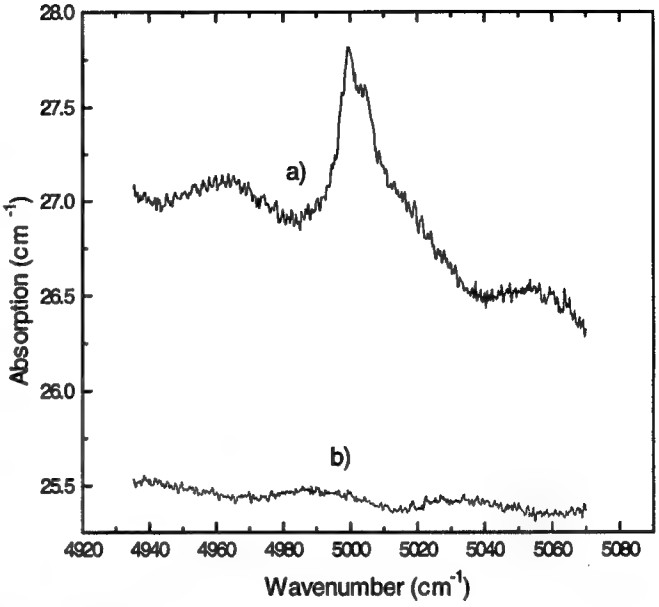

Figure 5.8-Absorption of the 5000 cm^{-1} band with the light polarized both: a) perpendicular and b) parallel to c.

5.2.2 Characterization of the 5000 cm^{-1} Transition

A polarization study of the 5000 cm^{-1} band is the first indication that the defect responsible is a complex. Shown in figure 5.8 is the polarization study of the 5000 cm^{-1} defect. Figure 5.8a is the absorption band in the typical polarization condition (i.e. E⊥c axis) taken at liquid nitrogen temperatures. Whereas, for figure 5.8b, the light vector (E) is parallel to the c-axis. In the latter condition, either no absorption is observed, or the absorption is within the S/N ratio of the experiment. For cubic symmetry, the selection rules necessitate that light absorption experiments excite defects identically whether the light is polarized along the x, y or z (or any combination of x, y, or z). This statement stems from the fact that the polarization vector is triply degenerate under cubic symmetry,

and therefore the triple product of the initial symmetry, the polarization vector, and the final symmetry is identical for each polarization. From this significant change of the absorption in the different polarizing conditions, some anisotropy of the defect must be present (i.e. the symmetry must be lower than cubic). The first likely symmetry is C_{3v}. This symmetry would imply a complex whose adjacent constituent species resides on a substitutional lattice site along the c-axis of the crystal.

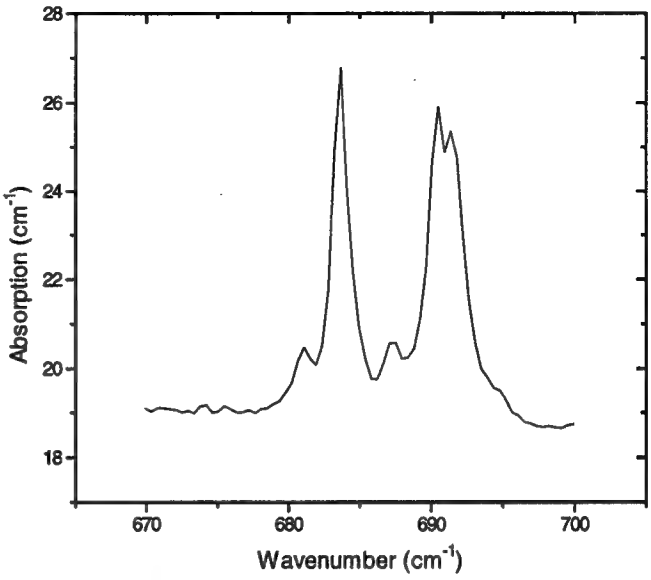

Figure 5.9-MIR absorption bands attributed to the vibrational modes of the V-X complex

5.2.2.1 Vibrational Transition of the V-X Complex

As described earlier (section 5.2.1.1) , a set of phonon replicas was observed adjacent to the electronic transition attributed to this complex. These replicas were mostly comprised of silicon carbide lattice modes. However, one replica at 683 cm^{-1} was not related to a lattice mode. Shown in figure 5.9 is a MIR absorption band structure observed in nearly all silicon carbide spectra. These bands are intricate which makes interpretation difficult. However , they were correlated to the 5000 cm^{-1} absorption band (figure 5.10).

This correlation, coupled with the phonon replica observed near the electronic transition, indicates that the bands at 683 cm^{-1} are related to the V-X complex. Due to the position of the band in the energy spectrum, the vibration is not associated with the vanadium atom. Therefore, the cause of this absorption band must be the other constituent of the complex. This argument is confirmed in a later section (5.2.2.3). The structure of the vibrational absorption band is not yet understood, but may be related to the presence of the three inequivalent lattice sites in the 6H polytype, coupled with the low symmetry of the complex.

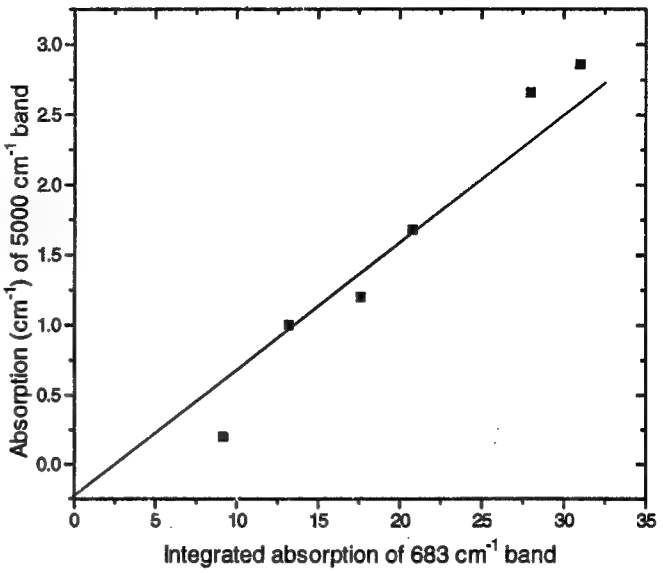

Figure 5.10-Correlation between the absorption intensities of the 683 and 5000 cm^{-1} bands

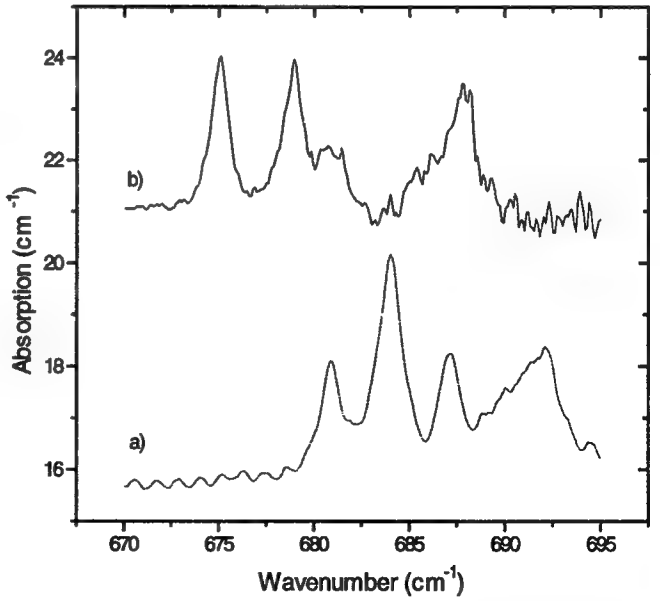

Figure 5.11-Absorption of the 683 cm^{-1} band with the light polarized: a) parallel and b) perpendicular to the c-axis

To further complicate the interpretation, yet to confirm the fact that this complex is of a low

symmetry, a polarization study of the 683 cm^{-1} absorption band is shown in figure 5.11. An examination of this figure illustrates that the complex is highly non-symmetric (i.e. not only linear, but also possessing a preferred orientation along the c-axis).[128]

5.2.2.2 Correlation Diagram Based upon Symmetry Arguments

With the assumption that this complex forms a center with C_{3v} symmetry, a correlation diagram can be constructed to show the likely transition which results in the 5000 cm^{-1} band. The correlation diagram shown in figure 5.12 depicts a C_{3v} center whose upper T_2 crystal field term is split into an upper A_1 and a lower E state.[129] This results in a crystal field splitting that has a low lying E state (termed E_1 in the diagram), an upper E state (termed E_2 in the diagram), and finally a uppermost A_1 state. From this correlation diagram, the ground state of the complex is the $^3A_2$ state, while the first excited state is the ^3E. From this, the transition involved in the observed absorption band is the $^3A_2 \rightarrow {}^3E$. In order to ascertain whether or not this

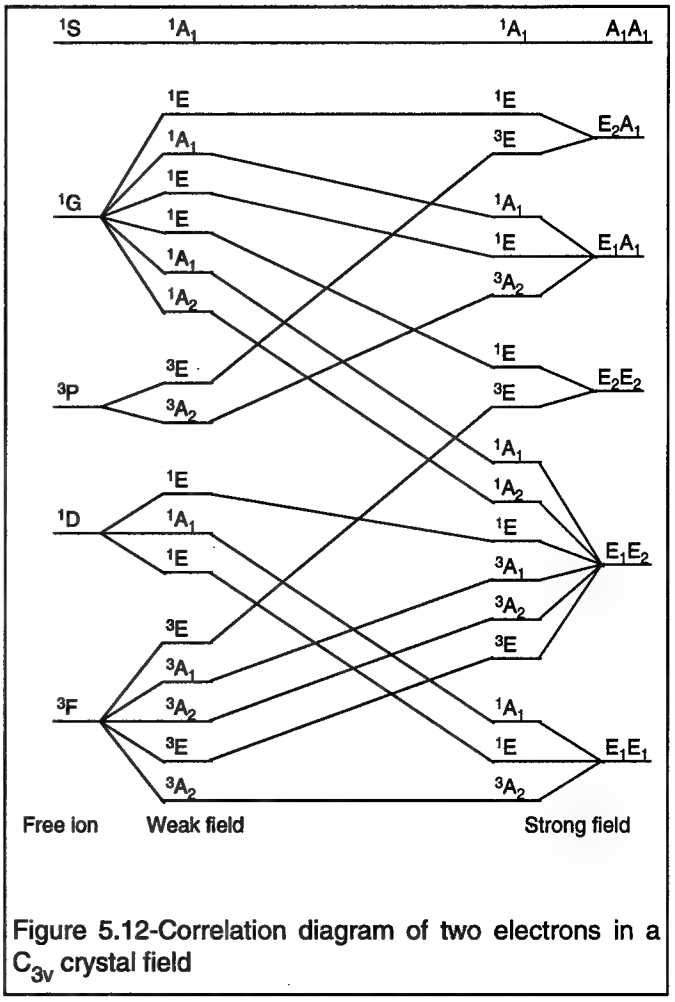

Figure 5.12-Correlation diagram of two electrons in a C_{3v} crystal field

transition correlates with the observed polarization study (figure 5.8), an evaluation of the selection rules is necessary. The transition is spin-allowed based upon the fact that the spin in the initial and final states are identical. In order to gauge whether the transition is orbitally allowed, the cross product of the initial symmetry, the electric dipole, and the final symmetry must contain the totally symmetric representation, A_1. This is illustrated by the following relationship:[130]

$$\begin{matrix} x,y \\ z \end{matrix} \Big| \; A_2 \begin{pmatrix} E \\ A_1 \end{pmatrix} E = \begin{pmatrix} A_2 + A_1 + E \\ E \end{pmatrix} \Big| \begin{matrix} \text{contains} \cdot A_1 \\ \text{does} \cdot \text{not} \end{matrix}$$

From this, the cross product of symmetries for light polarized along the x and y directions contain the totally symmetric representation (A_1), and therefore, the transition is orbitally allowed. The same is not true for light along the z direction which does not possess the A_1 term. These arguments suggest that the correlation diagram is valid for the observed bands, and the C_{3v} symmetry is most likely a correct descriptor of the defect's symmetry.

The other possible transitions that this symmetry would allow include: $^3A_2 \rightarrow {}^3A_2$, $^3A_2 \rightarrow {}^3A_1$, and $^3A_2 \rightarrow {}^3E$. The first two are orbitally forbidden. Section 5.2.3 will be used to show that the bottom-most $^3A_2$ state is 0.78 eV beneath the conduction band edge. The transition to the first ^3E state is 0.625 eV, and therefore, the upper state of the third transition (second ^3E) is most likely degenerate with the conduction band. This degeneracy would significantly shorten the time the defect would be allowed to exist in this ^3E configuration, which would broaden the transition so that it would not be observed.

5.2.2.3 Model of Defect

In order to explain the polarized absorption bands shown in figure 5.8, the complex must also be directed along the c-axis. A schematic of our model of the defect is shown in figure 5.13. The vanadium atom is substituted on the silicon sub-lattice and the unknown second element is shown directly above it on the carbon sub-lattice, orienting the complex along the c-axis.

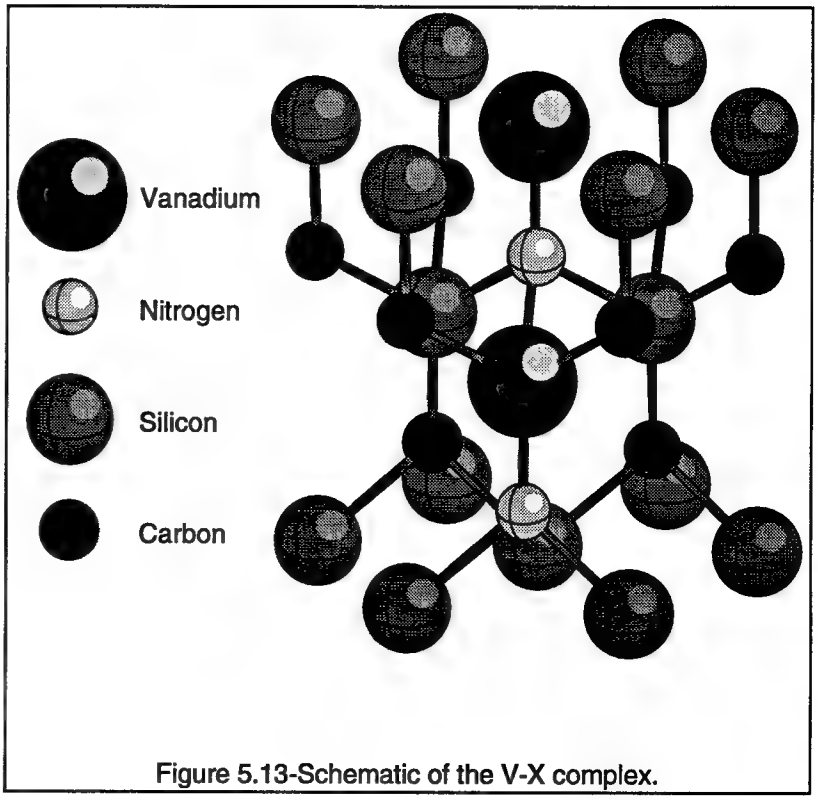

Figure 5.13-Schematic of the V-X complex.

At this juncture, speculation as to the chemical nature of the unknown element is in order. In order to isolate the species, the three primary restrictions are employed: a) that the total defect possesses two electrons, b) the second element is ubiquitous in silicon carbide, and c) the second element is light (will be discussed in figure 5.14). The first consideration is a result of research that Kunzer et. al.[79] performed which found that in n-type material, the complex contains two electrons. This factor will be used later to exclude configurations of the complex which result in too many or too few electrons.

The 683 cm^{-1} absorption band is observed in the vast majority of SiC samples, therefore it must result from an omnipresent impurity (i.e. condition two). The list of common contaminants in PVT-grown SiC include: H, N, B, Fe, Na, Mg, Al, S, Cl, K, Ca, Ti, V, Cr, Ni, and Zn.[45] Alternatively, the absorption bands may be the result of an intrinsic defect, such as a vacancy[131, 132], interstitial[133, 134], or an anti-site[135], which have been shown to exist in other semiconducting systems. However, the formation energies of such defects have been calculated to be much higher in SiC.[136] This higher formation energy is approximately 3 eV higher than in another comparable III-V compound; this increase translates into orders of magnitude fewer defects. Although they can be eliminated at this point, prudence dictates that they remain for further discussion.

The final consideration is a manifestation of the position of the 683 cm^{-1} band in the SiC vibrational spectrum. The Restrahlen region is a part of the absorption spectrum where the optical phonon branch completely extinguishes light passing through the sample. In SiC, the optical phonon band extends from 750 to about 875 cm^{-1}.[10] However, a region that extends from 700 to 1000 cm^{-1} completely absorbs light in PVT grown samples. The region between the bottom of the optical band and the top of the acoustical band is called the phonon gap. All modes which arise in this region are called gap modes (e.g. the 683 cm^{-1} band is a gap mode). All modes which arise from vibrations more energetic than the optical phonon bands are called localized vibrational modes (LVM). Figure 5.14 is a depiction of the means by which each of the modes can be created in a given semiconductor. In this, the M (m) refers to the mass of the heavier (lighter) atom in the lattice. The M' (m') represents the mass of the impurity which substitutes on the site of the heavier (lighter) atom.

The fact that these modes are within the phonon gap indicate that either the condition m'>m or M'<M is true. Secondly, if M'<M were true, the gap mode would originate from the acoustic band which reaches a maximum at 500 cm^{-1} which is 183 cm^{-1} below that band observed here. If this number were added to the top of the optical band, another set of absorption bands would be observed at about 1055 cm^{-1}. No such band has been observed, therefore, this condition (M'<M) cannot be correct, leaving the condition m'>m. This consideration is the most restrictive of the three. Therefore, neglecting the significant modification of the force between the impurity and the matrix (which would affect figure 5.14), the impurity examined must be heavier than the carbon atom it replaces. Since the band lies close to the optic band, one would expect the impurity to be only slightly heavier than the carbon atom. This argument alone is sufficient to eliminate all elements save nitrogen. However, in order to be complete all atoms with masses up to that of silicon will be considered. Coupled with the first limitation, the list of elements becomes: N, O, Cl, Na, and Al.

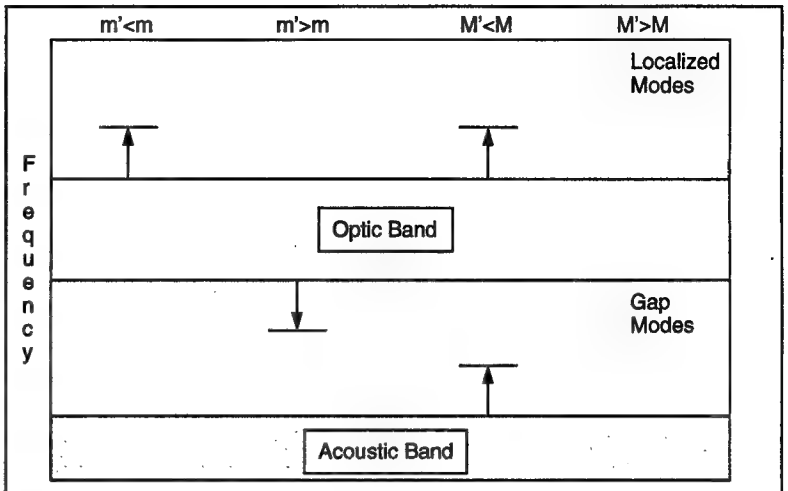

Figure 5.14-Schematic showing the relationship of the impurity's mass to the type of mode induced. The key for the masses is: M'-the impurity on heavy site, M-heavy atom, m'-the impurity on lighter site, m-light atom[54]

The third consideration immediately excludes all acceptor type impurities, since the addition of one hole to the one electron of the vanadium impurity results in zero electrons for the complex. Even if a vanadium-acceptor complex produced

an acceptor level within the band gap, it would add only one electron to the complex, not two. Therefore, all of the group III type impurities can be eliminated (i.e. B and Al). The next type of element considered are those belonging to group IV. Since the site is on the carbon sub-lattice, carbon is eliminated, as this would create the isolated vanadium impurity. A silicon anti-site is the next possibility, but extremely unlikely due to its weight. However, the possibility of the silicon anti-site cannot be completely excluded. The next category (group V) contains the most likely choice, nitrogen. This would contribute the necessary electron to yield the $\Delta m_s=2$ transition in the MCDA-ESR study. Nitrogen fulfills the three conditions previously delineated. Group VI and group VII elements would yield too many electrons (i.e. O and Cl). Conversely, group I (i.e. Na) yield too few electrons. At this point the list of possible elements contains only nitrogen and hydrogen.

Hydrogen is a natural choice for the second element due to its high diffusivity in most semiconducting compounds.[137, 138] Its electron would be needed to form the bond with vanadium; but, the complex could act as an acceptor state which would yield the extra electron observed in the ESR study. The main problem with hydrogen as the second component is its light weight. It tends to form LVMs, not gap modes. Even in more weakly bound semiconductors (e.g. GaP), the hydrogen in a complex vibrates at frequencies on the order of 2200 to 2400 cm^{-1}, or 3.5 times more energetic than that observed in the case of the 683 cm^{-1} band.[139, 140] The force constants between hydrogen and the silicon and vanadium nearest neighbors would need to be significantly reduced to make up for its extremely low mass. Therefore, it is a highly unlikely choice. Other modes of hydrogen exist which may vibrate at energies within the phonon gap, but the LVM should also be observed in the aforementioned range.

With most of the periodic table eliminated, except nitrogen, one other possibility remains: a carbon vacancy. The electronegativity difference between silicon and carbon (0.65) is as great as any of the non-nitride III-V compounds. From this, a carbon vacancy may yield the extra electron necessitated by the ESR experiment. However, a vacancy is not an appropriate choice, because vacancies do not produces absorption bands.

As a result of these arguments, the most likely candidate is nitrogen. Another issue which must be addressed is the preferential orientation of the complex along the c-axis. This is not difficult to rationalize because such a phenomenon is observed in another transition element complex (Ti-N), which preferentially orients perpendicular to the c-axis.[141] The reason behind this is not well understood, but if the Ti-N complex has a preferred orientation, not much rationalization is required to substantiate the preferred orientation of the vanadium-nitrogen complex.

5.2.3 Depth of the V-X Complex in the SiC Band gap

As was previously mentioned, one reason behind the study of this complex was to determine whether it would detract from the high-resistivity nature of vanadium doped silicon carbide boules. This is partly established through the determination of the depth of the V-X level in band gap. DLTS measurements on samples discussed in the previous chapter revealed that there were no other deep levels in the temperature range examined. For this reason, optical admittance spectroscopic (OAS) measurements were employed to correlate the 683 cm^{-1} absorption band to a deep level observed in the OAS spectrum. The OAS measurements were carried out by Evwaraye and Smith at Wright

Patterson AFB. Shown in figure 5.15 is the correlation between the 683 cm^{-1} absorption band and an OAS deep level at 0.78 eV. This figure was constructed from five samples (two at the origin and two at the upper right), and therefore, strongly suggests that the deep level and the 683 cm^{-1} absorption band are related. From this correlation, we conclude that the V-X complex creates a level at 0.78 eV from the conduction band edge.

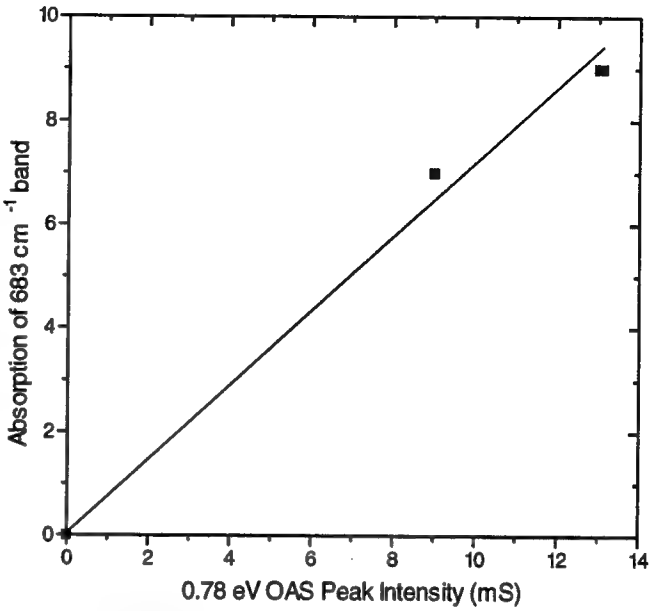

Figure 5.15-Correlation of the 683 cm^{-1} peak intensity with the intensity of an OAS peak at Ec-0.78 eV

If the V-X complex is actually a vanadium nitrogen complex, the type of deep level can now be determined. Since the MCDA-ESR study was performed on n-type samples, the Fermi level is presumably above the level of the V-X trap. In that study, the defect possessed two electrons which would be contributed by the vanadium and nitrogen. Therefore, since the trap is filled and the number of electrons equals the number that each constituent atom introduces, the unfilled trap will contain one less electron than the intrinsic configuration (i.e. (0/+)). This implies that the trap will contribute one electron to the conduction band. In other words, the trap is a deep donor.

There are two implications which derive from the fact that this level is deeper than that of the vanadium acceptor level. First, the complex should not detract from the resistivity of the crystal any more than that of the vanadium acceptor level. Second, the absorption band at 5000 cm^{-1} cannot be related to the acceptor level, as Kunzer et. al.[79] stated, since it is related to a deeper defect.

6. Summary of Results

The importance and utility of vanadium-doped silicon carbide is underscored by the present research. The data taken regarding the solubility limit, as well as the electronic levels produced, evince that vanadium is a viable deep level dopant in the SiC system. The three defects that were analyzed during this investigation into the nature of vanadium incorporation in SiC include: the vanadium donor, the vanadium acceptor, and the V-X complex.

6.1 The Vanadium Donor

These experiments confirmed the previous interpretation that vanadium produces a donor level (0/+) at 1.35 eV beneath the conduction band edge of the 6H polytype. This was accomplished using high temperature Hall effect measurements. The fact that the level at 1.35 eV was related to vanadium was confirmed using optical absorption measurements to selectively modify the population of vanadium centers. Additionally, boron, a major contaminant in undoped SiC, was shown to compensate the vanadium donor level.

6.2 The Vanadium Acceptor

The position of the vanadium acceptor level (0/-) was established at 0.66 (0.80) eV beneath the conduction band edge for the 6H (4H) polytype. Both Hall effect coupled with absorption and DLTS were used in the case of the 4H polytype, whereas only Hall effect was used in the 6H samples. A unique doping scheme using both nitrogen and vanadium greatly assisted in the discernment of this

level. The DLTS measurements aided in providing a deeper understanding of the vanadium impurity. The complementary SSMS data indicated that vanadium had reached the solubility limit. The DLTS showed that there were $3x10^{17}$ cm^{-3} electrically active vanadium centers. At this level of incorporation, the vanadium donor is a viable mechanism for the production of high-resistivity silicon carbide.

6.3 Other Vanadium Defects

This study showed that vanadium in its $3d^1$ configuration binds excitons. These excitons are manifested in the form of a set of absorption bands in the near-band-edge absorption spectrum. The lines do not shift with the band edge and are in the range from 2.76 to 2.92 eV.

The other defect vanadium incorporation produces, a complex, is responsible for an electronic transition ($^3A_2 \rightarrow {}^3E$) in the near infrared spectrum at 5000 cm^{-1}. Absorption experiments have shown that the complex aligns along the c-axis. The other component of the complex is undetermined, but experimental evidence strongly suggests nitrogen. This complex has also been shown to create a deep level at E_c-0.78 eV (OAS). This information is in conflict with another model proposing that these 5000 cm^{-1} absorption bands are related to the vanadium acceptor level.[79]

6.4 Future Research

The first item which must be addressed concerns the nature of the vanadium complex. The best course of action would be to study the effect of polarization

on samples of the three predominant polytypes in an effort to characterize the vibrational absorption bands observed in the middle infrared spectrum. A careful, high resolution study of the electronic transition in these three polytypes would also be helpful. One point not yet established is whether the band of lines in the MIR relate to more than one defect. A study of the relative intensities of the 683 cm^{-1} absorption band in a variety of samples would aid in solving this problem. Beyond these absorption studies, an orientation dependent examination of the MCDA-ESR spectrum of the 5000 cm^{-1} band would further confirm this as a linear defect. The ESR should also be able to elucidate the chemical nature of the complex's other component.

The other aspect of this research remaining unresolved concerns the position of the vanadium donor level in the 4H polytype. Although optical admittance spectroscopy has shown that the level is closer to the exact middle of the band gap, Hall effect should be employed since this technique yields a result which can be more readily compared with other studies.

References

1 J.A. Lely, Ber. Dtsch. Keram. Ges. **32,** 229(1955).

2 H. Morkoc, S. Strite, G.B. Gao, M.E. Lin, B. Sverdlov, and M. Burns, J. Appl. Phys. **76,** 1363(1994).

3 T.S. Ellman, R.B. Price, and D.N. Sunderman, Trans. Am. Nuc. Soc. **6,** 384(1963).

4 L.W. Aukerman, H.C. Gordon, R.K. Willardson, and V.E. Bryson, in *Silicon Carbide*, J.R. O'Conner and J. Smiltens, Editors. 1960, Pergamon: Oxford. p. 388.

5 P.C. Canepa, P. Malineric, R.B. Cambell, and J. Ostroski, IEEE Trans. Nucl. Sci. **NS-11,** 262(1964).

6 Committee on Materials for High-Temperature Semiconductor Devices, *Materials for High-Temperature Semiconductor Devices*, . 1995, (National Academy Press: Washington, DC).

7 R.W. Keyes, Proc. IEEE **60,** 225(1972).

8 E.O. Johnson, RCA Rev. **26,** 163(1965).

9 K. Shenai, R.S. Scott, and B.J. Baliga, IEEE Trans. Electron Dev. **36,** 1811(1989).

10 W. von Munch, *Silicon Carbide (SiC)*, in *Landolt-Bornstein: Numerical Data and Functional Relationships in Science and Technology*, O. Madelung, Editor. 1982, Springer-Verlag: New York. p. 132.

11 L.S. Ramsdell, Am. Mineral. **32,** 64(1947).

12 Y.A. Vodakov, G.A. Lomakina, and E.N. Mokhov, Sov. Phys. Solid State **24,** 780(1982).

13 M. Kanaya, J. Takahashi, Y. Fujiwara, and A. Moritani, Appl. Phys. Lett. **58,** 56(1991).

14 R.A. Stein and P. Lanig, J. Cryst. Growth **131,** 71(1993).

15 L. Hoffman, G. Ziegler, D. Theis, and C. Weyrich, IEEE Trans. Electron Devices **ED-30,** 277(1983).

16 J.W. Hong, N.F. Shin, T.S. Jen, S.L. Ning, and C.Y. Chang, IEEE Electron Device Lett. **EDL-13,** 375(1992).

17 J.A. Edmond, H.S. Kong, and J. C. H. Carter, Physica B **185,** 453(1993).

18 W. Muench, P. Hoeck, and E. Pettenpaul, Tech. IEEE Digest , 337.(1977)

19 J.W. Palmour, J.A. Edmond, H.S. Kong, and C.H. Carter, Physica B **185,** 461(1993).

20 P. Glasgow, G. Zeigler, W. Zuttrop, G. Pensl, and R. Helbig, Proc. SPIE **868,** 40(1987).

21 J.W. Palmour, H.S. Kong, and R.F. Davis, J. Appl. Phys. **64,** 2168(1988).

22 Y. Kondo, T. Takahashi, K. Ishii, Y. Hayashi, E. Sakuma, S. Misawa, H. Daimon, M. Yamanaka, and S. Yoshida, IEEE Electron. Dev. Lett. **EDL-7,** 404(1986).

23 G. Kelner, S. Binari, M. Shur, and J. Palmour, Electron. Lett. **27,** 1038(1991).

24 G. Kelner, S. Binari, K. Sleger, and H. Kong, IEEE Electron. Dev. Lett. **EDL-8,** 428(1987).

25 G. Kelner, M.S. Shur, S. Binari, K.J. Sleger, and H. Kong, IEEE Electron Devices **ED-36,** 1045(1989).

26 W. von Munch, J. Elect. Mater. **6,** 449(1977).

27 B.I. Vishnevskaya, V.A. Dmitriev, I.D. Kovalenko, L.M. Kogan, Y.V. Morozenko, V.S. Rodkin, A.L. Syrkin, B.V. Tsarenkov, and V.E. Chelnokov, Sov. Phys. Semicond. **22,** 414(1988).

28 L.G. Matus, J.A. Powell, and C.S. Salupo, Appl. Phys. Lett. **59,** 1770(1991).

29 P.G. Neudeck, D.J. Larkin, J.A. Powell, L.G. Matus, and C.S. Salupo, Appl. Phys. Lett. **64,** 1386(1994).

30 H. Funaki, A. Nakagawa, and I. Omura. *Numerical analysis of silicon carbide Schottky diodes and Power MOSFETs.* in *1995 International Symposium on Power Semiconducting Devices and IC's.* 1995. Monterey CA: IEEE.

31 K.V. Vassilevski, V.A. Dmitriev, and A.V. Zorenko, J. Appl. Phys. **74,** 7612(1993).

32 M. Bhatnagar and B.J. Baliga, IEEE Trans. Electron Dev. **ED-40,** 645(1993).

33 R.G. Verenchikova, Y.A. Vodakov, D.P. Litvin, E.N. Mokhov, A.D. Roenkov, and V.I. Sankin, Sov. Phys. Semicond. **26,** 565(1992).

34 D.M. Brown, E. T. Downey, M. Ghezzo, J. W. Kretchmer, R. J. Saia, Y. S. Liu, J. A. Edmond, G. Gati, J. M. Pimbley, W. E. Schneider, IEEE Trans. Electron Dev. **ED-40,** 325(1993).

35 J.S. Shor, D. Goldstein, and A.D. Kurtz, IEEE Trans. Electron Dev. **ED-40,** 1093(1993).

36 C.T. Gardner, J.A. Cooper, M.R. Melloch, J.W. Palmour, and C.H. Carter, Appl. Phys. Lett. **61,** 1185(1992).

37 G. Kelner and M.S. Shur, in *Properties of Silicon Carbide*, G. Harris, Editor, IEE: England.

38 R.F. Davis, Z. Sitar, B. E. Williams, H. S. Kong, H. J. Kim, J. W. Palmour, J. A. Edmond, J. Ryu, J. T. Glass, C. H. Carter, Jr.., Mater. Sci. Engr. B **1,** 77(1988).

39 H.M. Hobgood, R.C. Glass, G. Augustine, R.H. Hopkins, J.R. Jenny, M. Skowronski, W.C. Mitchel, and M. Roth, Appl. Phys. Lett. **66,** 1364(1995).

40 Y.M. Tairov and V.F. Tsvetkov, J. Cryst. Growth **43,** 209(1978).

41 Y.M. Tairov and V.F. Tsvetkov, J. Cryst. Growth **52,** 146(1981).

42 H.M. Hobgood, J.P. McHugh, J. Greggi, R.H. Hopkins, and M. Skowronski *Large diameter 6H-SiC for microwave device applications.* in *Silicon Carbide and Related Materials* 1993 Washington, DC. Institute of Physics Publishing.

43 Data from a study performed by Dr. W. C. Mitchel and A. Saxler at Wright-Patterson AFB, OH

44 P.A. Glasow *6H-SiC Studies and developments at the corporate research laboratory of Seimens AG and the Institute for Aplied Physics of the University in Erlangen (FRG).* in *Amophous and Crystalline Silicon Carbide and Related Materials.* 1987. Washington, DC: Springer-Verlag.

45 H.M. Hobgood, D. L. Barrett, J. P. McHugh, R. C. Clarke, S. Sriram, A. A. Burk, J. Greggi, C. D. Brandt, R. H. Hopkins, W. J. Choyke, J. Crystal Growth **137,** 181(1994).

46 K. Maier, J. Schneider, W. Wilkening, S. Leibenzeder, and R. Stein, Mat. Sci. & Engr. B **11,** 27(1992).

47 L. Solymar and D. Walsh, *Lectures on the Electrical Properties of Materials.* Fourth ed. (1988, Ney York: Oxford University Press) p. 465.

48 R.F. Pierret, *Semiconductor Fundamentals.* Second ed. Modular Series on Solid State Devices, ed. R.F. Pierret and G.W. Neudeck. Vol. Volume One. (1988, Reading: Addison-Wesley Publishing Co.) p. 146.

49 S.M. Sze, *Physics of Semiconductor Devices.* second edition ed. (1981, New York: John Wiley & Sons) p. 868.

50 W. Suttrop, G. Pensl, W.J. Choyke, R. Stein, and S. Leibenzeder, J. Appl. Phys. **72,** 3708.(1992)

51 W. Suttrop, G. Pensl, W.J. Choyke, A. Dornen, S. Leibenzeder, and R. Stein. *Hall effect and infrared absorption measurements on nitrogen donors in 6H-SiC.* in *Silicon Carbide and Related Materials.* 1991: Springer-Verlag.

52 L.J. van der Pauw, Philips Technical Review **20,** 220(1958).

53 L.J. van der Pauw, Philips Res. Repts. **13,** 1(1958).

54 D.W. Palmer, in *Growth and Characterization of Semiconductors*, R.A. Stradling and P.C. Klipstein, Editors. 1990, Adam Hilger: Bristol, England. p. 187.

55 G.L. Miller, D.V. Lang, and L.C. Kimmerling, *Capacitance Transient Spectroscopy*, in *Annual Review of Materials Science*, R.A. Huggins, R.H. Bube, and R.W. Roberts, Editors. 1977, Annual Reviews Inc.: Palo Alto, California. p. 377.

56 R.H. Bube, *Photoconductivity of Solids.* (1960, New York: John Wiley and Sons) p. 450.

57 P.L. Land, J. Phys. Chem. Solids **30,** 1693(1969).

58 A.G. Milnes, *Deep Impurities in Semiconductors.* (1973, New York, Ney York: Wiley) .

59 C.S. Williams and O.A. Becklund, *Optics: A Short Course for Engineers & Scientists.* (1972, New York, New York: Wiley-Interscience) p. 397.

60 E.G. Steward, *Fourier Optics: An Introduction.* (1983, Cichester, England: John Wiley & Sons) p. 185.

61 O.S. Heavens and R.W. Ditchburn, *Insight into Optics.* (1991, Chichester, England: John Wiley & Sons) p. 309.

62 L. Pauling, *General Chemistry.* (1988, New York, New York: Dover Publications) p. 959.

63 Y. Kato, Y. Mori, and K. Morizane, J. Crystal Growth **47,** 12(1979).

64 S.J. Bass, J. Crystal Growth **44,** 29(1978).

65 J. Schneider, H.D. Muller, K. Maier, W. Wilkening, F. Fuchs, A. Dornen, S. Leibenzeder, and R. Stein, Appl. Phys. Lett. **56,** 1184(1990).

66 J. Reinke, S. Greulich-Weber, and J.-M. Spaeth, Sol. St. Comm. **85,** 1017(1993).

67 A. Abragam and B. Bleany, *Electron paramagnetic resonance of transition ions.* (1986, New York: Dover Publications) p. 911.

68 M. Kunzer, H.D. Muller, and U. Kaufmann, Phys. Rev. B **48,** 10846(1993).

69 J. Reinke, H. Weihrich, S. Gruelich-Weber, and J.-M. Spaeth, Semicond. Sci. Tech. **8,** 1862(1993).

70 B. Clerjaud, J. Phys. C **18,** 3615(1985).

71 K. Maier, H.D. Muller, and J. Schneider, Materials Science Forum **83-87,** 1183(1992).

72 O.V. Vakulenko and O.A. Govorova, Sov. Phys. Solid State **13,** 520(1971).

73 U. Piekara, J.M. Langer, and B. Krukowska-Fulde, Solid State Comm. **23,** 583(1977).

74 D.R. Hamilton, W.J. Choyke, and L. Patrick, Phys. Rev. **131,** 127(1963).

75 N.P. Baran, V.Y. Bratus, A.A. Bugai, V.S. Vikhnin, A.A. Klimov, V.M. Maksimenko, T.L. Petrenko, and V.V. Romanenko, Phys. Solid State **35,** 1544(1993).

76 G. Lomakina, Sov. Phys. Solid State **7,** 475(1965).

77 J.S. Blakemore, *Semiconductor Statistics.* (1987, New York: Dover Publications) p. 365.

78 H.J. van Daal, W.F. Knippenberg, and J.D. Wasscher, J. Phys. Chem. Solids **24,** 109(1963).

79 M. Kunzer, U. Kaufmann, K. Maier, and J. Schneider, Mat. Sci. & Engr. B **29,** 118(1995).

80 J.R. Jenny, M. Skowronski, W.C. Mitchel, H.M. Hobgood, R.C. Glass, G. Augustine, and R.H. Hopkins, J. Appl. Phys. **78,** 3160(1995).

81 W.J. Choyke and L. Patrick, Phys. Rev. **127,** 1868 (1962).

82 P.J. Dean and R.L. Hartman, Phys. Rev. B **5,** 4911 (1972).

83 J.P. Bergman, C.I. Harris, O. Kordina, A. Henry, and E. Janzen, Phys. Rev. B **50,** 8305 (1994).

84 S.H. Hagen and C.J. Kapteyns, Philips Res. Rep. **25,** 1 (1970).

85 B.W. Wessels and H.C. Gatos, J. Phys. Chem. Solids **38,** 345 (1977).

86 D.L. Barrett and R.B. Cambell, J. Appl. Phys. **38,** 53 (1967).

87 R. Helbig, C. Haberstroh, T. Lauterbach, and S. Leibenzeder. *Material characterization of 6H- and 4H-SiC single crystals by optical measurements.* in *The Electrochemical Society-Fall Meeting.* 1988. Hollywood, Florida.

88 W.J. Moore, J.A. Freitas, and P.J. Lin-Chung, Sol. St. Comm. **93,** 389 (1995).

89 G.B. Dubrovskii and E.I. Radovanova, Phys. Stat. Sol. **48,** 875 (1971).

90 W.J. Moore, P.J. Lin-Chung, J. J. A. Freitas, Y.M. Altaiskii, V.L. Zuev, and L.M. Ivanova, Phys. Rev. B **48,** 12289 (1993).

91 O.V. Vakulenko and O.A. Guseva, Sov. Phys. Semicond. **15,** 886 (1981).

92 W. Gotz, A. Schoner, G. Pensl, W. Suttrop, W.J. Choyke, R. Stein, and S. Leibenzeder, J. Appl. Phys. **73,** 3332 (1993).

93 W.J. Choyke, D.R. Hamilton, and L. Patrick, Phys. Rev. **133,** A1163 (1964).

94 E. Beidermann, Sol. St. Comm. **3,** 343 (1965).

95 A.P. Krokhmal' and V.P. Koshelenko, Sov. Phys. Semicond. **24,** 420 (1990).

96 I.S. Gorban and A.P. Krokhmal, Sov. Phys. Solid State **11,** 623 (1969).

97 I.S. Gorban, A.P. Krokhmal, and S.N. Rud'ko, Sov. Phys. Solid State **10,** 312 (1968).

98 G.B. Dubrovskii and E.I. Radovanova, Sov. Phys. Solid State **11,** 545 (1969).

99 A.O. Evwaraye, S.R. Smith, and W.C. Mitchel, J. Appl. Phys. **75,** 3472 (1994).

100 C. Raynaud, C. Richier, P.N. Brounkov, F. Ducroquet, G. Guillot, L.M. Porter, R.F. Davis, C. Jaussaud, and T. Billon, Mat. Sci. & Engr. B **29,** 122 (1995).

101 G.W. Lehman and H.M. James, Phys. Rev. **100,** 1689 (1955).

102 G.L. Pearson and J. Bardeen, Phys. Rev. **75,** 865 (1949).

103 P.P. Debye and E.M. Conwell, Phys. Rev. **93,** 693 (1954).

104 M.V. Alekseenko, A.G. Zabrodskii, and M.P. Timofeev, Sov. Phys. Semicond. **21,** 494 (1987).

105 B. Segall, S.A. Alterovitz, E.J. Haugland, and L.G. Matus, Appl. Phys. Lett. **49,** 584 (1986).

106 W.J. Moore, J. Appl. Phys. **74,** 1805 (1993).

107 The term photoexcitation spectrum is vague, and may describe the absorption process. However, it has been used in the SiC system to describe the series of absorption lines in the middle infrared which result from the excitation of an impurity atom's electron to the successive higher hydrogenic levels.

108 I.S. Gorban and A.P. Krokhmal, Sov. Phys. Sol. St. **12,** 699 (1970).

109 M.A. Green, J. Appl. Phys. **67,** 2944 (1990).

110 W.J. Choyke, APS Bulletin **38,** 564 (1993).

111 A.O. Evwaraye, S.R. Smith, and W.C. Mitchel, Appl. Phys. Lett. **67,** 3319 (1995).

112 J.M. Langer and H. Heinrich, Phys. Rev. Lett. **55,** 1414 (1985).

113 J.M. Langer, C. Delerue, M. Lannoo, and H. Heinrich, Phys. Rev. B **38,** 7723 (1988).

114 D. Bois and G. Vincent, J. de Physique **38,** L351 (1977).

115 A.W.C. van Kemenade and S.H. Hagen, Sol. St. Comm. **14,** 1331 (1974).

116 J.R. Jenny, M. Skowronski, W.C. Mitchel, H.M. Hobgood, R.C. Glass, G. Augustine, and R.H. Hopkins, J. Appl. Phys. **79** (5) p. 2326 (1996)

117 L. Patrick, D.R. Hamilton, and W.J. Choyke, Phys. Rev. **132,** 2023 (1963).

118 L.L. Clemen, W.J. Choyke, R.P. Devaty, J.A. Powell, and H.-S. Kong. *Comparison of dilutely doped p-type 6H-SiC from a variety of sources.* in *International conference on silicon carbide and related materials.* (Springer-Verlag, Berlin, 1991) pp. 105-15

119 L.L. Clemen, R.P. Devaty, M.F. Macmillan, M. Yoganathan, W.J. Choyke, D.J. Larkin, J.A. Powell, J.A. Edmond, and H.S. Kong, Appl. Phys. Lett **62,** 2953 (1993).

120 T. Kimoto, H. Nishino, T. Ueda, A. Yamashita, W.S. Yoo, and H. Matsunami, Jpn. J. Appl. Phys. **30,** L289 (1991).

121 L. Patrick and W.J. Choyke, Phys. Rev. B **10,** 5091 (1974).

122 M. Ikeda, H. Matsunami, and T. Tanaka, Phys. Rev. B **6,** 2842 (1980).

123 K.M. Lee and G.D. Watkins, Phys. Rev. B **26,** 26 (1982).

124 K.M. Lee, L.S. Dang, G.D. Watkins, and W.J. Choyke, Phys. Rev. B **32,** 2273 (1985).

125 Private communication with Dr. M. Kunzer.

126 G. Aszodi and U. Kaufmann, Phys. Rev. B **32,** 7108 (1985).

127 M.J. Kane, M.S. Skolnick, P.J. Dean, W. Hayes, B. Cockayne, and W.R. MacEwan, J. Phys. C **17,** 6455 (1984).

128 Private communication with Dr. Micheal Stavola. He claimed that the large number of lines in either polarization was indicative of the phenomenon mentioned in the text.

129 F.A. Cotton, *Chemical Applications of Group Theory.* (1963, New York: Interscience Publishers) p. 295.

130 D.C. Harris and M.D. Bertolucci, *Symmetry and Spectroscopy: An Introduction to Vibrational and Electronic Spectroscopy.* (1989, New York: Dover Publications) p. 550.

131 Z. Jing, L.H. Yang, C. Mailhiot, T.D. de la Rubia, and G.H. Gilmer, Nucl. Instrum. Methods **B102,** 29 (1994).

132 S.B. Zhang and J.E. Northrup, Phys. Rev. Lett. **67,** 2339 (1991).

133 T. Soma, S. Tahata, and H.-M. Kagaya, Phys. Stat. Sol. B **157,** 509 (1990).

134 T.Y. Tan, Mater. Chem. Phys. **40,** 245 (1995).

135 J.I. Landman, C.G. Morgan, and J.T. Schick, Phys. Rev. Lett. **74,** 4007 (1995).

136 C. Wang, J. Berholz, and R.F. Davis, Phys. Rev. B **38,** 12752.(1988)

137 R.C. Newman, Philos. Trans. R. Soc. A, Phys. Sci. Eng. (UK) **350,** 215 (1995).

138 S.J. Pearton, C.R. Abernathy, C.B. Vartuli, J.D. Mackenzie, R.J. Shul, R.G. Wilson, and J.M. Zavada, Electron. Lett. (UK) **31,** 836 (1995).

139 M.D. McCluskey, E.E. Haller, J. Walker, and N.M. Johnson. *Local vibational mode spectroscopy of berillium and zinc-hydrogen complexes in GaP.* in *Twenty-First International Symposium on Compound Semiconductors.* 1994. San Diego, CA: IOP Publishing.

140 M.D. McCluskey, E.E. Haller, J. Walker, and N.M. Johnson, Phys. Rev. B **52,** 11859 (1995).

141 V.S. Vainer, V.A. Il'in, V.A. Karachinov, and Y.M. Tairov, Sov. Phys. Solid State **28,** 201 (1986).